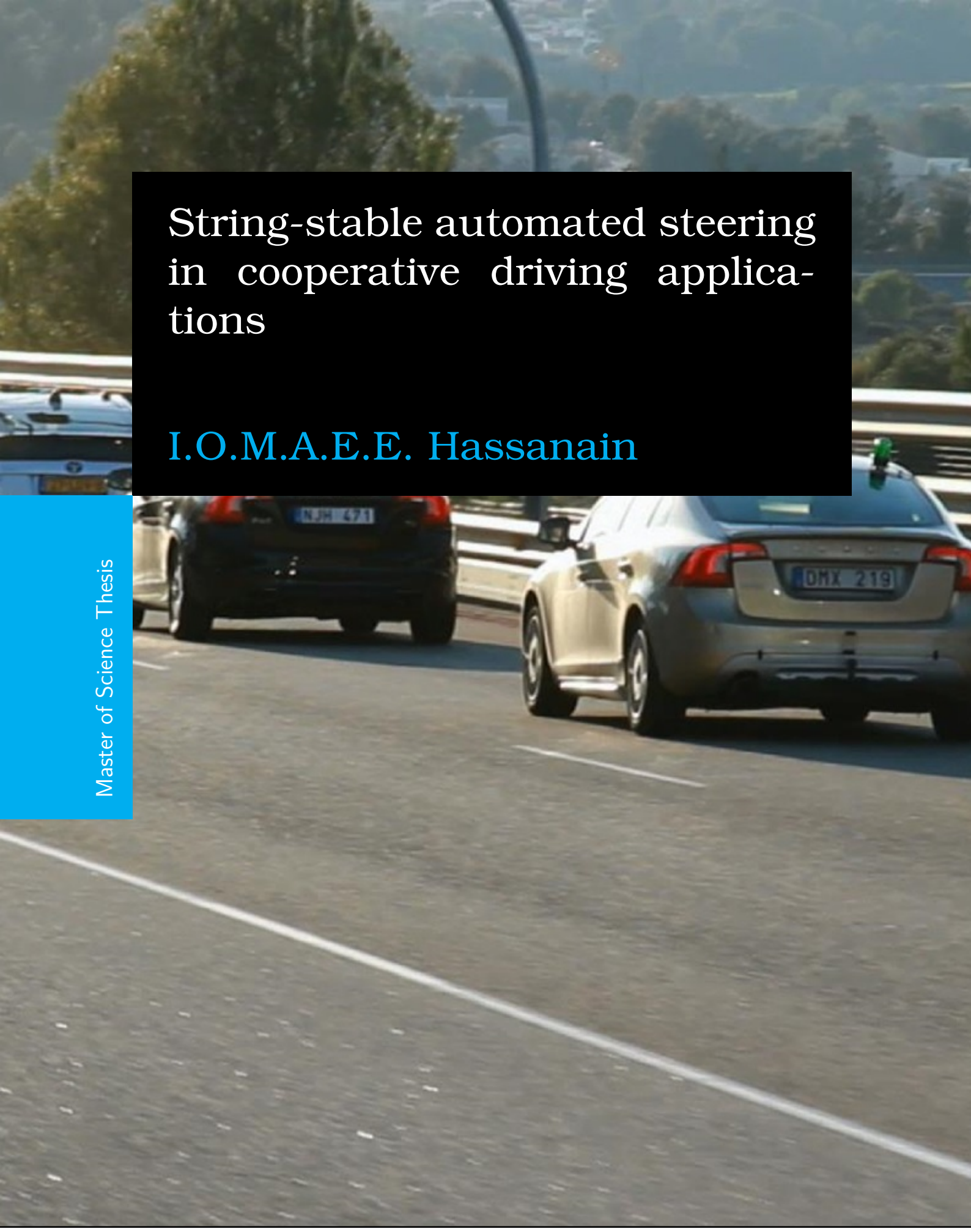

String-stable automated steering in cooperative driving applications

I.O.M.A.E.E. Hassanain

Master of Science Thesis

TU Delft Delft University of Technology

Delft Center for Systems and Control

String-stable automated steering in cooperative driving applications

Master of Science Thesis

For the degree of Master of Science in Systems and Control at Delft University of Technology

I.O.M.A.E.E. Hassanain

November 22, 2017

Faculty of Mechanical, Maritime and Materials Engineering (3mE) · Delft University of Technology

The work in this thesis was supported by TNO Automotive. Their cooperation is hereby gratefully acknowledged.

Delft University of Technology
Department of
Delft Center for Systems and Control (dcsc)

The undersigned hereby certify that they have read and recommend to the Faculty of Mechanical, Maritime and Materials Engineering (3mE) for acceptance a thesis entitled

String-stable automated steering in cooperative driving applications

by

I.O.M.A.E.E. Hassanain

in partial fulfillment of the requirements for the degree of

Master of Science Systems and Control

Dated: November 22, 2017

Supervisor(s):

Prof.dr.ir. Nathan van de Wouw

Dr. Mohsen Alirezaei

Dr.ir. Jeroen Ploeg

Reader(s):

Dr.ir. Jan-Willem van Wingerden

Abstract

The ever-increasing road transport demand in the developing and the developed world has resulted in road-traffic networks nearing maximum capacity. Traditional approaches to this problem, such as increasing road capacity, do not offer long-term solutions. Combined with rising environmental concerns, the demand for smarter solutions has never been higher. One such solution, which has gained significant ground in the past decades, is automated vehicle platooning.

A vehicle platoon is an interconnected dynamical system consisting of automated vehicles driving in close proximity, coordinating their movement through measurements and sometimes inter-vehicular communication. By allowing driving in close proximity, platoons have the potential to increase road capacity, whilst reducing fuel consumption. Platoons are subject to safety and performance requirements. In order to meet these requirements the vehicle platoon needs be string stable, such that effects of disturbances are not amplified in the upstream direction of the string of vehicles. String-stable platoons also help preventing ghost traffic jams, typically caused by human driver behaviour. Advancements in vehicle platooning research have mostly been concerned with longitudinal automation, and consequently with longitudinal string stability. However, driving at small inter-vehicular gaps also requires lateral automation. Naturally, this means that string stability in the lateral sense is required.

Therefore, the objective of this MSc thesis is to develop a lateral control method for automated vehicle platoons that yield string-stable behaviour. In the first part, an error model based on a vehicle-following control strategy, which uses vehicle path following, is derived. This model is then used to describe the path-following problem within a platoon. In the second part, a control strategy is proposed using the $\mathcal{H}_\infty$ framework, such that path following and lateral string stability are guaranteed a-priori.

The robustness properties and the performance of the designed controller are analysed by means of frequency-domain analysis and time-domain simulations. Finally, path following and the string-stability properties of the controller have been validated experimentally. The experiments performed confirm the theoretical analysis, thereby showing that lateral string stability is obtainable using the proposed method.

Glossary

List of Acronyms

ITS	Intelligent Transportation Systems
CACC	Cooperative Adaptive Cruise Control
ACC	Adaptive Cruise Control
V2V	Vehicle-to-Vehicle
AICC	Autonomous Intelligent Cruise Control
LTI	Linear Time-Invariant
PAS	Park Assist System
LFT	Linear Fractional Transformation
HMI	Human Machine Interface
CAN	Controller Area Network
LPV	Linear Parameter Varying
VeHIL	Vehicle Hardware In the Loop

List of Symbols

Subscripts

α	side-slip
c	center of gravity
d	disturbance
e	error
f	front

fb	feedback
ff	feed-forward
i	index; input
k	index; sample
LA	look-ahead
m	measurement; length
max	maximum
min	minimum
n	natural
o	global origin
p	p-norm; perturbed
r	rear; reference
s	path variable; sampling
t	time; angular rate
unc	uncertainty
us	under-steer
x	x-direction
y	y-direction
z	z-direction

Roman Symbols

A	system matrix
B	input matrix
C	output matrix; cornering slip stiffness
c	polynomial coefficient
D	delay transfer function
d	disturbance; separation distance
F	force
G	transfer function
I	inertia
K	polynomial; under-steer coefficient
L	length
m	mass
N	closed-loop system
n	number of states
P, $\mathcal{P}$	plant model
q	road's angular velocity
R	rotation matrix
r	reference;relative uncertainty
S	sensitivity transfer function
s	Laplace variable; generalised position

T	transformation matrix
t	time
u	input
v, V	vehicle velocity; sensed outputs
w	exogenous input; disturbance
x	global x-position
y	global y-position
z	exogenous outputs; discrete time operator

Greek Symbols

α	lateral slip; class $\mathcal{K}$ function
β	body slip angle; class $\mathcal{K}$ function
Δ	interval
δ	steering angle
Γ	complementary sensitivity function
ω	frequency
ϕ	time delay
Π	set of perturbed plants
ψ	yaw angle
ρ	curvature
σ	time constant
τ	time constant
θ	tangent of the road at measuring point
ζ	damping coefficient

Mathematical Notations

$\cdot$	(dot) product
ϵ	arbitrary value
$\mathbb{C}$	set of complex numbers
$\mathbb{R}^n$	real coordinate space of n dimensions
$\mathbb{Z}$	set of all integers
$\mathbb{Z}$	set of all positive integers
$\|\cdot\|$	vector norm
$\|\cdot\|_{\mathcal{H}_\infty}$	$\mathcal{H}_\infty$ system norm
$\|\cdot\|_{\mathcal{L}_p}$	$\mathcal{L}_p$ signal norm, $p \in \{1, 2, \infty\}$
$f(\cdot)$	real-valued function
$h(\cdot)$	real-valued function
S_m	set of all vehicles in a platoon of length m
$\mathrm{Re}(\cdot)$	real part

Table of Contents

List of Figures

List of Tables

Acknowledgements

Throughout the graduation process I have had the privilege of being surrounded with people that helped me in many ways, I would like to take this opportunity to thank all of them.

First of all, I would like to thank my supervising professor Nathan van de Wouw for giving me the opportunity to work under his guidance. Nathan, you have taught me to approach problems in a more critical and systematic way. Moreover, I would like to thank you for always being critical towards my work and providing excellent feedback on all my progress reports, my literature review and final thesis. I feel that I have grown a lot in the past year, and part of this, I credit to working under your supervision.

I would also like to thank my supervisors form TNO, Mohsen Alirezaei and Jeroen Ploeg. Your daily supervision and guidance has been really helpful. I would like to thank both of you for making the time for our weekly progress meetings, and the meaningful discussions we had during and outside of those meetings, I have learned a lot from both of you. Mohsen, thank you for reading all my reports, and for going above and beyond to ensure that I had some experimental results to present. Jeroen, thank you for always finding the time to read my reports, and for always quickly replying to my emails.

Finally, I would like to thank my family. Mum, Dad, and Hagar thank you for always being there for me. Mum and Dad, thank you for supporting me throughout my life and throughout my 5 years at the university. I will forever be grateful for enabling me to do what I am passionate about, I would not be where I am today without your love, trust, and support.

Delft, University of Technology — I.O.M.A.E.E. Hassanain
November 22, 2017

Chapter 1

Introduction

1-1 Cooperative driving

The rise of developing countries in the world economy, and the continuing economical growth of the developed world has led to an increase in traffic demand. As a result, the existing road-traffic networks are nearing maximum capacity. Since this demand is expected to keep increasing, the existing infrastructure will not be able to provide sufficient capacity [3]. The traditional approach of increasing physical road capacity does not offer a long-term solution [4]. With this knowledge in mind, combined with rising environmental concerns and the desire to increase traffic safety, the demand for smarter solutions has never been higher.

A smart solution would be to better utilise the existing road capacity through the increase of road throughput. It is possible to increase road throughput by reducing inter-vehicular distances without reducing operating speeds, whilst also maintaining equal accelerations, thereby avoiding phenomena such as ghost traffic jams. Unfortunately, these requirements can not be met by the human driver; the "human controller" is simply not fast nor accurate enough. Hence automation is required, which has led to the emergence of Intelligent Transportation Systems (ITS) in the past decades.

The added benefit of automating vehicles, is the increase in safety on the road. It was reported that the majority of traffic accidents are due to preventable human errors [5]. Casualties caused by inattentive, fatigued, and reckless drivers could be eliminated through full vehicle automation. The market-ready vehicles equipped with automated systems, are mostly still at level 1 with a few exceptions at level 2 of automation [6]. These systems can take over longitudinal and lateral control within predefined driving conditions. A promising level 2 ITS application, which has gained significant ground in the past decades, is vehicle platooning.

A vehicle platoon is best described as an interconnected dynamical system consisting of a group of vehicles driving in close proximity, coordinating their movement through measurements and sometimes inter-vehicular communication. Within a platoon, one can distinguish two types of platoon members, the leading vehicle and the following vehicles. Typically, the

leading vehicle is human driven and the following vehicles are automated in longitudinal direction. Platooning is often facilitated using inter-vehicular communication, however, it should also be possible without, e.g., in case of communication failure. Platooning not only increases road throughput but also has the potential to increase fuel efficiency, truck platooning being a good example thereof [7, 8].

Several research projects [1, 9, 10, 11, 12, 13] have been able to achieve safe platooning, albeit that most projects were concerned with longitudinal automation only, i.e., manual steering is still required. Commonly, platooning is facilitated by Cooperative Adaptive Cruise Control (CACC). CACC is an extension to Adaptive Cruise Control (ACC), widely implemented in consumer cars, that uses Vehicle-to-Vehicle (V2V) communication to maintain operational safety whilst allowing for smaller gaps/ headways on the road.

A phenomenon that does not occur in "regular" dynamic systems, which has to be accounted for in interconnected systems, is the propagation of disturbances in upstream direction of the string of interconnected subsystems. The amplification of these disturbances in the case of a vehicle string, may compromise safety or cause traffic flow instability, which is the reason for ghost traffic jams on motorways. Preventing the amplification of these disturbances up the string of vehicles is therefore a prerequisite for vehicle platooning. The stability of platoons against disturbances, is described by the notion of string stability, and is arguably the most important property of a platoon.

In contrast to the progress made in platooning with only longitudinal automation, advancements in platooning with lateral automation have been slow. At lower speeds, it is still possible to perform lateral manoeuvres within a platoon using a human operator. However, at higher velocities and at small time gaps, manual operation becomes unsafe [14]; the time gap refers to the time required to bridge the distance to the preceding vehicle. Naturally, the next evolutionary step would be the development of control methods for lateral automation within a platoon. Several research projects have devised methods for lateral automated driving [11, 12, 13, 15, 16, 17], successfully achieving lateral automation for a single vehicle. The implementation for platooning applications, however, has not been as heavily researched.

For lateral control, the objective is for the vehicle to follow a desired path by means of steering. There exist two main approaches to generate a reference for lateral control, those being lanekeeping and vehicle-following methods. Lanekeeping methods rely on the detection of lane markings to calculate the position of the lane's centerline, yielding an absolute reference for lateral control. As a result, the platoon members are not interconnected in the lateral sense. However, not all roads have clear road markings, and for smaller inter-vehicular distances it is not possible to detect the lane-markings reliably [13], thus, leaving vehicle following as the only viable option for lateral automation within a platoon. By using this approach, the lateral dynamics of the platoon members become interconnected. Meaning that any disturbances in the lateral motion of the leading vehicles will be amplified in the upstream direction of the platoon. This could lead to the following vehicles ending up in neighbouring lanes, potentially causing collisions with neighbouring traffic. To guarantee safe platooning, it is required that this system is string stable in the lateral sense.

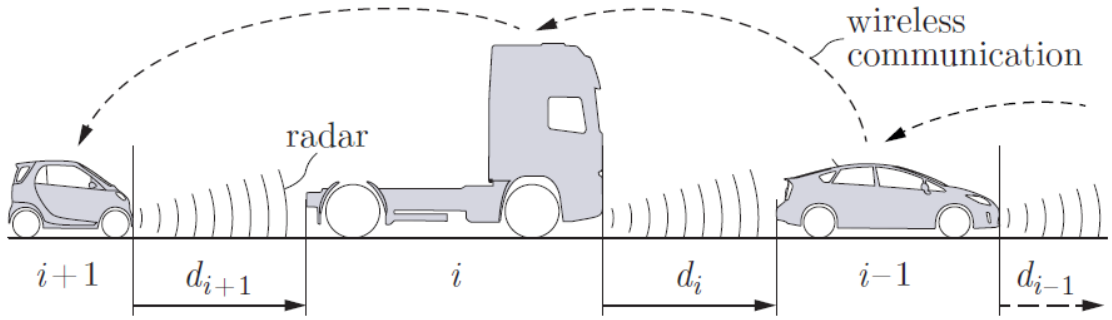

Figure 1-1: An illustration of a vehicle platoon [1].

1-2 Background for lateral control for cooperative driving

Whilst many strategies exist for lateral control, the majority of those have been developed for autonomous driving and are not suitable for platooning applications. Phenomenona that occur in an interconnected system, such as string (in-)stability, have to be accounted for during the design process. Furthermore, the deployed control strategy will dictate the behaviour of the following vehicles, e.g., the occurrence of the corner cutting phenomenon [18]. This section will therefore highlight the most important aspects with regards to the lateral control problem within a platoon, and attempts to quantify them. First, Section 1-2-1 will give a description of the motorway platooning scenario. Next, Section 1-2-2 will provide the approaches to the vehicle-following problem and argue their applicability for the set objective. Finally, in Section 1-2-3, the notion of string stability in both the general and lateral sense will be introduced.

1-2-1 Motorway platooning

This section aims to provide a comprehensive description of the motorway platooning scenario. Generally, a platoon consists of a group of vehicles that travel in a coordinated manner, with close proximity to each other. When all the vehicles in a platoon are identical, i.e., have same dynamics and controller, the platoon is said to be homogeneous. For platooning to be possible, system states of platoon members are used to determine an appropriate following strategy. States that could possibly be of interest may include a platoon member's steering input, their acceleration and velocity. The collection of these states is usually facilitated by on-board sensors and wireless inter-vehicular communication.

The objective of the follower vehicles is to follow the path driven by the leading vehicle whilst maintaining a predefined inter-vehicular separation distance. Figure 1-1 serves to illustrate what a vehicle platoon looks like. In this figure, the leading platoon member is illustrated as vehicle $i-1$. The inter-vehicular distance that separates the vehicles is given by d_i.

1-2-2 The vehicle following problem

The method deployed for vehicle following determines the general behaviour of the platoon members. In this section, the most commonly deployed methods for vehicle following used to

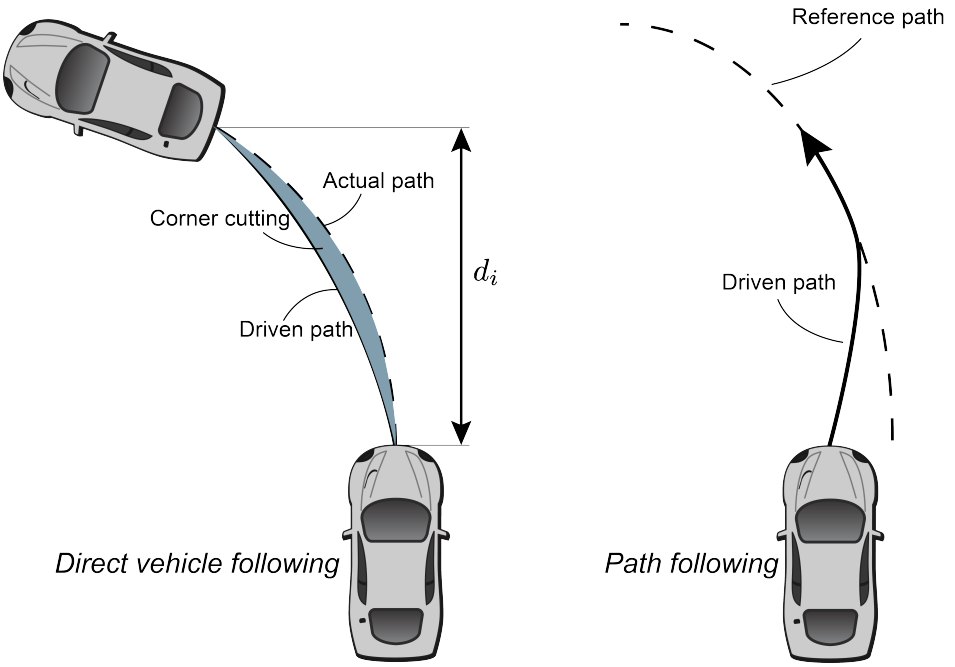

Figure 1-2: An illustration of the direct vehicle-following method (left) and the path-following method (right).

achieve lateral automation will be highlighted. Based on the system requirements, it will be argued why deploying one method over the other would be more beneficial.

Two main approaches to vehicle following can be distinguished, being direct vehicle-following and the path-based vehicle-following approaches. In Figure 1-2, both approaches have been illustrated. The direct-following approach is the simplest solution to the vehicle following problem. As a result thereof, it is also the most encountered one in literature [11, 19, 13, 20]. The objective for this concept is to steer towards a reference located on the preceding vehicle. This reference is the relative position of the preceding vehicle as measured from the trailing vehicle. Often this reference is chosen to be a point on the rear bumper of the preceding vehicle. The problems that arise with this approach is that the path driven by the following vehicle will not be equal to the one driven by the preceding vehicle. This could lead to corner-cutting phenomena, which are undesirable for platooning, especially when the platoons are long, as it would lead to potentially hazardous situations.

The second strategy is the path-based vehicle-following method [21, 17]. In this approach, measurements of the relative position and states of the preceding vehicle are obtained. These measurements, are used to construct an estimate of the path driven by the preceding vehicle, which is typically done using interpolation techniques. The drawback of this approach, however, is that it increases the complexity of the system. But when deployed properly, this approach does not suffer from the same corner-cutting phenomenon as in the vehicle following approach.

1-2-3 String Stability: A comprehensive Overview

When dealing with interconnected dynamical systems, string stability becomes a matter of concern. String stability differs from conventional stability, in that it is concerned with the propagation of system responses along a string of interconnected systems, instead of with the dynamics of individual systems. String stability is the primary performance criterion for platooning, as a string-stable platoon guarantees that initially bounded spacing errors will remain bounded, thereby enabling safe platooning. Moreover, string-stable platoons are desired to prevent ghost traffic jams on motorways. The stability of an individual sub-system does not necessarily warrant the string stability of the interconnected system, even if the system consists of identical sub-systems. In regular motorway traffic, string instability is often encountered, also with human operated vehicles. The "human controller" can be described as a stabilising controller, however, applying this "controller" yields a string unstable interconnected system. This often results in so-called ghost traffic jams, which are congestions that appear on the motorway for no apparent reason. The upcoming paragraphs will attempt to summarise the most prevalent definitions encountered in literature.

String stability has been studied from as early as 1974 [22]. In an informal approach, [23] argued that string stability, within the context of platooning, should ensure that, "disturbances in all frequency ranges are attenuated along the platoon to ensure that they do not became unreasonably large by the end". Accordingly, [23] referred to (asymptotic) string stability as the "monotonic decrease along the platoon". This (asymptotic) stability, is not a by-product of a "good" controller, but should be accounted for during controller design. Later on, in their work on Autonomous Intelligent Cruise Control (AICC), [24] referred to this phenomenon as the "slinky effect". Within the context of autonomous driving, this referred to the "amplification of disturbances in the values of deviation, velocities and accelerations of the following vehicles" [24].

Having established the most prevalent descriptions of string stability, as they have been encountered in literature, one can formulate a general definition for string stability. Fundamentally, the different definitions that have been discussed attempt to describe a system property that prevents the propagation of variations in system states through the string of interconnected systems. This definition will be maintained when "string stability" is referred to in the remainder of this report.

A mathematical definition for string stability

In this section, the mathematical definition for string stability will be introduced, such that the string-stability criterion can be quantified. In [25], a general definition for the string stability of interconnected systems was formulated. This definition was based on the propagation of initial conditions perturbations, in which they consider systems of the following form:

$$\dot{x}_i = f(x_i, x_{i-1}, \cdots, x_{i-r+1}), \tag{1-1}$$

where $i \in \mathbb{Z}$, $x_i = 0 \, \forall \, i \leq 0$, $x \in \mathbb{R}^n, f : \underbrace{\mathbb{R}^n \times \cdots \times \mathbb{R}^n}_{r \text{ times}} \mapsto \mathbb{R}^n$ and $f(0, \cdots, 0) = 0$, with $\mathbb{Z}$ being the set of all integers and $\mathbb{R}^n$ the real vector space of size n. For systems of the form (1-1), the following definition for string stability is derived.

Definition 1. [25] *The origin $x_i = 0$, $i \in \mathbb{Z}$ of the system* (1-1) *is $\mathcal{L}_p$ string stable if for all $\epsilon > 0$ $\exists \delta > 0$ such that,*

$$\|x_i(0)\|_p < \delta \Rightarrow \sup_t \Big(\sum_{i=1}^{\infty} |x_i(t)|^p \Big)^{\frac{1}{p}} < \epsilon,$$

where for all $p < \infty$, $\|f_i\|_p$ denotes $(\int_0^\infty |f_i(t)|^p dt)^{\frac{1}{p}}$ and $\|f_i(0)\|_p$ denotes $\big(\sum_{i=1}^{\infty} |f_i(0)|^p\big)^{\frac{1}{p}}$. Definition 1 presents the so-called $\mathcal{L}_p$ string stability condition. This definition implies that for bounded initial states smaller than δ, of the interconnected system, the states remain bounded with a value smaller than ϵ, for all times t. This definition, however, does not take the directionality of the error propagation into account. Moreover, the input-output behaviour of the interconnected system is not included in the system description.

In [1] a novel definition of string stability, based on $\mathcal{L}_p$ string stability, is presented, which addresses the shortcomings of the definition in [25]. First the following cascaded system is defined

$$\begin{aligned} \dot{x}_0 &= f_r(x_0, u_r) \\ \dot{x}_i &= f_i(x_i, x_{i-1}),\ i \in S_m \\ y_i &= h(x_i),\ i \in S_m, \end{aligned} \tag{1-2}$$

describing a general interconnected (cascaded) system. Herein $S_m = \{i \in \mathbb{Z} \mid 1 \leq i \leq m\}$ is the set of all vehicles in a platoon of length $m \in \mathbb{Z}$, $u_r \in \mathbb{R}^q$ denotes the external input, $x_i \in \mathbb{R}^n$, $i \in S_m \cup \{0\}$, is the state vector, and $y_i \in \mathbb{R}^l$, $i \in S_m$, is the output. Furthermore, $f_r : \mathbb{R}^n \times \mathbb{R}^q \mapsto \mathbb{R}^n$, $f_i : \mathbb{R}^n \times \mathbb{R}^n \mapsto \mathbb{R}^n$, $i \in S_m$ and $h : \mathbb{R}^n \mapsto \mathbb{R}^l$. For the model in (1-2) the following string stability condition is proposed.

Definition 2. [1] *Consider the interconnected system* (1-2). *Let $x^T = (x_0^T, x_1^T, \ldots, x_m^T)$ be the lumped state vector and let $\bar{x}^T = (\bar{x}_0^T, \ldots, \bar{x}_0^T)$ denote a constant equilibrium solution of* (1-2) *for $u_r \equiv 0$. The system of* (1-2) *is $\mathcal{L}_p$ string stable if there exist class $\mathcal{K}$ functions α and β, such that, for any initial state $x(0) \in \mathbb{R}^{(m+1)n}$ and any $u_r \in \mathcal{L}_p^q$,*

$$\|y_i(t) - h(\bar{x}_0)\|_{\mathcal{L}_p} \leq \alpha(\|u_r(t)\|_{\mathcal{L}_p}) + \beta(\|x(0) - \bar{x}\|),\ \forall i \in S_m \text{ and } \forall\, m \in \mathbb{Z}.$$

If, in addition, with $x(0) = \bar{x}$, it also holds that

$$\|y_i(t) - h(\bar{x}_0)\|_{\mathcal{L}_p} \leq \|y_{i-1}(t) - h(\bar{x}_0)\|_{\mathcal{L}_p}, \quad \forall i \in S_m \setminus \{1\} \text{ and } \forall\, m \in \mathbb{Z} \setminus \{1\},$$

then the system (1-2) *is strictly $\mathcal{L}_p$ string stable with respect to its input $u_r(t)$.*

Here, $\|\cdot\|$ denotes any vector norm, $\|\cdot\|_{\mathcal{L}_p}$ denotes the signal p-norm [26], and $\mathcal{L}_p^q$ is the q-dimensional space of vector signals that are bounded in the $\mathcal{L}_p$ sense. Furthermore, a continuous function $\alpha : \mathbb{R}_{\geq 0} \mapsto \mathbb{R}_{\geq 0}$ is said to belong to class $\mathcal{K}$ if it is strictly increasing and $\alpha(0) = 0$.

Through the class $\mathcal{K}$ function $\alpha(\|u_r(t)\|_{\mathcal{L}_p})$, Definition 2 takes external disturbances into account. Furthermore, by including the class $\mathcal{K}$ function $\beta(\|x(0) - \bar{x}\|)$, initial condition

perturbations are considered. This notion is applicable to both linear and non-linear systems, and has been applied for string stability analysis of platooning in automated highway systems in [1].

When linear systems are considered, it is more convenient to analyse string stability in the frequency domain. Definition 2, can be used to obtain a frequency domain representation of the string stability condition. For this condition to be valid, however, one has to assume that the sub-systems describe linear homogeneous systems. The formal derivations and conditions are further explained in [27]. In [28], a similar approach was used to assess string stability of a platoon. In this work, it was proposed to describe the platoon dynamics using a transfer function $H_i(s)$ that describes the relation from $E_{i-1}(s)$ to $E_i(s)$, with the signal E denoting the error in the Laplace domain. This error could, for instance, represent the deviation in nominal separation between vehicles. For a homogeneous platoon $H_i(s) = H(s)\,\forall i$. In order to ensure string stability, the following condition should hold,

$$\|H(s)\|_\infty \leq 1, \quad \forall s \in \mathbb{C}. \tag{1-3}$$

The string-stability notions presented in the previous section provide a generic description of string stability. To incorporate the notion of string stability for lateral automation, one has to determine the states required to do so. The next section briefly discusses the attempts made in literature to extend the notion of string stability in the lateral sense.

Lateral string stability

As has been noted in Section 1-1, there still is significant ground to be gained in lateral control for platooning. Although several studies for lateral automation exist, the majority does not consider string stability in the lateral sense; this yields these studies impractical for the application at hand, since lateral string stability is sought after to ensure safe platooning. When lateral string stability is of concern, one often refers to the propagation of lateral displacement errors along the platoon of vehicles. Different attempts have been made to define the notion of string stability in the lateral sense. This section will attempt to summarise those.

In [18], an attempt was made to quantify a definition for lateral string stability. In this approach, the propagation of lateral errors was investigated such that the following definition could be given.

Definition 3. *[18] A group of n vehicles is said to be laterally platoon stable in the $\mathcal{L}_p$ sense if* $\forall\, i \in [2, n]$ $\left\|y_r^{(i)}(t)\right\|_{\mathcal{L}_p} < \left\|y_r^{(i-1)}(t)\right\|_{\mathcal{L}_p}$.

Here $y_r^{(i-1)}(t)$ and $y_r^{(i)}(t)$ are the lateral deviations with respect to a reference path of the $(i-1)$-th and i-th vehicle at time t, respectively. The author argued that since lateral error propagation is analysed, it is preferred to use the $\mathcal{L}_\infty$ stability condition, which is concerned with the amplification of the maximum lateral deviation. If $y_r^{(i)}$ is a scalar, the $\mathcal{L}_\infty$ conditions become,

$$\max_t |y_r^{(i)}(t)| < \max_t |y_r^{(i-1)}(t)|. \tag{1-4}$$

This condition can be represented in the frequency domain when linear systems are considered, yielding the following condition:

$$\left| \frac{Y_r^{(i)}(j0)}{Y_r^{(i-1)}(j0)} \right| < 1, \tag{1-5}$$

and the impulse response should not change sign. These conditions imply that the impulse response of $Y_r^{(i)}$ should be smaller than or equal to that of $Y_r^{(i-1)}$, moreover the impulse response not changing signs entails that the system has negative real poles, yielding a damped response. This approach is inspired by the work of [25] and is analogous to the longitudinal case.

Recently, [29] conducted a study on vehicle following control for highly actuated vehicles in a platoon. In this case, lateral string stability was assessed by investigating the ratio between the reference curvature (that of the leading vehicle's path), and the following vehicle's curvature. This means that for the system to be $\mathcal{L}_2$ string stable, the curvature of the preceding vehicle's path should not be amplified, for which the following condition can be expressed,

$$\left\| \frac{\rho_i(j\omega)}{\rho_{i-1}(j\omega)} \right\|_{\mathcal{H}_\infty} \leq 1, \quad i \in \{1, \ldots, N_{PL}\}. \tag{1-6}$$

Here $N_{PL}+1$ denotes the number of vehicles in the platoon including the platoon leader, and ρ_i the curvature of vehicle i. Appendix A provides a definition for the $\mathcal{H}_\infty$ norm, which will be adopted in the remainder of this report when the $\mathcal{H}_\infty$ norm is considered.

In this section, different approaches to describe the notion of string stability were reviewed. In the remainder of this thesis, the definition given by [1] will be used for further analysis, as this definition takes both the initial condition perturbations, and disturbances into account. For adopting this string-stability definition in the lateral sense, a condition inspired by the one defined in [29] is chosen, i.e., the curvature of the preceding vehicle should not be amplified.

1-3 Problem statement

Having established the theoretical framework in which most aspects regarding (cooperative) lateral control have been introduced, it is now possible to formulate the most important challenges. The aim of this master thesis is to develop a lateral controller which renders the set of interconnected vehicles in a platoon string stable. In doing so, the notion of string stability in the lateral sense needs to be defined.

The development of said controller will be based on a vehicle-following approach, such that platooning with small time gaps is possible. To ensure safety, path following will be the means of generating a control reference as opposed to direct vehicle following. This choice was made to prevent the occurrence of the corner-cutting phenomenon, and also to implicitly warrant a certain degree of safety. The interconnection between the vehicles' state is not obvious when using a path-following method, as opposed to direct vehicle-following. Hence, it is desired to obtain a means of quantifying this dynamic interconnection of vehicles, for this approach.

Furthermore, most control approaches treat the string stability condition as an afterthought, as the string stability requirement is never explicitly taken into account. This work will explicitly take this statement into account, such that string stability can be guaranteed *a-priori*. Moreover, the theoretical results will be validated experimentally using platooning-ready vehicles provided by TNO.

Platooning mostly limits itself to regular driving conditions, i.e., the absence of limit handling behaviour. As a result, the decoupling of the longitudinal and lateral dynamics becomes possible. In this work, only homogeneous platoons are considered, where all platoon members are identical.

1-4 Report outline

This section aims to present the approach to the challenges presented previously, which relates to the layout of the report. First in Chapter 2 a system model will be developed, which describes the lateral dynamics of the vehicle. The model of the system will be based on a control-oriented approach for regular driving scenarios, such that certain simplifications can be made. This will be followed by the development of an error model that describes the relation between a vehicle's position and orientation with respect to a predefined path. Furthermore, a system model will be developed such that the interconnection between the vehicles is quantified. Next in Chapter 3, the string stability conditions will be given and a control method will be designed such that the path-following and string stability objectives can be guaranteed *a-priori*. Moreover, the controller should ensure the (internal) stability of the individual systems. In Chapter 4, the designed controller will be analysed in both time and frequency domain, such that a conclusion can be drawn about its stability and performance properties. Chapter 5, focusses on the practical implementation of the controller, and presents test results. Finally, Chapter 6 summarises the main conclusions of this thesis and presents recommendations regarding future works in this field.

Chapter 2

System modelling: A control oriented approach

In this chapter, the model of a vehicle in a homogeneous platoon is derived; the aim is to express the lateral dynamics of a path-following vehicle in terms of its own dynamics and the dynamics of its preceding vehicle. The vehicle's dynamics will be described using a bicycle model [20], which will be used to obtain the error dynamics deemed necessary to design a controller capable of fulfilling the path-following objective. Finally, the interconnection between the current vehicle's and the preceding vehicle's dynamics will be defined.

This chapter is organised as follows: Section 2-1 provides the equations of motion for a vehicle driving in motorway conditions. Afterwards, the error dynamics for the path-following problem will derived in Section 2-2. Finally, in Section 2-3, the complete system dynamics will be derived and posed in Linear Time-Invariant (LTI) state-space form.

2-1 The single track bicycle model

The single track bicycle model is commonly used to describe the lateral dynamics of a vehicle for normal driving conditions [30], since it provides a relatively accurate description of the vehicle states without having to resort to complex modelling and parametrisation efforts. Figure 2-1 presents an illustration of the bicycle model. Here, the front and rear tyres are represented by a single tyre on each axle. The points r and f are defined to be the imaginary contact points where the tyre forces act on, and are located along the center of the axle. Furthermore, it is assumed that the vehicle's mass is concentrated at the center of gravity C, which remains at a constant position along the longitudinal axis of the vehicle. Moreover, all lifting, rolling, and pitching motion is neglected, and the wheel-load distribution between the front and rear axle is assumed to be constant. Given the assumptions presented above, this model is able to describe a vehicle's behaviour, provided that the lateral acceleration remains low [30], i.e., smaller than approximately $4\,\mathrm{m\,s^{-2}}$.

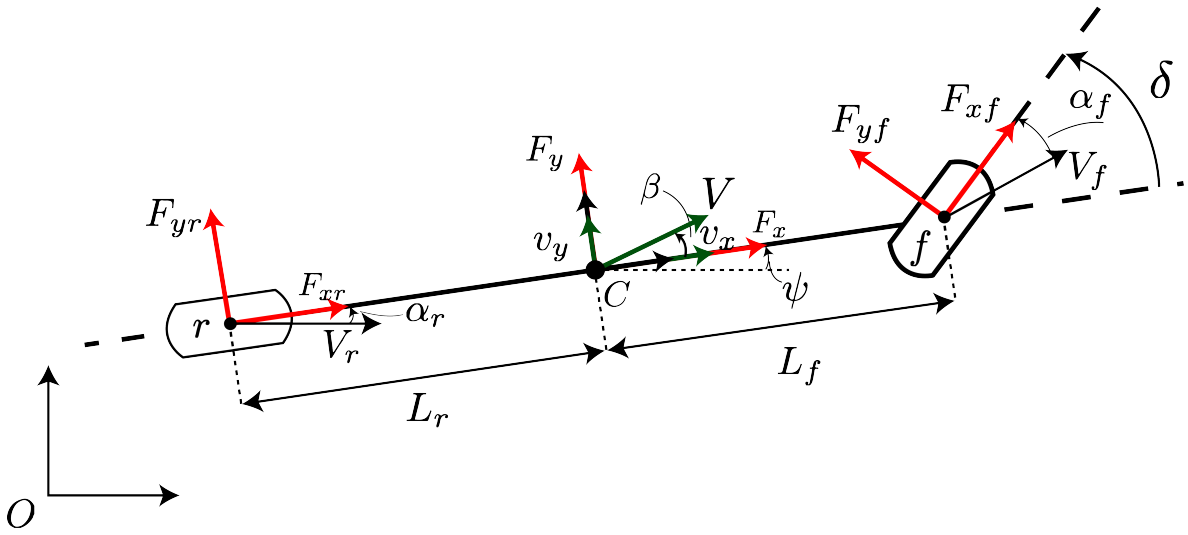

Figure 2-1: The single track bicycle model.

The equations of motion for the single track model as derived in Appendix B are expressed as

$$\begin{aligned} \dot{v}_x &= \frac{1}{m}(F_{xr} + F_{xf}) + \dot{\psi} v_y \\ \dot{v}_y &= \frac{1}{m}(F_{yr} + F_{yf}) - \dot{\psi} v_x \\ \ddot{\psi} &= \frac{1}{I_z}(L_f F_{yf} - L_r F_{yr}), \end{aligned} \tag{2-1}$$

here v_x, v_y and $\dot{\psi}$ denote the longitudinal, lateral, and yaw velocity, respectively. Furthermore, m and I_z respectively represent the vehicle's mass and its moment of inertia around the z-axis, which is pointing outwards at the frame of reference. Moreover, F_{xj} represents the longitudinal forces generated at the tyres, and F_{yj} denotes the lateral forces generated at the tyres, with $j \in \{r, f\}$. Finally, the steering angle of the front wheel is denoted by δ, which also acts as the input to the system.

2-1-1 Adjustments for motorway platooning conditions

The dynamics as expressed by (2-1) depend on the forces, F_{xj} and F_{yj}. Since the aim is to eventually design a lateral controller, the lateral forces are of interest. These forces are generated by the tyres and depend on the slip angles α_j, with $j \in \{r, f\}$, which describe the difference in direction of the wheel's velocity vector and its orientation. The exact mapping depends on the tyre model deployed to describe this relation, which can vary in complexity depending on the required accuracy. Since only regular motorway driving conditions are considered, it is expected that the tyres will operate in their linear regime. The linear tyre model can be deployed to describe these forces [31]. Where the lateral force depends proportionally on the slip angle α_j, with $j \in \{r, f\}$, which has a proportionality constant $C_{\alpha j}$, also known as the cornering stiffness. As a result, these forces can be expressed as

$$\begin{aligned} F_{yr} &= C_{\alpha r}\alpha_r \\ F_{yf} &= C_{\alpha f}\alpha_f, \end{aligned} \tag{2-2}$$

where the cornering stiffnesses and the slip angles of the rear (r) and the front (f) tyres are denoted by their respective subscripts. The slip angles at the front and rear tyres are defined as,

$$\begin{aligned} \alpha_r &= -\beta_r \\ \alpha_f &= \delta - \beta_f. \end{aligned} \tag{2-3}$$

Herein, β_j, with $j \in \{r, f\}$, is the angle that the velocity vector at the rear and front wheels makes with the longitudinal axis of the vehicle, respectively. The angle β_j is defined as

$$\beta_j = \arctan\left(\frac{v_{y,j}}{v_{x,j}}\right), \tag{2-4}$$

where $v_{y,j}$ and $v_{x,j}$ with $j \in \{r, f\}$ denote the lateral and longitudinal velocity components in either the rear or front wheel. The longitudinal component at both wheels is equal to the longitudinal velocity at the center of gravity, since both wheels are located at the vehicle's longitudinal axis. The lateral velocity components depend on the lateral velocity at the center of gravity and the yaw rate, which yields the following expressions for the slip angles:

$$\begin{aligned} \alpha_r &= -\arctan\left(\frac{v_y - L_r\dot{\psi}}{v_x}\right) \approx \frac{v_y - L_r\dot{\psi}}{v_x} \\ \alpha_f &= \delta - \arctan\left(\frac{v_y + L_f\dot{\psi}}{v_x}\right) \approx \delta - \frac{v_y + L_f\dot{\psi}}{v_x}. \end{aligned} \tag{2-5}$$

where $v_{y,i}$ is the lateral velocity and The arctangent could be omitted since the argument is expected to remain within the (low-slip) linear region; therefore it is possible to use the small angle approximation. By substitution of (2-2) and (2-5) into (2-1) the equations of motion for the single track bicycle model become

$$\begin{aligned} \dot{v}_x &= \frac{1}{m}(F_{xr} + F_{xf}) + \dot{\psi}v_y \\ \dot{v}_y &= -\frac{1}{v_x}\left(\frac{C_{\alpha r} + C_{\alpha f}}{m}\right)v_y + \left(\frac{1}{v_x}\left(\frac{C_{\alpha r}L_r - C_{\alpha f}L_f}{m}\right) - v_x\right)\dot{\psi} + \left(\frac{C_{\alpha f}}{m}\right)\delta \\ \ddot{\psi} &= \frac{1}{v_x}\left(\frac{C_{\alpha r}L_r - C_{\alpha f}L_f}{I_z}\right)v_y - \frac{1}{v_x}\left(\frac{C_{\alpha r}L_r^2 + C_{\alpha f}L_f^2}{I_z}\right)\dot{\psi} + \left(\frac{C_{\alpha f}L_f}{I_z}\right)\delta. \end{aligned} \tag{2-6}$$

From (2-6), it can be observed that the lateral and longitudinal dynamics are coupled. Since the focus is to develop a lateral controller for a platooning application, it may be assumed that $F_{xr} + F_{xf}$ is such that v_x remains constant at all times. This is a valid assumption since, v_x is typically held constant by a longitudinal controller in platooning applications. As

a result, v_x becomes a (time-dependent) system parameter instead of a state, and the first equation of motion in (2-6) becomes irrelevant. For this assumption to hold, however, the longitudinal force equilibrium at the tyres should be equal to $F_{xr} + F_{xf} = -m\dot{\psi}v_y$.

Finally, the platooning-ready vehicles available at TNO are equipped with a Park Assist System (PAS) to perform the steering input as commanded by the controller. This PAS is a dynamic system, and has been identified to be a second-order system [32], described by the following equation:

$$\ddot{\delta} = -2\zeta\omega_n\dot{\delta} + \omega_n^2\left(\delta_{ref} - \delta\right), \tag{2-7}$$

where ζ denotes the damping term, ω_n the natural frequency, and δ_{ref} the reference angle at the steering wheel. Combining the previous results, yields the following equations of motion

$$\begin{aligned}
\dot{v}_y &= -\frac{1}{v_x}\left(\frac{C_{\alpha r} + C_{\alpha f}}{m}\right)v_y + \left(\frac{1}{v_x}\left(\frac{C_{\alpha r}L_r - C_{\alpha f}L_f}{m}\right) - v_x\right)\dot{\psi} + \left(\frac{C_{\alpha f}}{m}\right)\delta \\
\ddot{\psi} &= \frac{1}{v_x}\left(\frac{C_{\alpha r}L_r - C_{\alpha f}L_f}{I_z}\right)v_y - \frac{1}{v_x}\left(\frac{C_{\alpha r}L_r^2 + C_{\alpha f}L_f^2}{I_z}\right)\dot{\psi} + \left(\frac{C_{\alpha f}L_f}{I_z}\right)\delta \\
\ddot{\delta} &= -2\zeta\omega_n\dot{\delta} + \omega_n^2\left(\delta_{ref} - \delta\right).
\end{aligned} \tag{2-8}$$

2-2 Error dynamics

In this section, the error dynamics for the path-following problem will be derived. Figure 2-2 provides a schematic illustration of the path following problem, where the path is defined as an arbitrary curve K. Here, three coordinate frames of reference can be distinguished; the space-fixed reference frame $P^O = \{\mathbf{O}, \underline{\vec{e}}^o\}$, the body-fixed frame $P^C = \{\mathbf{C}, \underline{\vec{e}}^c\}$, and the frame $P^S = \{\mathbf{S}, \underline{\vec{e}}^s\}$, where $\mathbf{S}$ is the orthogonal projection of the point $\mathbf{O}$ onto K. Here $\underline{\vec{e}}^j$, $j \in \{o, c, s\}$, represents the coordinate system as described by a set of orthonormal vectors

$$\underline{\vec{e}}^j = \begin{pmatrix} \vec{e}_x^j & \vec{e}_y^j \end{pmatrix}^T. \tag{2-9}$$

The yaw angle ψ is defined as the angle between $\underline{\vec{e}}^o$ and $\underline{\vec{e}}^c$. Furthermore, θ_s is the angle between $\underline{\vec{e}}^o$ and $\underline{\vec{e}}^s$. Two errors can be distinguished: the heading error ψ_e and the lateral error y_e. The heading error is defined as the angular difference between the tangent to K at $\mathbf{S}$, and the heading direction of the vehicle (not to be confused with the difference in orientation)

$$\psi_e = \beta + \psi - \theta_s. \tag{2-10}$$

Here, β denotes the vehicle's side-slip and is defined as $\beta = \arctan\left(\frac{v_y}{v_x}\right)$. Furthermore, the lateral error y_e, describes the shortest distance between $\mathbf{C}$ and K, which is defined as the following dot product

$$y_e = \vec{r}_{c/s} \cdot \vec{e}_y^s, \tag{2-11}$$

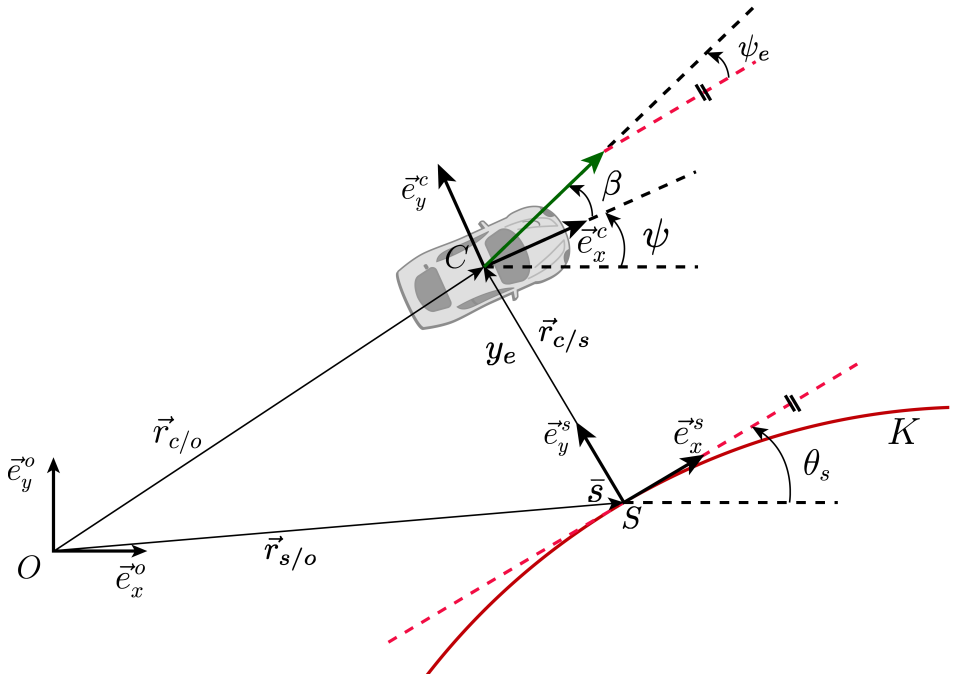

Figure 2-2: Schematic representation of the error dynamics with respect to a reference path.

where $\vec{r}_{c/s}$ denotes the position vector from P^S to P^C. To successfully perform path following, the aim is to reduce the errors such that,

$$\begin{aligned} \lim_{t\to\infty} y_e(t) &= 0 \\ \lim_{t\to\infty} \psi_e(t) &= 0. \end{aligned} \tag{2-12}$$

Hence the dynamics of these errors must be derived. First, the time derivative of the heading error $\dot{\psi}_e$ follows from (2-10) as

$$\begin{aligned} \dot{\psi}_e &= \dot{\beta} + \dot{\psi} - \dot{\theta}_s \\ &= \left(\frac{v_x}{v_x^2 + v_y^2} \dot{v}_y - \frac{v_y}{v_y^2 + v_x^2} \dot{v}_x \right) + \dot{\psi} - \dot{\theta}_s, \end{aligned} \tag{2-13}$$

For motorway platooning conditions, $v_x \gg v_y$ and $\dot{v}_x \approx 0$, therefore (2-13) can be reduced to

$$\dot{\psi}_e = \frac{\dot{v}_y}{v_x} + \dot{\psi} - \dot{\theta}_s, \tag{2-14}$$

where $\dot{\theta}_s$ denotes the rate of change of the road orientation at the path coordinate $\bar{s}$. Substitution of (2-8) into (2-14) yields the dynamics in terms of the system states,

$$\dot{\psi}_e = -\frac{1}{v_x^2}\left(\frac{C_{\alpha r} + C_{\alpha f}}{m}\right) v_y + \frac{1}{v_x^2}\left(\frac{C_{\alpha r} L_r - C_{\alpha f} L_f}{m}\right) \dot{\psi} + \frac{1}{v_x}\left(\frac{C_{\alpha f}}{m}\right) \delta - \dot{\theta}_s. \tag{2-15}$$

For the time derivative of the lateral error y_e one can write

$$\dot{y}_e = \dot{\vec{r}}_{c/s} \cdot \vec{e}_y^s + \vec{r}_{c/s} \cdot \dot{\vec{e}}_y^s. \tag{2-16}$$

By definition P^S only moves in the direction of $\vec{e}_x^s$, hence $\dot{\vec{e}}_y^s = 0$, and thus $\dot{y}_e = \dot{\vec{r}}_{s/c} \cdot \vec{e}_y^s$. Here $\dot{\vec{r}}_{c/s}$ denotes the velocity vector of P^C with respect to P^S, and is defined as

$$\dot{\vec{r}}_{c/s} = \dot{\vec{r}}_{c/o} - \dot{\vec{r}}_{s/o}. \tag{2-17}$$

According to the bicycle model as derived in Appendix A

$$\dot{\vec{r}}_{c/o} = \begin{pmatrix} v_x & v_y \end{pmatrix} \underline{\vec{e}}^c, \tag{2-18}$$

when expressed with respect to P^S yields,

$$\begin{aligned} \dot{\vec{r}}_{c/o} &= \begin{pmatrix} v_x & v_y \end{pmatrix} \underline{\vec{e}}^c \\ &= \begin{pmatrix} v_x & v_y \end{pmatrix} R(\psi - \theta_s)^T \underline{\vec{e}}^s \\ &= \begin{pmatrix} v_x \cos(\psi - \theta_s) - v_y \sin(\psi - \theta_s) & v_x \sin(\psi - \theta_s) + v_y \cos(\psi - \theta_s) \end{pmatrix} \underline{\vec{e}}^s. \end{aligned} \tag{2-19}$$

Herein, $\psi - \theta_s$ denotes the orientation error between the vehicle and road. Moreover $R(\psi - \theta_s)$ denotes the rotation matrix defined as

$$R(\psi - \theta_s) = \begin{pmatrix} \cos(\psi - \theta_s) & -\sin(\psi - \theta_s) \\ \sin(\psi - \theta_s) & \cos(\psi - \theta_s) \end{pmatrix}. \tag{2-20}$$

Furthermore, the following relation at the path coordinate $\bar{s}$ holds:

$$\dot{\vec{r}}_{s/o} = \dot{\bar{s}} \vec{e}_x^s, \tag{2-21}$$

since P^S can only move in the direction of the line defined tangent to K at S, i.e, the direction of $\vec{e}_x^s$. Substitution of (2-19) and (2-21) into (2-17) yields,

$$\dot{\vec{r}}_{c/s} = \begin{pmatrix} v_x \cos(\psi - \theta_s) - v_y \sin(\psi - \theta_s) - \dot{\bar{s}} & v_x \sin(\psi - \theta_s) + v_y \cos(\psi - \theta_s) \end{pmatrix} \underline{\vec{e}}^s. \tag{2-22}$$

With $\dot{y}_e = \dot{\vec{r}}_{c/s} \cdot \vec{e}_y^s$ one obtains

$$\dot{y}_e = v_x \sin(\psi - \theta_s) + v_y \cos(\psi - \theta_s). \tag{2-23}$$

From (2-10), it can be observed that $\psi - \theta_s = \psi_e - \beta$, such that (2-23) can be expressed as

$$\dot{y}_e = v_x \sin(\psi_e - \beta) + v_y \cos(\psi_e - \beta). \tag{2-24}$$

Using the small angle approximation,

$$\begin{aligned} \sin(\psi_e - \beta) &\approx \psi_e - \beta \\ \cos(\psi_e - \beta) &\approx 1 \\ \beta &\approx \frac{v_y}{v_x}, \end{aligned} \tag{2-25}$$

and substituting (2-25) into (2-24) yields,

$$\begin{aligned} \dot{y}_e &\approx v_y + v_x \left(\psi_e - \frac{v_y}{v_x} \right) \\ &= v_x \psi_e. \end{aligned} \tag{2-26}$$

Hereby, all the expressions necessary to describe the error dynamics for the path following problem have been derived. When augmented into a single state vector, these equations of motion can be written in the LTI state-space form, such that the following error model is obtained

$$\begin{pmatrix} \dot{v}_y \\ \ddot{\psi} \\ \dot{y}_e \\ \dot{\psi}_e \\ \ddot{\delta} \end{pmatrix} = \underbrace{\begin{pmatrix} \frac{-1}{v_x}\frac{C_{\alpha r}+C_{\alpha f}}{m} & \frac{1}{v_x}\frac{C_{\alpha r}L_r - C_{\alpha f}L_f}{m} - v_x & 0 & 0 & \frac{C_{\alpha f}}{m} & 0 \\ \frac{1}{v_x}\frac{C_{\alpha r}L_r - C_{\alpha f}L_f}{I_z} & -\frac{1}{v_x}\frac{C_{\alpha r}L_r^2 + C_{\alpha f}L_f^2}{I_z} & 0 & 0 & \frac{C_{\alpha f}L_f}{I_z} & 0 \\ 0 & 0 & 0 & v_x & 0 & 0 \\ \frac{-1}{v_x^2}\frac{C_{\alpha r}+C_{\alpha f}}{m} & \frac{1}{v_x^2}\frac{C_{\alpha r}L_r - C_{\alpha f}L_f}{m} & 0 & 0 & \frac{1}{v_x}\frac{C_{\alpha f}}{m} & 0 \\ 0 & 0 & 0 & 0 & 0 & 1 \\ 0 & 0 & 0 & 0 & -\omega_n^2 & -2\zeta\omega_n \end{pmatrix}}_{A} \begin{pmatrix} v_y \\ \dot{\psi} \\ y_e \\ \psi_e \\ \delta \\ \dot{\delta} \end{pmatrix} + \underbrace{\begin{pmatrix} 0 \\ 0 \\ 0 \\ 0 \\ 0 \\ \omega_n^2 \end{pmatrix}}_{B_1} \delta_{ref} + \underbrace{\begin{pmatrix} 0 \\ 0 \\ 0 \\ -1 \\ 0 \\ 0 \end{pmatrix}}_{B_2} \dot{\theta}_s, \tag{2-27}$$

with state vector

$$x = \begin{pmatrix} v_y & \dot{\psi} & y_e & \psi_e & \delta & \dot{\delta} \end{pmatrix}^T, \tag{2-28}$$

input $u = \delta_{ref}$, and disturbance $d = \dot{\theta}_s$ its compact form is given by:

$$\dot{x}(t) = Ax(t) + B_1 u(t) + B_2 d(t). \tag{2-29}$$

Because of the introduced error states, y_e and ψ_e, a 6^{th}-order system is now obtained, as opposed to the 4^{th}-order system introduced in (2-8). It should be noted that the time dependencies in (2-27) have been omitted for clarity. From (2-27) it can be observed that $\dot{\theta}_s$ acts as a disturbance to the system, and that δ_{ref} is the only input to the system.

2-3 Platoon system model

The error model in (2-27) does not provide an interconnection between the vehicle's dynamics, and the dynamics of its preceding vehicle. To gain insight on how the platoon is connected, a complete system model is needed. Consider to this end a homogeneous platoon consisting of m vehicles. The aim would be for vehicle i to exactly follow the path of its predecessor, vehicle $i-1$. In this section and in the remaining chapters, the subscript i will be added to indicate the vehicle's position within the platoon.

Assuming the reconstructed path will be identical to the path driven by vehicle $i-1$, the rate of change of the road orientation for vehicle i, $\dot{\theta}_{s,i}(t)$, will be equal to the rate of change of the preceding vehicle's heading angle with a time delay Δt, such that

$$\dot{\theta}_{s,i}(t) = \dot{\psi}_{i-1}(t-\Delta t) + \dot{\beta}_{i-1}(t-\Delta t). \tag{2-30}$$

This time delay Δt is approximately the time gap between the vehicles and can be assumed constant during regular platooning conditions. Using $\dot{\beta}_i(t) \approx \frac{\dot{v}_{y,i}(t)}{v_{x,i}(t)}$, and substituting $\dot{v}_{y,i}(t)$ from (2-8), yields

$$\dot{\beta}_{i-1}(t) + \dot{\psi}_{i-1}(t) = -\frac{1}{v_{x,i-1}^2}\left(\frac{C_{\alpha r}+C_{\alpha f}}{m}\right) v_{y,i-1}(t) + \frac{1}{v_{x,i-1}^2}\left(\frac{C_{\alpha r}L_r - C_{\alpha f}L_f}{m}\right)\dot{\psi}_{i-1}(t) + \frac{1}{v_{x,i-1}}\left(\frac{C_{\alpha f}}{m}\right)\delta_{i-1}(t). \tag{2-31}$$

From the expressions in (2-31) and (2-30), the following relation can be obtained

$$\dot{\theta}_{s,i}(t) = -\frac{1}{v_{x,i-1}^2}\left(\frac{C_{\alpha r}+C_{\alpha f}}{m}\right) v_{y,i-1}(t-\Delta t) + \frac{1}{v_{x,i-1}^2}\left(\frac{C_{\alpha r}L_r - C_{\alpha f}L_f}{m}\right)\dot{\psi}_{i-1}(t-\Delta t) + \frac{1}{v_{x,i-1}}\left(\frac{C_{\alpha f}}{m}\right)\delta_{i-1}(t-\Delta t). \tag{2-32}$$

From (2-32), it can be observed that the disturbance $\dot{\theta}_{s,i}$ depends on the states of vehicle $i-1$, which can be expressed in terms of the following output equation,

$$\dot{\theta}_{s,i}(t) = C_t x_{i-1}(t-\Delta t), \tag{2-33}$$

with,

$$C_t = \begin{pmatrix} -\frac{1}{v_{x,i-1}^2}\frac{C_{\alpha r}+C_{\alpha f}}{m} & \frac{1}{v_{x,i-1}^2}\frac{C_{\alpha r}L_r - C_{\alpha f}L_f}{m} & 0 & 0 & \frac{1}{v_{x,i-1}}\frac{C_{\alpha f}}{m} & 0 \end{pmatrix}, \tag{2-34}$$

and x_{i-1} denoting the state vector of vehicle $i-1$. Substituting (2-33) in (2-27), yields

$$\begin{pmatrix} \dot{v}_{y,i}(t) \\ \ddot{\psi}_i(t) \\ \dot{y}_{e,i}(t) \\ \dot{\psi}_{e,i}(t) \\ \ddot{\delta}_i(t) \\ \dddot{\delta}_i(t) \end{pmatrix} = \underbrace{\begin{pmatrix} \frac{-1}{v_{x,i}}\frac{C_{\alpha r}+C_{\alpha f}}{m} & \frac{1}{v_{x,i}}\frac{C_{\alpha r}L_r-C_{\alpha f}L_f}{m} - v_{x,i} & 0 & 0 & \frac{C_{\alpha f}}{m} & 0 \\ \frac{1}{v_{x,i}}\frac{C_{\alpha r}L_r-C_{\alpha f}L_f}{I_z} & -\frac{1}{v_{x,i}}\frac{C_{\alpha r}L_r^2+C_{\alpha f}L_f^2}{I_z} & 0 & 0 & \frac{C_{\alpha f}L_f}{I_z} & 0 \\ 0 & 0 & 0 & v_{x,i} & 0 & 0 \\ \frac{-1}{v_{x,i}^2}\frac{C_{\alpha r}+C_{\alpha f}}{m} & \frac{1}{v_{x,i}^2}\frac{C_{\alpha r}L_r-C_{\alpha f}L_f}{m} & 0 & 0 & \frac{1}{v_{x,i}}\frac{C_{\alpha f}}{m} & 0 \\ 0 & 0 & 0 & 0 & 0 & 1 \\ 0 & 0 & 0 & 0 & -\omega_n^2 & -2\zeta\omega_n \end{pmatrix}}_{A_i} \begin{pmatrix} v_{y,i}(t) \\ \psi_i(t) \\ y_{e,i}(t) \\ \psi_{e,i}(t) \\ \delta_i(t) \\ \dot{\delta}_i(t) \end{pmatrix}$$
$$+ \underbrace{\begin{pmatrix} 0 \\ 0 \\ 0 \\ 0 \\ 0 \\ \omega_n^2 \end{pmatrix}}_{B} \delta_{ref,i}(t) + \underbrace{\begin{pmatrix} 0 & 0 & 0 & 0 & 0 & 0 \\ 0 & 0 & 0 & 0 & 0 & 0 \\ 0 & 0 & 0 & 0 & 0 & 0 \\ \frac{1}{v_{x,i-1}^2}\frac{C_{\alpha r}+C_{\alpha f}}{m} & -\frac{1}{v_{x,i-1}^2}\frac{C_{\alpha r}L_r-C_{\alpha f}L_f}{m} & 0 & 0 & -\frac{1}{v_{x,i-1}}\frac{C_{\alpha f}}{m} & 0 \\ 0 & 0 & 0 & 0 & 0 & 0 \\ 0 & 0 & 0 & 0 & 0 & 0 \end{pmatrix}}_{A_{i-1}} \begin{pmatrix} v_{y,i-1}(t-\Delta t) \\ \dot{\psi}_{i-1}(t-\Delta t) \\ y_{e,i-1}(t-\Delta t) \\ \psi_{e,i-1}(t-\Delta t) \\ \delta_{i-1}(t-\Delta t) \\ \dot{\delta}_{i-1}(t-\Delta t) \end{pmatrix}, \tag{2-35}$$

or in its shorter hand notation

$$\dot{x}_i(t) = A_i x_i(t) + B u_i(t) + A_{i-1} x_{i-1}(t - \Delta t). \tag{2-36}$$

The established interconnection between the vehicles in a platoon will prove to be useful for string stability analysis, as will be further elaborated in Chapter 3.

Chapter 3

Controller Design

Controllers for laterally automated vehicles aim to generate a steering input such that a predefined trajectory can be followed. For safe operation, a platoon equipped with these controllers needs to be string stable in the lateral sense, such that the effect of disturbances will not be amplified. A control design method is proposed such that the string-stability and the path-following requirement are explicitly included in the design process. To do so, the conditions for $\mathcal{L}_2$ string stability in the lateral sense are presented, which motivates the use of an $\mathcal{H}_\infty$ approach for controller synthesis. However, for this to be possible the system introduced in Chapter 2 has to be formulated within this framework. Using the developed framework, one is able to obtain an $\mathcal{L}_2$ string stable platooning strategy.

This chapter is organised as follows. Section 3-1 defines the control objectives for the path-following problem qualitatively. Section 3-2 formulates the string stability problem for path following, and presents the conditions for string stability in the lateral sense. In Section 3-3 the $\mathcal{H}_\infty$ control problem is introduced, upon which Section 3-4 casts the platooning control problem into the $\mathcal{H}_\infty$ framework. The conditions for $\mathcal{L}_2$ string stability in this framework are presented in Section 3-5, such that the actual controller can be designed and synthesised in Sections 3-6 and 3-7, respectively.

3-1 The control objectives

The desired operation of the vehicle is to accurately follow a predefined path. Therefore, the objective is to regulate the vehicle such that it follows a reference path by means of a feedback-feedforward controller. The measurements available for the control of vehicle i are the distance error $y_{e,i}$, the heading error $\psi_{e,i}$, and the rate of change of the road orientation $\dot{\theta}_{s,i}$, as defined in the preceding chapter. The vehicle can be controlled by means of the steering angle at the steering wheel $\delta_{ref,i}$. The synthesised controller should be able to,

1. Asymptotically follow a predefined path, i.e, the path following errors should be reduced

to zero:

$$\begin{aligned} \lim_{t\to\infty} y_{e,i}(t) &= 0 \\ \lim_{t\to\infty} \psi_{e,i}(t) &= 0, \end{aligned} \tag{3-1}$$

2. Guarantee the satisfaction of closed-loop performance specifications, such as disturbance rejection and limitation on the magnitude of the control action;
3. Guarantee string stability a-priori;
4. Ensure the (internal) stability of the closed-loop system.

3-2 String stability

In this section, the definition for $\mathcal{L}_2$ string stability will be discussed. Here a homogeneous platoon of m vehicles, all driving at a constant velocity v_x, is considered. The leading vehicle is human driven and will be identified by index $i = 0$. The remaining platoon members are automated and are equipped with identical steering control systems. This platoon can be formulated as a linear cascaded system of the form:

$$\begin{aligned} \dot{x}_0(t) &= A_r x_0(t) + B_r u_r(t) \\ \dot{x}_i(t) &= A_0 x_i(t) + A_1 x_{i-1}(t-\Delta t) \quad \forall i \in S_m \\ y_i(t) &= C x_i(t) \quad \forall i \in S_m. \end{aligned} \tag{3-2}$$

Here, A_r represents the state matrix of the human driven vehicle, and B_r represents the input matrix to that vehicle, with state vector x_0 defined similarly as x_i. The dynamics of the human driven vehicle are then given by,

$$\begin{pmatrix} \dot{v}_{y,0} \\ \ddot{\psi}_0 \\ \dot{y}_{e,0} \\ \dot{\psi}_{e,0} \\ \dot{\delta}_0 \\ \ddot{\delta}_0 \end{pmatrix} = \underbrace{\begin{pmatrix} \frac{-1}{v_{x,0}}\frac{C_{\alpha r}+C_{\alpha f}}{m} & \frac{1}{v_{x,0}}\frac{C_{\alpha r}L_r - C_{\alpha f}L_f}{m} - v_{x,0} & 0 & 0 & \frac{C_{\alpha f}}{m} & 0 \\ \frac{1}{v_{x,0}}\frac{C_{\alpha r}L_r - C_{\alpha f}L_f}{I_z} & -\frac{1}{v_{x,0}}\frac{C_{\alpha r}L_r^2 + C_{\alpha f}L_f^2}{I_z} & 0 & 0 & \frac{C_{\alpha f}L_f}{I_z} & 0 \\ 0 & 0 & 0 & 0 & 0 & 0 \\ 0 & 0 & 0 & 0 & 0 & 0 \\ 0 & 0 & 0 & 0 & 0 & 1 \\ 0 & 0 & 0 & 0 & -\omega_n^2 & -2\zeta\omega_n \end{pmatrix}}_{A_r} \begin{pmatrix} v_{y,0} \\ \dot{\psi}_0 \\ y_{e,0} \\ \psi_{e,0} \\ \delta_0 \\ \dot{\delta}_0 \end{pmatrix} + \underbrace{\begin{pmatrix} 0 \\ 0 \\ 0 \\ 0 \\ 0 \\ \omega_n^2 \end{pmatrix}}_{B_r} \delta_{ref,0}. \tag{3-3}$$

Moreover, A_0 and A_1 are constant closed-loop system matrices which follow from (2-35) after a state-feedback controller for u_i has been designed, and they depend on the control architecture chosen, in addition C denotes the output matrix. Furthermore, $S_m = \{i \in \mathbb{Z} | \, 1 \leq i \leq m\}$ is the set of all vehicles in a platoon of length $m \in \mathbb{N}$, where $\mathbb{N}$ is the set of all positive integers. Finally, $u_r \in \mathbb{R}^q$ is the external input, $x_i \in \mathbb{R}^n$, $i \in S_m \cup \{0\}$, is the state vector, and $y_i \in \mathbb{R}^l$, $i \in S_m$ is the system output. For a platoon the system states are defined as $x_i^T = \begin{pmatrix} v_{y,i} & \dot{\psi}_i & y_{e,i} & \psi_{e,i} & \delta_i & \dot{\delta}_i & \cdots \end{pmatrix}$, $i \in S_m \cup \{0\}$, indicating possible extension with additional states due to, for example, controller dynamics.

It is possible to assume the time gap Δt to be zero. In Section 3-5 it will be motivated why this assumption does not affect the string stability properties of the system, such that the platoon dynamics of (3-2) can be written in matrix form, yielding

$$\begin{pmatrix} \dot{x}_0 \\ \dot{x}_1 \\ \vdots \\ \dot{x}_m \end{pmatrix} = \begin{pmatrix} A_r & & & O \\ A_1 & A_0 & & \\ & \ddots & \ddots & \\ O & & A_1 & A_0 \end{pmatrix} \begin{pmatrix} x_0 \\ x_1 \\ \vdots \\ x_m \end{pmatrix} + \begin{pmatrix} B_r \\ 0 \\ \vdots \\ 0 \end{pmatrix} u_r. \tag{3-4}$$

In its shorthand notation, the system is given by,

$$\dot{x} = Ax + Bu_r, \tag{3-5}$$

with $x^T = \begin{pmatrix} x_0^T & x_1^T & \cdots & x_m^T \end{pmatrix}$, and their corresponding state and input matrices given by A and B, respectively. The output is defined as, $y_i = C_i x$, $i \in S_m$ with an output matrix of choice, $C_i = \begin{pmatrix} 0_{l\times n(i-1)} & C & 0_{l\times n(m-i)} \end{pmatrix}$. In the Laplace domain, this model is defined as follows:

$$y_i(s) = P_i(s)u_r(s) + O_i(s)x(0),\ i \in S_m, \tag{3-6}$$

where, $x(0) \in \mathbb{R}^{(m+1)n}$ is the initial condition, $P_i(s)$ denotes the complementary sensitivity transfer function, and $O_i(s)$ represents the initial condition transfer function. $P_i(s)$ and $O_i(s)$ are given as

$$\begin{aligned} P_i(s) &= C_i(sI - A)^{-1}B \\ O_i(s) &= C_i(sI - A)^{-1}. \end{aligned} \tag{3-7}$$

This notation allows for the use of the following theorem to define the string stability conditions [1].

Theorem 1. [1] *Let* (3-5) *represent a linear unidirectionally-interconnected system of which the input-output behaviour is described by* (3-6) *and* (3-7)*. Assume that the pair* (C_i, A) *is such that unstable and marginally stable modes are unobservable and that* $P_i(s)$ *is square and nonsingular for all* $i \in \mathbb{N}$*. Then the system* (3-5)*, is* $\mathcal{L}_2$ *string stable if*

1. $\|P_1(s)\|_{\mathcal{H}_\infty} < \infty$ *and*
2. $\|\Gamma_i(s)\|_{\mathcal{H}_\infty} \leq 1, \quad \forall i \in \mathbb{N} \setminus \{1\}$,

with the string stability complementary sensitivity function, $\Gamma_i(s)$*, given by*

$$\Gamma_i(s) = P_i(s)P_{i-1}^{-1}(s), \tag{3-8}$$

assuming $P_i(s)$ *is nonsingular for all* i*, thus guaranteeing the existence of* $P_{i-1}^{-1}(s)$*. Moreover, the system is strictly* $\mathcal{L}_2$ *string stable if and only if conditions 1 and 2 hold.*

For the proof, the reader is referred to [1]. For platooning, one is interested in the propagation of the disturbance in upstream direction of the interconnected vehicles. In the lateral sense this is described by the relation between $\dot{\beta}_i(t)+\dot{\psi}_i(t)$ and $\dot{\beta}_{i-1}(t)+\dot{\psi}_{i-1}(t)$ for their respective vehicles. Hence, the output matrices C_i and C_{i-1} should be defined such that $P_i(s)$ and $P_{i-1}(s)$ are the transfer functions from the input to the states of interest, as a result the string stability complementary sensitivity function $\Gamma_i(s)$ can be defined. These conditions will be formulated within the $\mathcal{H}_\infty$ control framework, such that lateral string stability can be assessed and guaranteed.

3-3 The $\mathcal{H}_\infty$ control problem

In this section, the general $\mathcal{H}_\infty$ control configuration will be described, after which the system will be cast into this framework. The inputs and outputs to this framework play an important role in fulfilling the control objectives, and should be selected accordingly.

First, a general method of formulating control problems in the $\mathcal{H}_\infty$ framework is provided. This general formulation requires the system to be configured as presented in Figure 3-1, where $\mathcal{P}$ and $\mathcal{K}$ represent the generalised plant and generalised controller, respectively. Moreover, d represents the (weighted) exogenous inputs, u indicates the control signals, z denotes the (weighted) exogenous outputs, and v describes the controller inputs or the sensed outputs. The generalised plant $\mathcal{P}$ does not include the controller, and represents the transfer function from $\begin{pmatrix} d & u \end{pmatrix}^T$ to $\begin{pmatrix} z & v \end{pmatrix}^T$, such that

$$\begin{pmatrix} z \\ v \end{pmatrix} = \underbrace{\begin{pmatrix} \mathcal{P}_{11} & \mathcal{P}_{12} \\ \mathcal{P}_{21} & \mathcal{P}_{22} \end{pmatrix}}_{\mathcal{P}} \begin{pmatrix} d \\ u \end{pmatrix}. \tag{3-9}$$

The size of the matrices $\mathcal{P}_{ij}, i, j \in \{1, 2\}$, depends on the dimensions of their corresponding inputs and outputs. In the generalised feedback configuration of Figure 3-1, the controller $\mathcal{K}$ is separated from the generalised plant $\mathcal{P}$. This is useful for controller design, as the objective is to minimise the $\mathcal{H}_\infty$ norm from d to z. Qualitatively, this means that one needs to find a controller $\mathcal{K}$, which uses the measurements v, to generate a control signal u, such that the influences of d on z are minimised.

To obtain the closed-loop system, the controller $\mathcal{K}$ can be absorbed into the control structure, such that the controlled system N is obtained, i.e,

$$z = Nd, \tag{3-10}$$

where N is a function of $\mathcal{K}$. Using the partitioning of $\mathcal{P}$ in Equation (3-9), and the controller equation,

$$u = \mathcal{K}v \tag{3-11}$$

one obtains through substitution,

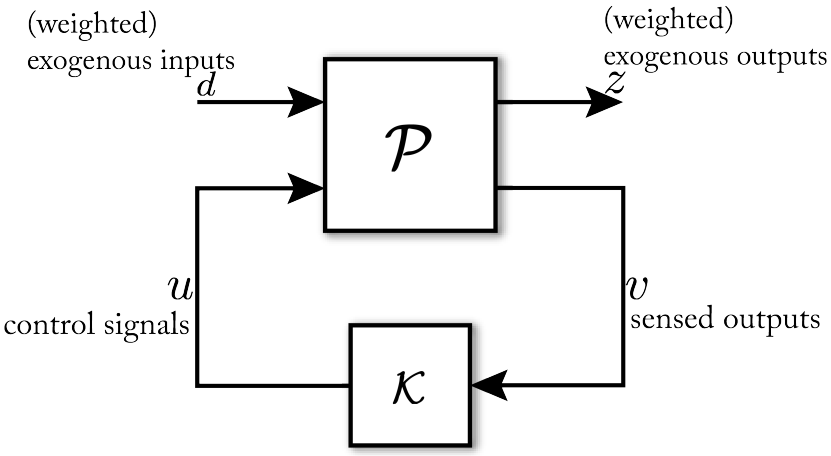

Figure 3-1: General control configuration.

$$N = \mathcal{P}_{11} + \mathcal{P}_{12}\mathcal{K}(I - \mathcal{P}_{22}\mathcal{K})^{-1}\mathcal{P}_{21} \triangleq F_l(\mathcal{P}, \mathcal{K}). \tag{3-12}$$

Here $F_l(\mathcal{P}, \mathcal{K})$ denotes the lower Linear Fractional Transformation (LFT) of $\mathcal{P}$ with $\mathcal{K}$ as the parameter. To obtain a controller $\mathcal{K}$, the following $\mathcal{H}_\infty$ optimisation problem has to be solved:

$$\mathcal{K} = \arg\min_{\mathcal{K}} \|N(\mathcal{K})\|_\infty , \tag{3-13}$$

where $\mathcal{K}$ is an internally stabilising controller. A system is said to be internally stable if none of its components contain hidden or unstable modes. Furthermore, the injection of any bounded external inputs results in a bounded external output. This means that the controller does not cancel any unstable or marginally stable plant poles.

One of the most important properties of the generalised plant description, from a control point of view, is that input and output weights can be included in $\mathcal{P}$, such that the plant will be as illustrated in Figure 3-2. Here $\widetilde{\mathcal{P}}$ represents the generalised plant without any weighting applied, furthermore W_z and W_d represent the input and output weights, respectively. The use of these weights means that weighted inputs $\left(\widetilde{d} = W_d d\right)$, and weighted outputs $(z = W_z \widetilde{z})$ are considered. The weights W_d and W_z are typically frequency dependent, and are used to shape the behaviour of the outputs z to the disturbance d, such that predefined control objectives can be achieved.

3-3-1 Adopting the model to the $\mathcal{H}_\infty$framework

The $\mathcal{H}_\infty$-control framework makes use of the frequency domain descriptions, as it allows for insightful analysis using simple frequency domain tools. Hence a frequency domain description of the system will be adopted. Typically, for a system description in the frequency domain, $G(s)$ will represent the transfer function from the input u to the output y, and in the presence of a disturbance d, $G_d(s)$ will describe the effect of d on y, yielding,

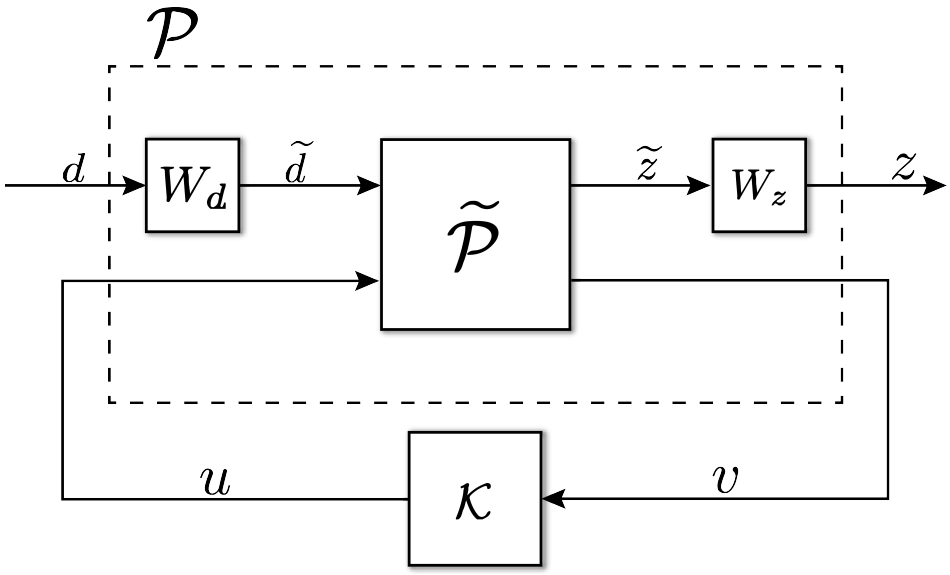

Figure 3-2: Weighted general control configuration.

$$y(s) = G(s)u(s) + G_d(s)d(s). \tag{3-14}$$

The expression in (3-14) takes advantage of the superposition principle for linear systems, i.e., a change in y can be found through summation of the independent effects of u and d.

For the path-following objective, the aim is to reduce the lateral and heading errors for a vehicle i, $y_{e,i}$ and $\psi_{e,i}$ respectively, to zero. These states, therefore, represent the outputs of interest for the control problem. For the control problem, the error model of (2-27) will be used, since all the necessary states are present. To extract these states, the output matrix C is defined as

$$C = \begin{pmatrix} 0 & 0 & 1 & 0 & 0 & 0 \\ 0 & 0 & 0 & 1 & 0 & 0 \end{pmatrix}. \tag{3-15}$$

In the frequency domain, the open-loop dynamics of vehicle i are then given by

$$\begin{pmatrix} y_{e,i} \\ \psi_{e,i} \end{pmatrix} := \begin{pmatrix} G(s) & G_d(s) \end{pmatrix} \begin{pmatrix} \delta_{ref,i} \\ \dot{\theta}_{s,i} \end{pmatrix}, \tag{3-16}$$

with $G(s)$ and $G_d(s)$ denoting the transfer functions from the input $\delta_{ref,i}$, and the disturbance $\dot{\theta}_{s,i}$ to the output $\begin{pmatrix} y_{e,i} & \psi_{e,i} \end{pmatrix}^T$, respectively. The transfer matrices $G(s)$ and $G_d(s)$ are described by,

$$\begin{aligned} G(s) &= C(sI - A)^{-1}B_1 \\ G_d(s) &= C(sI - A)^{-1}B_2, \end{aligned} \tag{3-17}$$

where $B_1 = \begin{pmatrix} 0 & 0 & 0 & 0 & 0 & \omega_n^2 \end{pmatrix}^T$, $B_2 = \begin{pmatrix} 0 & 0 & 0 & -1 & 0 & 0 \end{pmatrix}^T$, and A is as defined in (2-27). The dynamics of (3-16) can be written in the form of (3-14) such that,

$$y_i(s) = G(s)u_i(s) + G_d(s)d_i(s) \tag{3-18}$$

with $y_i(s)$ being the output $\begin{pmatrix} y_{e,i} & \psi_{e,i} \end{pmatrix}^T$, $u_i(s)$ being the input $\delta_{ref,i}$, and $d_i(s) = \dot{\theta}_{s,i}$. The model of (3-18) is not enough to describe a controlled vehicle in a platoon, hence in the next section the platoon model will be derived.

The open-loop system described in (3-16), has six poles. Two of which are due to the vehicle's dynamics. In general vehicles are understeered and stable, hence these poles will be confined to the left-half plane. Moreover, there are two poles at the origin due to the error model, as a result the system is marginally stable. The last two pole are due to the second-order steering dynamics, and are also located in the left-half plane. It should be noted that the location of the poles related to vehicle dynamics will change with the longitudinal velocity, since the system in (3-16) is linear parameter varying. Finally, the system is both controllable and observable.

3-4 The platoon model

In this section, the frequency domain description of a controlled vehicle in a platoon is provided. In Section 2-3, it was established that there is an interconnection between the preceding and the following vehicle through the following relation $\dot{\theta}_{s,i}(t) = \dot{\beta}_{i-1}(t - \Delta t) + \dot{\psi}_{i-1}(t - \Delta t)$. This interconnection, which is present in the system model of (2-35), is not explicitly defined in the error model of (2-27), therefore an equivalent representation is desired.

In (2-31), the rate of change of the heading angle was described in terms of its own states. To this end, let $\dot{\beta}_i + \dot{\psi}_i$ be denoted by q_i. In the frequency domain this yields

$$q_i(s) = G_t(s)\delta_{ref,i}(s). \tag{3-19}$$

From (2-27) it can be observed that $\dot{\theta}_{s,i}$ only affects the error states $y_{e,i}$ and $\psi_{e,i}$. Since (2-31) does not depend on the error states, q_i will not depend on $\dot{\theta}_{s,i}$. $G_t(s)$ is then given by

$$G_t(s) = C_t \left(sI - A\right)^{-1} B_1, \tag{3-20}$$

with the output matrix C_t defined as

$$C_t = \begin{pmatrix} -\frac{1}{v_{x,i}^2}\frac{C_{\alpha r}+C_{\alpha f}}{m}, & \frac{1}{v_{x,i}^2}\frac{C_{\alpha r}L_r - C_{\alpha f}L_f}{m}, & 0, & 0, & \frac{1}{v_{x,i}}\frac{C_{\alpha f}}{m}, & 0 \end{pmatrix}. \tag{3-21}$$

Moreover A and B_1 are identically defined as for (3-17). The disturbance term $d_i(s)$ of (3-18) is then given by

$$d_i(s) = D(s)q_{i-1}(s). \tag{3-22}$$

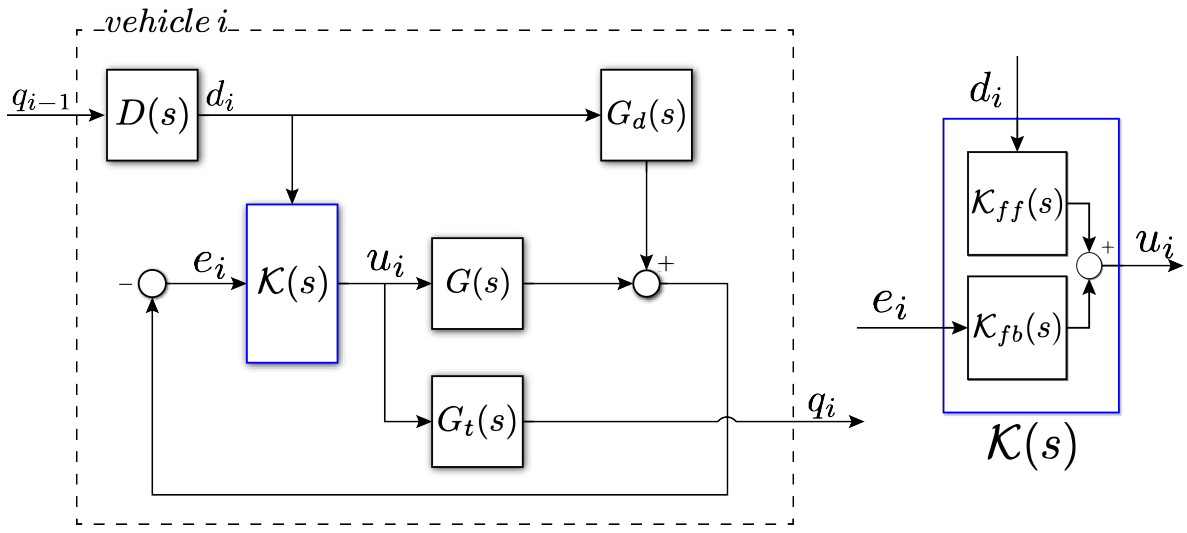

Figure 3-3: Representation of controlled vehicle i within a platoon.

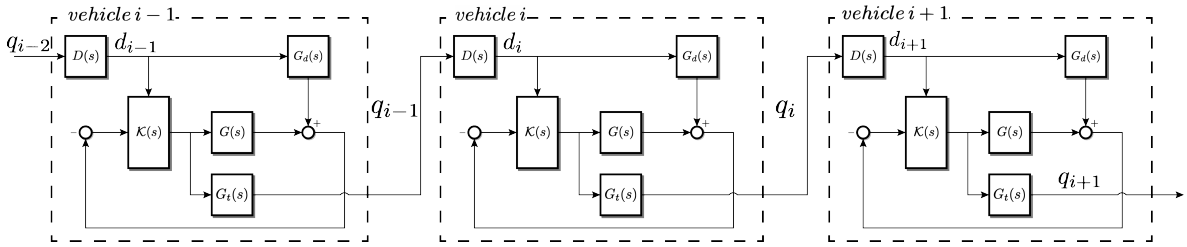

Figure 3-4: Illustration of a homogeneous platoon model representation within the presented control framework.

where $D(s)$ denotes the delay induced by the time gap Δt and is defined as,

$$D(s) = e^{-\Delta t s}. \tag{3-23}$$

Now that the interconnection has been established, the frequency-domain description for a controlled vehicle in a platoon is as depicted by the block diagram of Figure 3-3. Where $\mathcal{K}(s) = \begin{pmatrix} \mathcal{K}_{ff}(s) & \mathcal{K}_{fb}(s) \end{pmatrix}$ represents a general control structure, which includes a feedforward and a feedback controller. The input signal to the feedforward controller $\mathcal{K}_{ff}(s)$ is $d_i(s)$, since the aim is to reduce the errors to zero, $e_i = -y_i$, is the input to the feedback controller $\mathcal{K}_{fb}(s)$.

The diagram illustrates the dynamics of a controlled vehicle i within a platoon, where the disturbance d_i is obtained from the delayed signal q_{i-1} of the preceding vehicle, and q_i is sent to the following vehicle. In a homogeneous platoon, these inputs and outputs will be connected to the identical preceding and following vehicles, respectively, which yields the platoon model as depicted in Figure 3-4.

3-5 Lateral string stability

In this section, the conditions for lateral string stability within the presented platoon model will be given. From Theorem 1, it is known that $\mathcal{H}_\infty$-norm of the transfer function from the "disturbance" output q_{i-1} of the interconnected subsystem $i-1$ to the "disturbance" output q_i of subsystem i, should be investigated to assess string stability. From the platoon model depicted in Figure 3-4, it can be observed that the system contains the following input/output relation between the disturbances q_{i-1} and q_i

$$q_i = \underbrace{G_t \left((1 + \mathcal{K}_{fb} G)^{-1} \mathcal{K}_{ff} - \mathcal{K}_{fb} \left(I + G\mathcal{K}_{fb} \right)^{-1} G_d \right)}_{\Gamma} D q_{i-1}, \tag{3-24}$$

where the Laplace variable s has been omitted for clarity. $\Gamma(s)$ denotes the string stability complementary sensitivity function, and is equivalent to the string stability condition discussed in Theorem 1. For the system to be $\mathcal{L}_2$ string stable, the following condition has to hold:

$$\begin{aligned} \|\Gamma(s)\|_{\mathcal{H}_\infty} &= \left\| \frac{q_i(s)}{D(s) q_{i-1}(s)} \right\|_{\mathcal{H}_\infty} \\ &= \left| \frac{1}{D(s)} \right| \left\| \frac{q_i(s)}{q_{i-1}(s)} \right\|_{\mathcal{H}_\infty} \\ &= \left\| \frac{q_i(s)}{q_{i-1}(s)} \right\|_{\mathcal{H}_\infty} \leq 1. \end{aligned} \tag{3-25}$$

Since $\left| \frac{1}{D(s)} \right| = \left| \frac{1}{e^{-\Delta t s}} \right| = 1$, the influence of the delay on the string stability complementary sensitivity function cancels out, hence it can be concluded that the time delay Δt has no influence on the string stability of the platoon. Therefore, it is valid to assume that $D(s)$ in Figure 3-3 and in Γ can be omitted for controller design and string-stability analysis. As a result the disturbances can be defined as, $d_i(s) = q_{i-1}(s)$ and $d_{i+1}(s) = q_i(s)$, which yields the following string stability condition

$$\|\Gamma(s)\|_{\mathcal{H}_\infty} = \left\| \frac{d_{i+1}(s)}{d_i(s)} \right\|_{\mathcal{H}_\infty} \leq 1. \tag{3-26}$$

This only holds if the controller is distributed, as will be the case in this work. However, if it is desired to design a single controller for the entire platoon, the delays can no longer be neglected. Furthermore, it should be noted that for Γ the index i has been omitted, since for a homogeneous platoon the block diagram of Figure 3-3 holds for all vehicles, meaning that the controller will be independent of i.

3-6 Controller design

In order to support controller design, and to satisfy performance specifications, the weighted outputs z_i, with $i \in \{1, 2, 3\}$, are introduced to the closed-loop system of Figure 3-3 and the

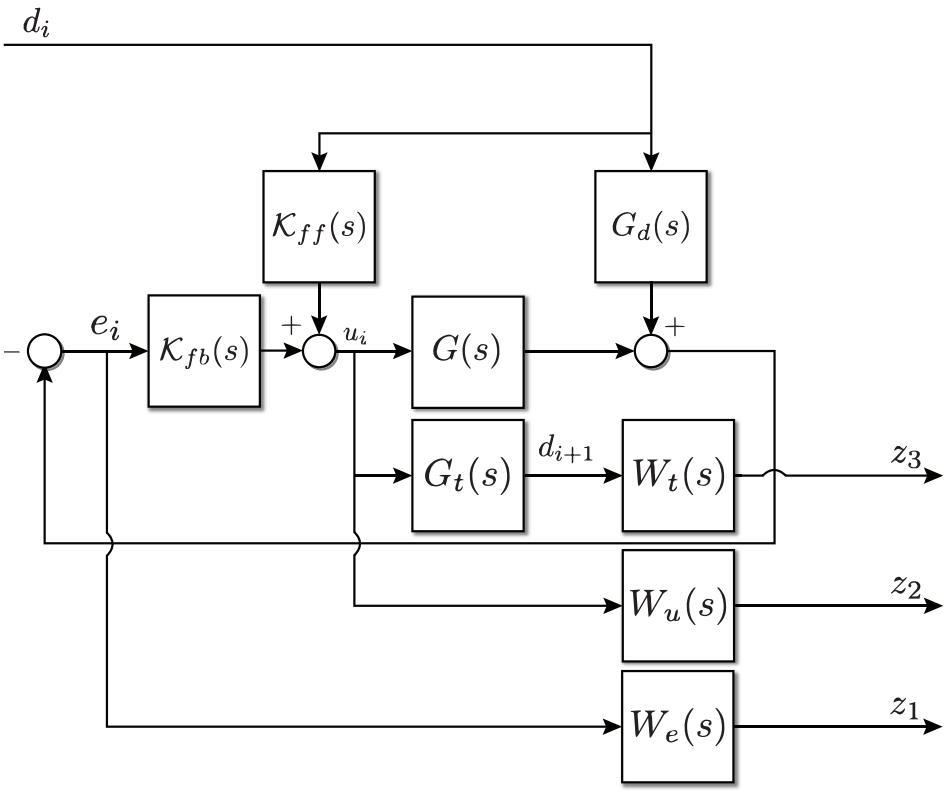

Figure 3-5: Block diagram of the weighted closed-loop system.

delay $D(s)$ is disregarded, yielding the system in Figure 3-5. Here, the output z_1 is defined as

$$z_1(s) = -W_e(s)\widetilde{S}_o(s)d_i(s), \tag{3-27}$$

with,

$$\widetilde{S}_o(s) = S_o(s)\left(G(s)\mathcal{K}_{ff}(s) + G_d(s)\right), \tag{3-28}$$

which denotes the transfer function from the disturbance d_i to the error e_i. Here,

$$S_o(s) = \left(I + G(s)\mathcal{K}_{fb}(s)\right)^{-1}, \tag{3-29}$$

is the output sensitivity. With z_1 as a weighted output, the weighting filter $W_e(s)$ can be used to shape $\widetilde{S}_o$, such that the path-following and disturbance rejection objectives stated in Section 3-1 can be met. The second output z_2 is defined as:

$$z_2 = W_u S_{\mathcal{K}} d_i. \tag{3-30}$$

Here,

$$S_{\mathcal{K}}(s) = S_i(s)\mathcal{K}_{ff}(s) - \mathcal{K}_{fb}(s)S_o(s)G_d(s), \tag{3-31}$$

denotes the transfer function from the disturbance d_i to the input u_i. With,

$$S_i(s) = \left(1 + \mathcal{K}_{fb}(s)G(s)\right)^{-1}, \tag{3-32}$$

denoting the input sensitivity. Choosing z_2 allows one to impose a bound on the magnitude of $S_{\mathcal{K}}$, by means of the weight W_u. In this way, it is possible to restrict the magnitude of u_i, if need be. Finally, the third output of the system z_3 is defined as

$$z_3 = W_t \Gamma d_i. \tag{3-33}$$

By including z_3 as an output it is thus possible to shape Γ by means of the weighting filter W_t, such that string stability can be guaranteed a-priori. It should be noted that by choosing the signals z_1 and z_2 (for e_i and u_i) as weighted outputs of the generalised plant, it is possible to guarantee internal stability [33].

With these weighted outputs, the generalised plant $\mathcal{P}$ is defined as

$$\begin{pmatrix} z_1 \\ z_2 \\ z_3 \\ d_i \\ e_i \end{pmatrix} = \underbrace{\begin{pmatrix} W_e(s) & 0 & 0 & 0 & 0 \\ 0 & W_u(s) & 0 & 0 & 0 \\ 0 & 0 & W_t(s) & 0 & 0 \\ 0 & 0 & 0 & I & 0 \\ 0 & 0 & 0 & 0 & I \end{pmatrix} \widetilde{\mathcal{P}}}_{\mathcal{P}} \begin{pmatrix} d_i \\ u_i \end{pmatrix}, \tag{3-34}$$

with,

$$\widetilde{\mathcal{P}} = \left(\begin{array}{c|c} -G_d(s) & -G(s) \\ 0 & I \\ 0 & G_t(s) \\ \hline I & 0 \\ -G_d(s) & -G(s) \end{array}\right). \tag{3-35}$$

Here it can be observed that the output vector indeed contains the weighted exogenous outputs z_i with $i \in \{1, 2, 3\}$. Moreover, d_i and e_i are the sensed outputs, used for the feedforward and the feedback controller. Furthermore, the exogenous input, and the control signal are d_i and u_i, respectively.

With $\mathcal{P}$ defined, it is now possible to state the mixed sensitivity control problem. The aim for this mixed sensitivity control problem is to compute a stabilising controller $\mathcal{K}(s) = \begin{pmatrix} \mathcal{K}_{ff}(s) & \mathcal{K}_{fb}(s) \end{pmatrix}$, such that $\|N(s)\|_{\mathcal{H}_\infty}$ is minimised. Here, the control law is defined as

$$u_i(s) = \begin{pmatrix} \mathcal{K}_{ff}(s) & \mathcal{K}_{fb}(s) \end{pmatrix} \begin{pmatrix} d_i(s) \\ e_i(s) \end{pmatrix}, \tag{3-36}$$

and $z = Nd_i$, with $N = F_l(\mathcal{P}, \mathcal{K})$, is expressed as

$$\begin{pmatrix} z_1 \\ z_2 \\ z_3 \end{pmatrix} = \underbrace{\begin{pmatrix} -W_e(s)\widetilde{S}_o(s) \\ W_u(s)S_{\mathcal{K}}(s) \\ W_t(s)\Gamma(s) \end{pmatrix}}_{N} d_i. \tag{3-37}$$

Here, it can be observed that indeed $N(s)$ contains all the aforementioned transfer functions. If $\|N(s)\|_{\mathcal{H}_\infty} = \gamma$, it follows that

$$\|N(s)\|_{\mathcal{H}_\infty} = \gamma \Rightarrow \|W_t(s)\Gamma(s)\|_{\mathcal{H}_\infty} \leq \gamma. \tag{3-38}$$

For steady-state driving, the vehicle states of vehicles i and vehicles $i-1$ should be identical. Which implies

$$\lim_{\omega \to 0} |\Gamma(j\omega)| = 1 \Rightarrow \|\Gamma(s)\|_{\mathcal{H}_\infty} \geq 1. \tag{3-39}$$

According to the condition derived in (3-25) string stability is achieved for any value of $\gamma \leq 1$. However since at lower frequencies Γ can not be smaller than 1, it can be concluded that string stability is obtained if,

$$\|N(s)\|_{\mathcal{H}_\infty} = 1, \tag{3-40}$$

provided $W_t(s)$ is designed such that the string-stability condition is enforced. As a result the objective of the $\mathcal{H}_\infty$ control problem will be to obtain a closed-loop system with $\|N(s)\|_{\mathcal{H}_\infty} = 1$, with the weighting filters designed accordingly.

3-7 Weighting filter design

In this section, the weighting filters introduced in Section 3-6 will be designed, such that the control objectives can be satisfied. For string-stable platooning, the system response should be damped, which can be achieved by penalising the heading error $\psi_{e,i}$ [17]. At the same time the lateral error $y_{e,i}$ should be reduced to zero. Large controller gains on $y_{e,i}$ can induce oscillatory behaviour, thereby causing string instability. However, having small controller gains combined with large damping action will yield steady-state errors. Therefore, a trade-off between damping and having a steady state error is required. With this in mind the following controller objectives have been determined:

- The vehicle should be able to perform a worst-case lane-change manoeuvre, i.e. it should be able to follow a road-profile with a magnitude of approximately 3 deg s^{-1} and a period of 5 s (frequency of 0.2 Hz) at a design velocity of 20 m s^{-1};
- A maximum allowable steady-state error of 15 cm [34] (approximately tyre width);
- Guarantee strict string stability for the chosen nominal speed.

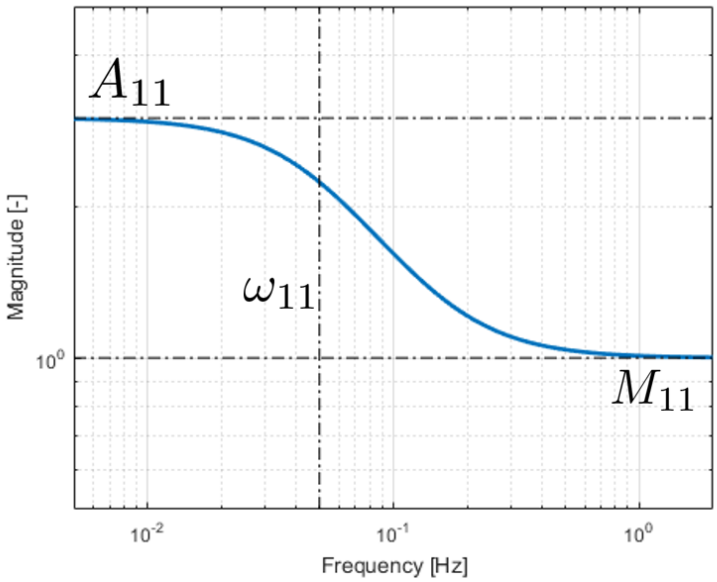

Figure 3-6: Inverse of the weight $|w_{e,11}|$.

The weighting filters will be designed specifically such that these objectives are met. From Section 3-6 it is known that $W_e(s)$ is used to shape $\widetilde{S}_o$, which determines the disturbance rejection properties of the system, and thus can be used to meet the path-following requirement. This filter is defined as,

$$W_e(s) = \begin{pmatrix} w_{e,11} & 0 \\ 0 & w_{e,22} \end{pmatrix} = \begin{pmatrix} \frac{\frac{s}{M_{11}}+\omega_{11}}{s+\omega_{11}A_{11}} & 0 \\ 0 & w_{e,22} \end{pmatrix}, \tag{3-41}$$

with $w_{e,11}$ acting on $y_{e,i}$ and $w_{e,22}$ acting on $\psi_{e,i}$. The average turn radius on Dutch motorways is approximately 600 m [35], combined with driving speeds ranging from 20-30 $\mathrm{m\,s^{-1}}$ yields a maximum expected angular velocity of the road equal to $\dot{\theta}_i = 0.05\,\mathrm{rad\,s^{-1}}$. A maximum steady-state error of 15 cm corresponds to a three times amplification of this value, hence $A_{11} = 3$. Furthermore, $M_{11} = 1$ and ω_{11} was chosen to be $0.05 \cdot 2 \cdot \pi$, such that disturbances higher than ω_{11} are rejected. In this way, the worst-case lane-change manoeuvre at 0.2 Hz can be performed. The effect of these parameters on the shape of the inverse of $w_{e,11}$ is illustrated in Figure 3-6.

As stated earlier, applying a control action on the heading error $\psi_{e,i}$ has been known to increase the overall damping behaviour of the system; too much damping however would result in high derivative control actions at the higher frequencies. This would be undesired in practice as it would result in the system being very sensitive to high frequency noise. Moreover, penalising the heading error too much can result in the system becoming unstable [17]. To obtain adequate damping, such that string stability can be obtained, it was determined that $w_{e,22} = 20$.

Finally, since the steering dynamics are included in the system model, it is not required to apply a frequency-dependent weight for $W_u(s)$, hence $W_u(s)$ is a static gain with $W_u = 0.01$.

Table 3-1: Parameters for TNO Carlab.

Parameter	Value
L_r	$1.6\,\mathrm{m}$
L_f	$1.1\,\mathrm{m}$
$C_{\alpha r}$	$0.143\,\mathrm{MN\,rad^{-1}}$
$C_{\alpha f}$	$0.117\,\mathrm{MN\,rad^{-1}}$
m	$1650\,\mathrm{kg}$
I_z	$2900\,\mathrm{kg\,m^2}$
v_x	$20\,\mathrm{m\,s^{-1}}$
ω_n	$17.5\,\mathrm{rad\,s^{-1}}$
ζ	0.7 [-]

For $W_t(s)$, a static gain was selected equal to 1, as it is desired for $\|\Gamma\|_{\mathcal{H}_\infty} \leq 1$. The controller was synthesised for the Toyota Prius available at TNO, with parameters presented in Table 3-1.

The $\mathcal{H}_\infty$ procedure yields a 8^{th}-order state-space model controller. The order of this controller is reduced by removing the states associated with small Hankel singular values, yielding an expression of $\mathcal{K}(s)$ as a transfer function. Furthermore, a balanced order reduction is applied, such that poles and zeros outside the frequency region of interest are removed, yielding a fourth-order controller given by,

$$\begin{aligned}
\mathcal{K}_{ff}(s) &= \frac{0.031604(s+1.02\cdot10^7)(s+5.649)(s^2+44.6s+864.3)}{(s+319.1)(s+22.44)(s^2+1923s+1.072\cdot10^6)} \\
\mathcal{K}_{fb,y_e}(s) &= \frac{-0.13066(s-2.558\cdot10^5)(s+432.7)(s+36.02)(s+0.176)}{(s^2+345.7s+3.56\cdot10^4)(s^2+1304s+5.272\cdot10^5)} \\
\mathcal{K}_{fb,\psi_e}(s) &= \frac{-0.0073328(s-1.44\cdot10^6)(s+427.4)(s+35.48)(s+3.762)}{(s^2+345.7s+3.56\cdot10^4)(s^2+1304s+5.272\cdot10^5)}.
\end{aligned} \tag{3-42}$$

The subscripts y_e and ψ_e for the feedback controller denote which error the sub-controller acts on. This controller realises an internally stable system, as a-posteriori inspection of the closed-loop system reveals that the controller does not cancel any marginally stable poles, furthermore, $\|N\|_{\mathcal{H}_\infty} = 1.0039 \approx 1$. The $\mathcal{H}_\infty$ norm of N not being exactly equal to 1 is caused by $\lim_{\omega\to0}|\Gamma(j\omega)| = 1$ imposing a lower limit on $\|N\|_{\mathcal{H}_\infty}$, thereby leaving no margin for numerical imprecisions. However, inspection of the individual transfer functions reveals that all system requirements have been met, including $\mathcal{L}_2$ string stability. Figure 3-7 shows the controller magnitudes $|\mathcal{K}_{fb}(s)|$, where it can be noticed that around $0.01\,\mathrm{Hz}$ for $\mathcal{K}_{fb,y_e}(s)$ and $0.2\,\mathrm{Hz}$ for $\mathcal{K}_{fb,\psi_e}(s)$ the controller exhibits a differential action.

It can also observed that the steady-state gain of the feed-forward controller $\mathcal{K}_{ff}(0) = 0.2038$. This is equal to the steady-state gain $|G_t^{-1}(0)|$, where G_t is the transfer function from $\delta_{ref,i}$ to d_{i+1}. In the remaining frequency range, the feed-forward controller is approximately equal to a proper realisation of the inverse dynamics of $G_t^{-1}(s)$.

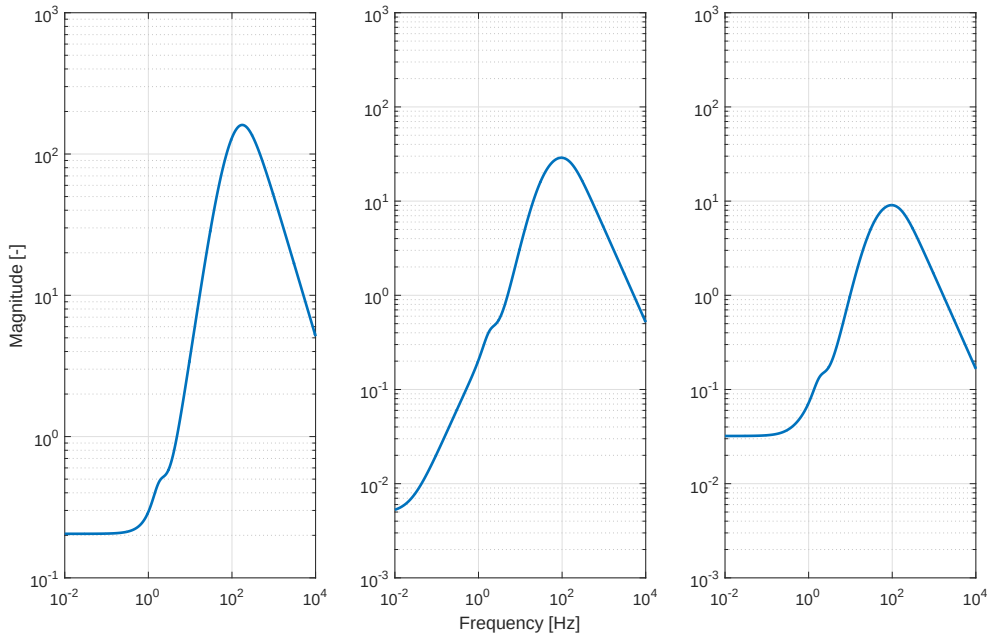

Figure 3-7: Frequency responses for the designed controller, from left to right $|\mathcal{K}_{ff}(j\omega)|$, $|\mathcal{K}_{fb,y_e}(j\omega)|$, $|\mathcal{K}_{fb,\psi_e}(j\omega)|$.

Chapter 4

Robustness and string stability analysis

In Chapter 3, a control framework for string-stable platooning based on path-following was introduced. This framework, in turn, was used to synthesise a controller using $\mathcal{H}_\infty$ optimal control, where the desired performance objectives were imposed through frequency-dependent weighting filters. In this chapter, the performance of the designed controller is assessed, by verifying that the sensitivity functions of interest satisfy the imposed constraints. All real systems will have a certain degree of uncertainty, which could either be parametric or dynamic in nature. For instance, parametric uncertainty can be caused by parameters in the model which are only known approximately or have been determined inaccurately. Dynamic uncertainty, on the other hand, can be caused by neglected dynamics. To assess the performance in the presence of these uncertainties, a $\mathcal{H}_\infty$ frequency-domain approach will be used. In this analysis, one is interested in how the path-following and the string-stability objectives are affected.

Moreover, a comparative analysis will be performed between the controller currently implemented at TNO, and the controller designed in Chapter 3. The lateral controller designed at TNO is also designed for path following, albeit with a slightly different error model, and has velocity-dependent gains. For both controllers, a response to an initial condition error will be considered, such that a better understanding of the difference in controller behaviour is obtained.

This chapter is organised as follows. First, Section 4-1 will provide a frequency-domain analysis of the controller designed in Chapter 3. In Section 4-2, the robustness of the controller will be determined against both parametric and dynamic uncertainties, which are caused by inaccurate parameter estimation and simplifications made during modelling. In Section 4-3, the state-feedback lateral controller, developed at TNO, will be introduced, after which the results of the time-domain simulations regarding the transient response and string stability performance will be given in Sections 4-4 and 4-5, respectively. Finally, this chapter will be concluded with a discussion.

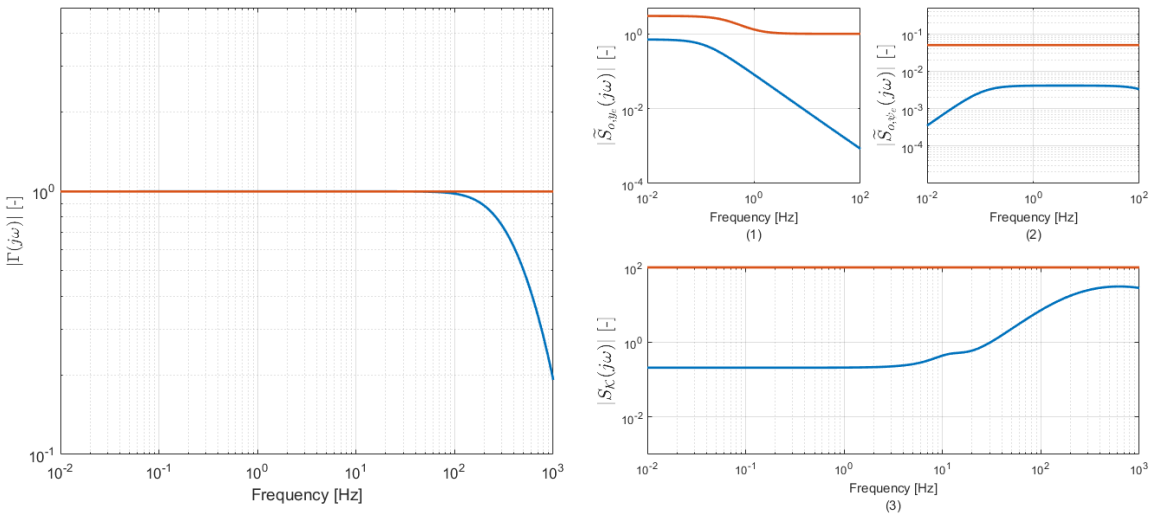

(a) **(b)**

Figure 4-1: Bode diagrams of the string stability complementary sensitivity function $|\Gamma(j\omega)|$ (blue) and its inverse weight $|W_t^{-1}|$ (orange) (a), output sensitivity functions $|\widetilde{S}_{o,y_e}(j\omega)|$(1),$|\widetilde{S}_{o,\psi_e}(j\omega)|$(2), and $|S_{\mathcal{K}}(j\omega)|$(3) (blue) and their respective inverse weights $|w_{e,11}^{-1}(j\omega)|$, $|w_{e,22}^{-1}|$, and $|W_u^{-1}|$ (orange) (b).

4-1 Controller analysis

In the previous chapter, it was concluded that the controller $\mathcal{K}$ yields the closed-loop system string stable, since $\|N\|_{\mathcal{H}_\infty} = 1$. This is confirmed by the frequency response of the magnitude of the string stability sensitivity function Γ presented in Figure 4-1a, from which it can be observed that $\|\Gamma\|_{\mathcal{H}_\infty} \leq 1$. This bound on the string stability complementary sensitivity function implies that input perturbations are not amplified in the upstream direction of the platoon.

Furthermore, the constraints applied on the other sensitivities have all been met. This is confirmed by Figure 4-1b, showing the frequency responses of the transfer functions $|\widetilde{S}_o(j\omega)|$ defined in (3-28) (from d_i to e_i), and $|S_{\mathcal{K}}(j\omega)|$ defined in (3-31) (from d_i to u_i), and their respective inverse weights. Since $|\widetilde{S}_{o,y_e}(j\omega)| < |w_{e,11}^{-1}(j\omega)|$, and $|\widetilde{S}_{o,\psi_e}(j\omega)| < |w_{e,22}^{-1}|$ it can be concluded that indeed, the path following objective as defined in Section 3-7 has been satisfied.

4-2 Uncertainty

In this section, the performance and stability properties of the closed-loop system will be investigated in the presence of uncertainty. Uncertainties are always present in real systems, and they usually come in the form of parametric or dynamic uncertainty. Therefore, the stability analysis for such systems plays an important role in controller design. The $\mathcal{H}_\infty$-framework provides enough tools to embed uncertainty analysis into it, which is often the

raison d'etre $\mathcal{H}_\infty$ optimisation is used for controller design. First, it will be explained how uncertainties are generally included into this framework.

To account for uncertainty, the dynamic behaviour will be described by a set Π which contains all possible perturbed plant models, such that

$$\begin{aligned} G(s) &\in \Pi - \text{nominal plant model (with no uncertainty)} \\ G_p(s) &\in \Pi - \text{perturbed plant model.} \end{aligned} \tag{4-1}$$

Here the perturbed model set Π, depends on the type of uncertainty considered. Moreover, a norm bounded uncertainty description is used where the set Π is generated by allowing $\mathcal{H}_\infty$ norm-bounded perturbations to the system. These perturbations are denoted by Δ, which has an $\mathcal{H}_\infty$ norm less than 1, i.e, $\|\Delta\|_{\mathcal{H}_\infty} \leq 1$. By "pulling out" the perturbations Δ from the system such that an input and an output can be associated with them, the $N\Delta$ structure of Figure 4-2 can be used to represent the perturbed system. Herein, y_Δ denotes the input to, and u_Δ denotes the output of the uncertainty block Δ; the structure is then denoted as

$$\begin{pmatrix} y_\Delta \\ z \end{pmatrix} = \begin{pmatrix} N_{11} & N_{12} \\ N_{21} & N_{22} \end{pmatrix} \begin{pmatrix} u_\Delta \\ d \end{pmatrix}. \tag{4-2}$$

The uncertainty Δ can be absorbed into the closed-loop system N such that $z = F(\Delta)d$ is obtained, with F

$$F = N_{22} + N_{21}\Delta(I - N_{11}\Delta)^{-1}N_{12} \triangleq F_u(N, \Delta), \tag{4-3}$$

where $F_u(N, \Delta)$ denotes the upper LFT of N and Δ. It can be observed that in this representation of $F(\Delta)$, N_{22} denotes the transfer function from d to z without uncertainty, which is equivalent to the weighted nominal system defined in (3-37). Using the $\mathcal{H}_\infty$ norm to define robust performance requires $\|F(\Delta)\|_{\mathcal{H}_\infty} \leq 1$ for all allowed Δ's [33], which is also implied by the condition in (3-40). Since F will include the perturbed realisations of the weighted sensitivity functions in N_{22}, the robust performance requirement thus implies that for all allowable perturbations the control objectives have to be met, i.e., the perturbed sensitivity functions have to be smaller than or equal to their respective inverse weights.

4-2-1 Dynamic Uncertainty

A class of uncertainty, that is often used in robustness analysis, is dynamic uncertainty. This type of uncertainty takes complex perturbations into account, which is often used to quantify uncertainty caused by unmodelled dynamics. Moreover, it can also be used to describe parametric uncertainty, since in the presence of multiple real perturbations, it becomes possible to lump real uncertainties into a single complex uncertainty [33].

The nominal system presented in Sections 3-3 and 3-4 potentially contains both dynamic and parametric uncertainty. Dynamic uncertainty in this case is caused by simplifications made during modelling in order to linearise the system, such as, using small angle approximations, decoupling the lateral dynamics from the longitudinal dynamics, and using the linear tyre model. Parametric uncertainty is also present in the system, since parameters such as the

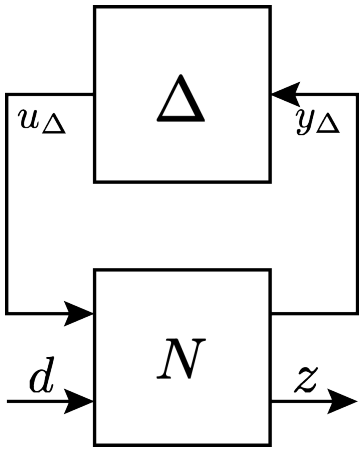

Figure 4-2: Block diagram of the $N\Delta$ structure.

cornering stiffnesses and vehicle mass might not have been accurately estimated and could change over time or during motion. These various sources of uncertainty can be lumped into a single input multiplicative uncertainty of the form:

$$\begin{aligned} \Pi_I: \quad G_p(s) &= G(s)(1 + w_I(s)\Delta_I(s)) \\ G_{p,t}(s) &= G_t(s)(1 + w_I(s)\Delta_I(s)), \end{aligned} \tag{4-4}$$

where $G_p(s)$ and $G_{p,t}(s)$ denote the perturbed representation of the systems in (3-17) and (3-20), with input u_i and outputs y_i and d_{i+1} respectively. In this way, it is possible to determine the robustness of the system against uncertainty, in terms of path following and string stability. Furthermore, Δ_I denotes the complex input uncertainty and can be any stable transfer function, and w_I is a weight that describes the uncertainty at each frequency, and can be used to normalise the perturbation to be less than 1 in magnitude. The perturbed system with input multiplicative uncertainty can then be represented by the diagram in Figure 4-3.

To describe the uncertainty in frequency domain the input uncertainty filter w_I was chosen to be

$$w_I = \frac{\sigma_I s + r_o}{\frac{\sigma_I}{r_\infty} s + 1}, \tag{4-5}$$

where $1/\sigma_I$ is approximately the frequency at which the relative uncertainty reaches 100 %, r_o is the relative uncertainty at steady-state, and r_∞ is the magnitude of the weight at high frequency. At lower frequencies, the system model provides an accurate description of the real system [36], hence parametric uncertainty will be dominant over dynamic uncertainty, in this frequency range. It is assumed that the system parameters, such as the cornering stiffnesses, the mass, and the longitudinal velocity are accurately estimated and that any variation from the estimated values does not exceed 10 % at any time, therefore $r_o = 0.1$. Moreover, at input frequencies higher than 2 Hz the linearised bicycle model no longer provides an accurate description of the true system [36], therefore at that frequency range dynamic uncertainty will be the more dominant source of uncertainty. This is accounted for by choosing $r_\infty = 1$

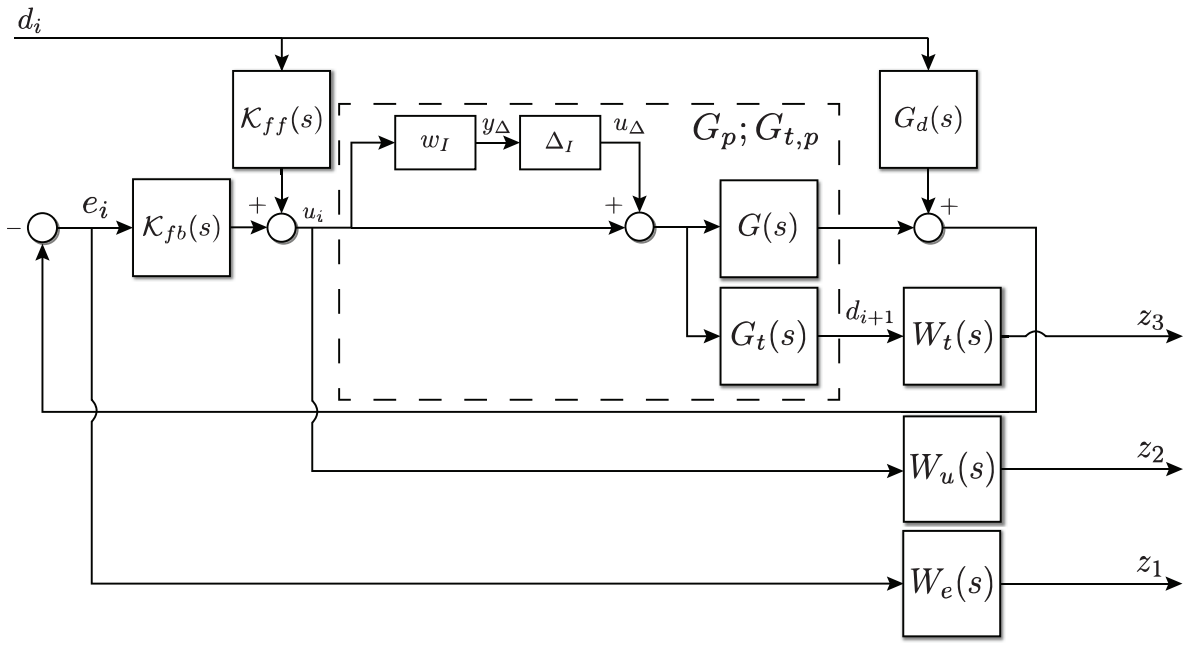

Figure 4-3: Plant with input multiplicative uncertainty.

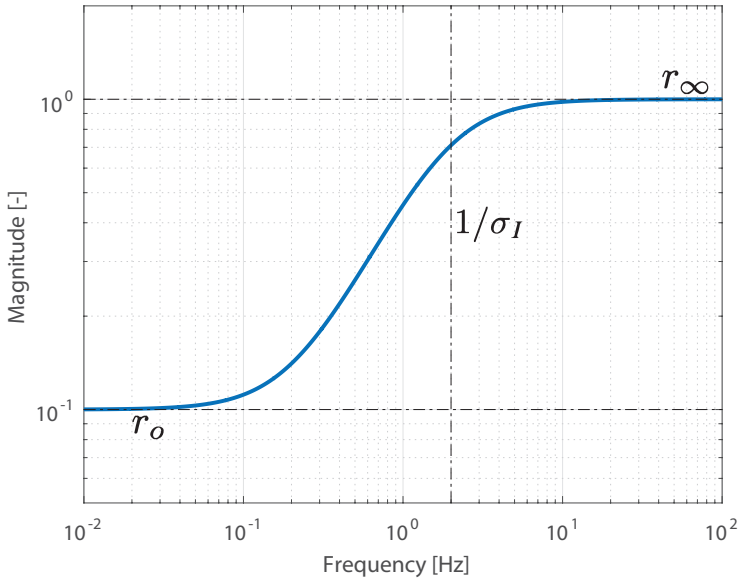

Figure 4-4: Multiplicative weight $w_I(s)$ for uncertainty in $G(s)$ and $G_t(s)$.

and $\sigma_I = 1/(2 \cdot 2 \cdot \pi)$, such that at frequencies higher than 2 Hz a hundred percent uncertainty is considered. The filter $w_I(s)$ with these parameter values is depicted in Figure 4-4.

The sensitivities of interest of the uncertain perturbed closed-loop system, for which Δ_I has been randomly sampled, and their inverse weights are presented in Figure 4-5. From which it can be concluded that for this type of uncertainty the system is still able to fulfil the path-following condition, since the magnitudes of $\widetilde{S}^p_{o,y_e}(j\omega)$ and $\widetilde{S}^p_{o,\psi_e}(j\omega)$, describing the transfer functions from d_i to e_i in the presence of uncertainty, are smaller than the magnitudes of the inverse of their respective weights $w^{-1}_{e,11}(j\omega)$ and $w^{-1}_{e,22}$. Here, $\widetilde{S}^p_{o,y_e}(j\omega)$ and $\widetilde{S}^p_{o,\psi_e}(j\omega)$ denote the perturbed representations of the sensitivity functions defined in (3-28). However, string stability is not guaranteed, since $\|F\|_{\mathcal{H}_\infty} > 1$, which is caused by the perturbed representation of the string-stability complementary sensitivity function in (3-24) $|\Gamma^p(j\omega)|$ being larger than 1, i.e., $|\Gamma^p(j\omega)| > |W_t^{-1}|$.

It can thus be concluded that the controller is not robust against perturbations of the presented form, which is caused by the string stability condition being violated in the presence of uncertainties. However, the system remains stable and the path-following objective is still fulfilled. Designing a robust controller, such that, both path following and string stability can be obtained in the presence of uncertainty is not possible without sacrificing one objective over the other. For example having a controller that remains string stable at different velocities, would require a certain degree of conservatism in the path-following properties of the system, i.e., lower bandwidth and larger steady-state errors. Moreover, the path-following condition implies that for $\omega \to 0$ the magnitude of the string stability complementary sensitivity function $\Gamma(j\omega)$ will always be equal to one, whereas the string-stability condition implies that $|\Gamma(j\omega)| \leq 1$. Both these conditions make it such that there are no margins for uncertainties at the lower-frequency range. The use of robust control methods does therefore not offer a feasible solution for dealing with these uncertainties. This only leaves the option of compensating for them, which is only possible if the uncertain parameters are measurable. For these uncertainties one could use alternative control methods, such as, Linear Parameter Varying (LPV) control. With this taken into consideration, it is decided that the designed optimal controller will be the one deployed for further analysis.

4-3 State feedback-feedforward controller

In this section, the controller as deployed at TNO will be introduced [37], such that in the upcoming sections, a comparative analysis can be provided in terms of performance. The controller is a state feedback-feedforward controller, with speed dependent gains. The goal for this controller is to calculate a suitable input such that the errors for path tracking are minimised,

$$\lim_{t \to \infty} e_i(t) = 0, \tag{4-6}$$

with $e_i(t) = \begin{pmatrix} y_{e,i} & \psi_{e,i} \end{pmatrix}^T$. Here, however, the errors are not identical to the ones introduced in the preceding chapters, but are as depicted in Figure 4-6. Here, the lateral error $y_{e,i}$, is defined as the lateral distance of the center of gravity of the vehicle from the desired path, perpendicular to the vehicle's orientation, and is positive in the depicted direction. The

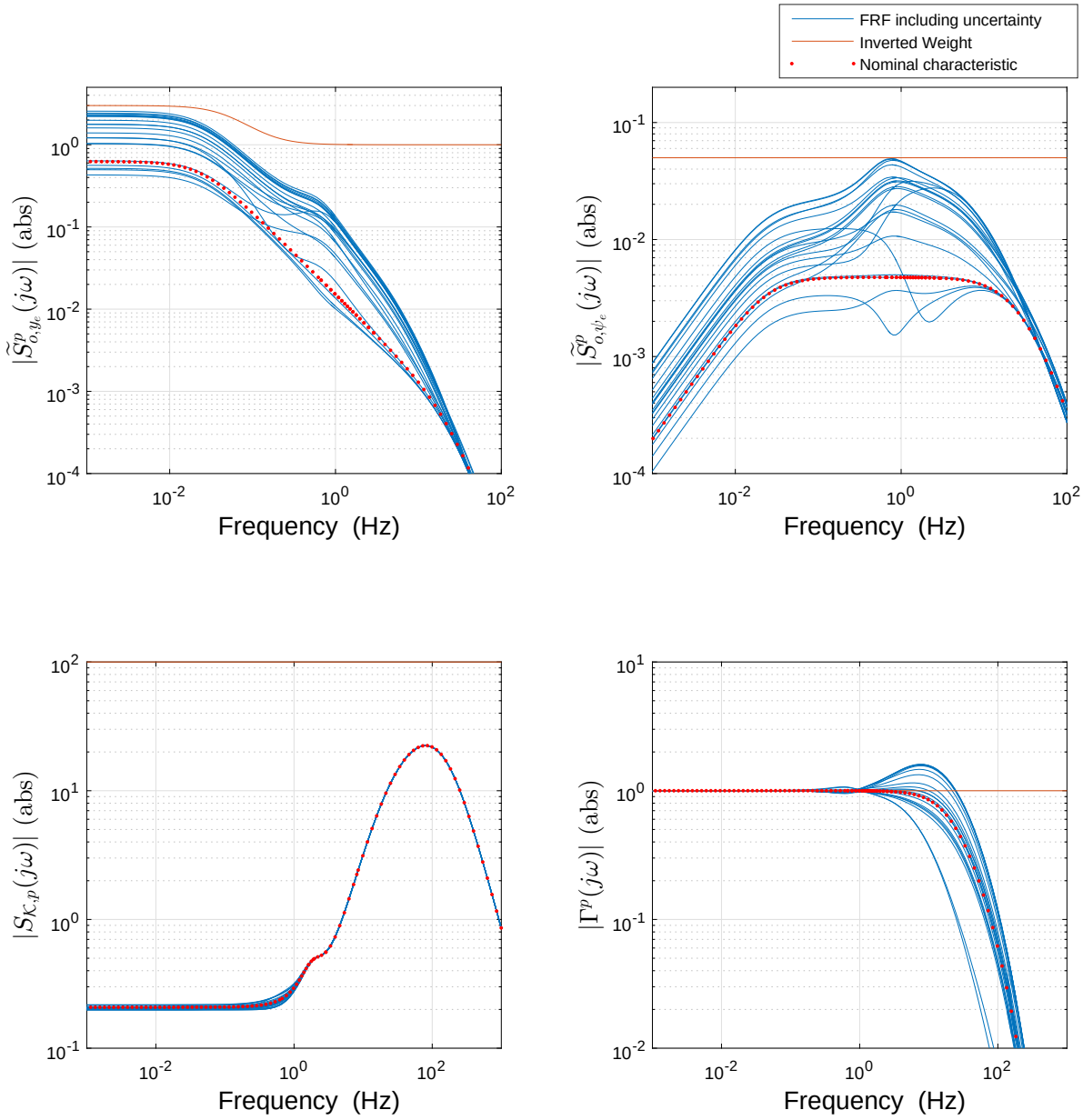

Figure 4-5: Sensitivity plots with dynamic uncertainty (blue), their inverse weights (orange), and the nominal system (red dots). The top left figure denotes the perturbed transfer function of $|\widetilde{S}^p_{o,y_e}(j\omega)|$ and the top right figure denotes $|\widetilde{S}^p_{o,\psi_e}(j\omega)|$, the bottom left figure denotes the perturbed transfer function $|S_{\mathcal{K},p}(j\omega)|$ and the bottom right figure presents the perturbed transfer function $|\Gamma^p(j\omega)|$.

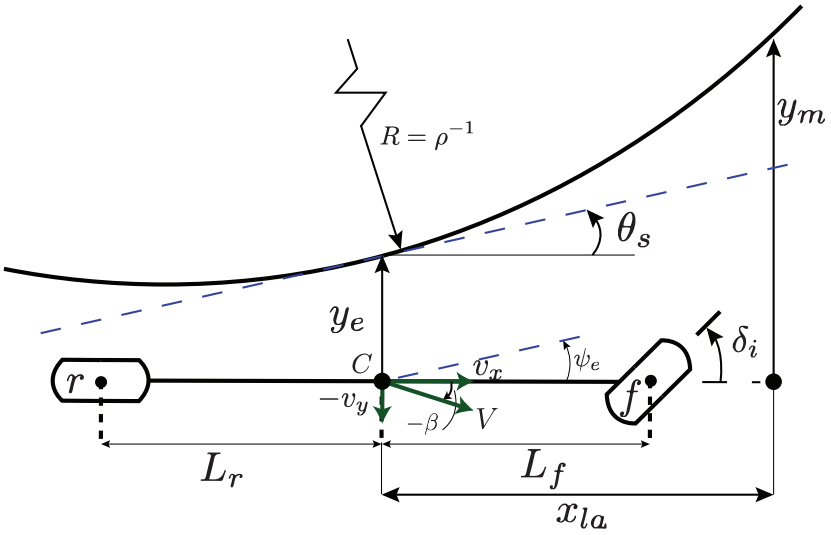

Figure 4-6: Schematic overview of the error model.

positive orientation error $\psi_{e,i}$ is defined as the difference between the actual orientation of the vehicle and the desired orientation angle of the road. This is opposed to the errors introduced in Chapter 2, where $y_{e,i}$ was perpendicular to the road and $\psi_{e,i}$ was defined as the difference between the heading of the vehicle and the road's orientation.

The vehicle dynamics were augmented with the dynamics of the defined errors, such that the following state-space error model is obtained:

$$\begin{pmatrix} \dot{v}_{y,i} \\ \ddot{\psi}_i \\ \dot{y}_{e,i} \\ \dot{\psi}_{e,i} \\ \dot{\delta}_i \\ \ddot{\delta}_i \end{pmatrix} = \begin{pmatrix} \frac{1}{v_{x,i}}\frac{C_{\alpha r}+C_{\alpha f}}{m} & \frac{1}{v_{x,i}}\frac{C_{\alpha f}L_f - C_{\alpha r}L_r}{m} - v_{x,i} & 0 & 0 & -\frac{C_{\alpha f}}{m} & 0 \\ \frac{1}{v_{x,i}}\frac{C_{\alpha f}L_f - C_{\alpha r}L_r}{I_z} & \frac{1}{v_{x,i}}\frac{C_{\alpha r}L_r^2 + C_{\alpha f}L_f^2}{I_z} & 0 & 0 & -\frac{L_f C_{\alpha f}}{I_z} & 0 \\ -1 & 0 & 0 & v_{x,i} & 0 & 0 \\ 0 & -1 & 0 & 0 & 0 & 0 \\ 0 & 0 & 0 & 0 & 0 & 1 \\ 0 & 0 & 0 & 0 & -\omega_n^2 & -2\zeta\omega_n \end{pmatrix} \begin{pmatrix} v_{y,i} \\ \dot{\psi}_i \\ y_{e,i} \\ \psi_{e,i} \\ \delta_i \\ \dot{\delta}_i \end{pmatrix} + \begin{pmatrix} 0 \\ 0 \\ 0 \\ 0 \\ 0 \\ \omega_n^2 \end{pmatrix} \delta_{ref,i} + \begin{pmatrix} 0 \\ 0 \\ 0 \\ 1 \\ 0 \\ 0 \end{pmatrix} \dot{\theta}_{s,i} \quad (4\text{-}7)$$

with state vector $x = \begin{pmatrix} v_{y,i} & \dot{\psi}_i & y_{e,i} & \psi_{e,i} & \delta_i & \dot{\delta}_i \end{pmatrix}^T$. The short notation of the system is given as

$$\dot{x}_i = A_a x_i + B_{a,1}\delta_{ref,i} + B_{a,2}\dot{\theta}_{s,i}, \quad (4\text{-}8)$$

here, $\delta_{ref,i}$ is the steering angle at the wheel, which is the input to the system. Furthermore, $\dot{\theta}_{s,i}$ denotes the rate of change of the road's orientation, and is the disturbance to the system.

For the errors as introduced above, a control law was developed, which reads:

$$\delta_i = \underbrace{k_{y_{e,i}} y_{e,i} + k_{\psi_{e,i}} \psi_{e,i}}_{feedback} + \delta_{i,ff}. \tag{4-9}$$

with the control parameters defined as,

$$\begin{aligned} k_{y_{e,i}} &= \frac{2(L + K_{us} v_{x,i}^2)}{d_{LA}^2} \\ k_{\psi_{e,i}} &= \frac{2(L + K_{us} v_{x,i}^2)}{d_{LA}^2} x_{LA}, \end{aligned} \tag{4-10}$$

here $L = L_r + L_f$ denotes the wheel-base, and $d_{LA} = x_{LA} + L_r$ is the look-ahead distance as taken from the rear axle; x_{LA} is the look-ahead distance defined from the center of gravity, given by $x_{LA} = v_{x,i} t_{LA}$ where t_{LA} is the time headway; finally the understeer gradient is defined as $K_{us} = \frac{m}{L}\left(\frac{L_r}{C_{\alpha f}} - \frac{L_f}{C_{\alpha r}}\right)$. The basic idea for determining these gains is based on the fact that while driving in steady-state conditions a front wheel steered vehicle can only move in circular movements. It is therefore desired to realise a certain radius R that reduces the error at a look-ahead distance $y_m = y_{e,i} + x_{LA}\psi_{e,i}$. Finally, the feedforward control input is given by

$$\delta_{i,ff} = \underbrace{(L + K_{us} v_{x,i}^2)/v_{x,i}}_{K_{ff}} \dot{\theta}_{s,i}, \tag{4-11}$$

which is designed such that errors are reduced during steady-state cornering. For the derivation the reader is referred to [37].

4-4 Comparison of the $\mathcal{H}_\infty$ and state feedback-feedforward controller

In this section, the response to an initial condition perturbation of the closed-loop system for both controllers will be investigated. The gains for the controller in Section 4-3 are calculated using the parameters presented in Table 3-1, combined with a time headway of 1 s, such that the following controller gains are obtained for a vehicle driving at $v_{x,i} = 20\,\mathrm{m\,s^{-1}}$:

$$\begin{aligned} k_{y_{e,i}} &= 0.0178 \\ k_{\psi_{e,i}} &= 0.3569 \\ k_{ff} &= 0.2081. \end{aligned} \tag{4-12}$$

In Appendix C, a comparison between the magnitude of the $\mathcal{H}_\infty$ controller and the state feedback-feedforward controller is provided. Moreover, a string stability analysis is performed, from which it is concluded that the state feedback-feedforward controller is not string stable.

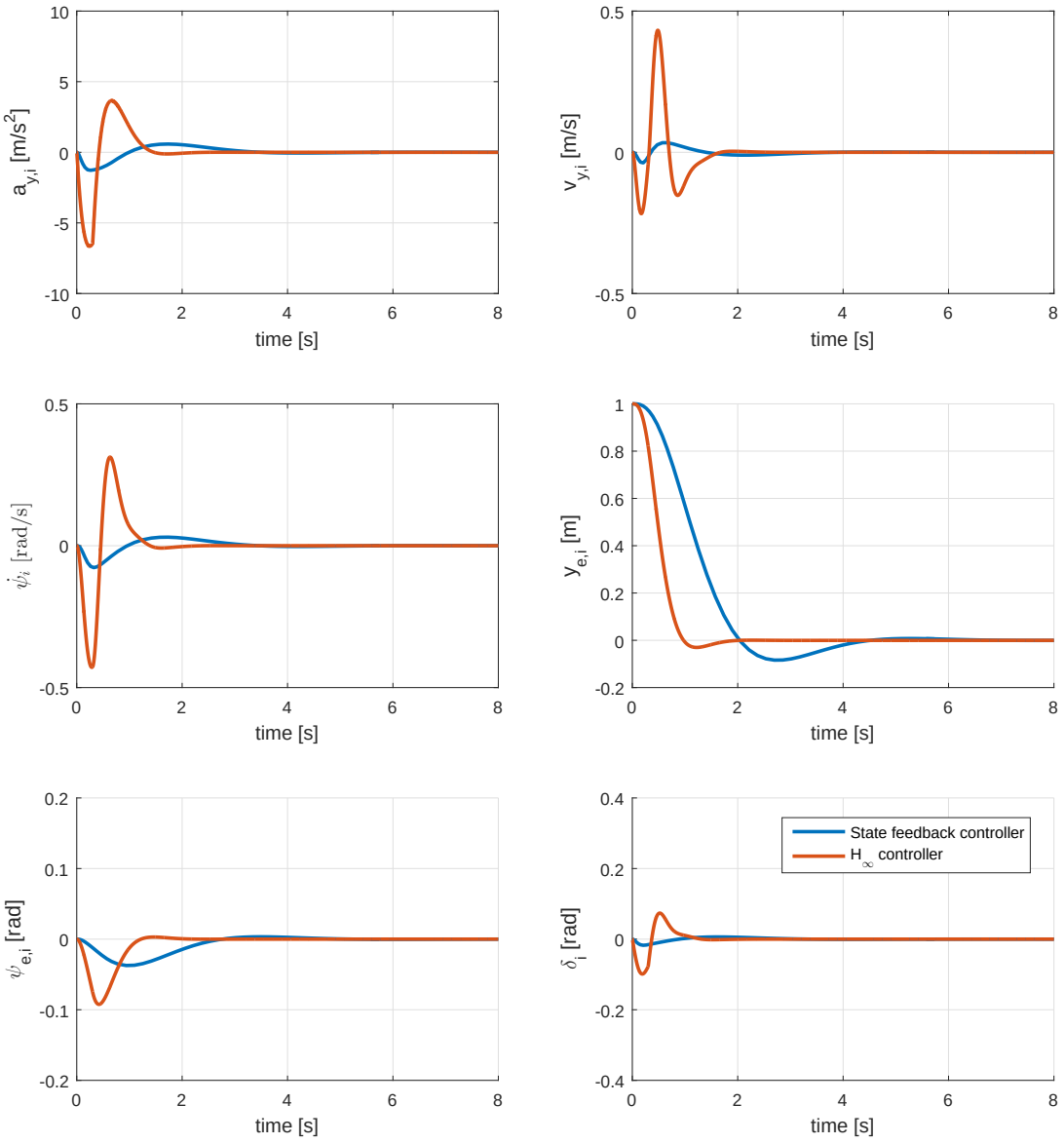

Figure 4-7: Transient response of the closed-loop system driving at $v_{x,i} = 20\,\mathrm{m\,s^{-1}}$, using the state feedback-feedforward controller and the $\mathcal{H}_\infty$ controller.

For the simulation, an offset of 1 m from the reference path is considered, such that $x(0) = (0,\ 0,\ 1,\ 0,\ 0,\ 0)^T$, moreover a disturbance $d_i = \dot{\theta}_{s,i} = 0$ is taken.

Figure 4-7 provides the time-response of multiple system states, here the lateral acceleration $a_{y,i} = \dot{v}_{y,i} + v_{x,i}\dot{\psi}_i$ is introduced as an additional state as it provides insight on how comfortable the response is. From the response of Figure 4-7 it can be confirmed that indeed both controllers yield a stable system response. Moreover, it can be observed that the dynamic $\mathcal{H}_\infty$ controller has an overall faster and more aggressive response to the initial condition error, as can be observed by the larger rates and magnitudes of $a_{y,i}$, $v_{y,i}$, and $\dot{\psi}_i$. However, the response of the $\mathcal{H}_\infty$ controller has better damping characteristics, which is characterised by the fast convergence and the lack of overshoot in $y_{e,i}$. This is caused by the closed-loop system having fast left half plane poles on the real axis. The higher lateral accelerations are caused by these poles exciting the relatively high feedback gains of the controller, yielding larger inputs. A plot of the poles and zeros of the closed-loop systems for both controllers is provided in Appendix D. The static feedback-feedforward controller has smaller gains and slower left-half plane poles that are closer to the imaginary axis, hence the smaller steering angles generated in response to the initial condition, and the slower convergence to zero. Moreover, the complex poles of this system yield a more oscillatory response.

The reason behind the difference in responses is caused by the design approach. The $\mathcal{H}_\infty$-controller was designed from an input-output perspective, with string stability being one of the main design criteria. It is expected to see the consequences of these design choices when string stability is concerned.

4-5 String stability properties

In this section, the string stability properties of the designed controller will be investigated in time domain, and compared to the existing state feedback-feedforward controller. In order to do so, a simulation model has to be obtained, which is schematically given in Figure 4-8. The simulation model describes a platoon consisting of 3 vehicles, and can be expanded to contain more. Each vehicle obtains $\dot{\theta}_{i-1}$ from its preceding vehicle's model, i.e., "System Model"; in a real life scenario this would be obtained from a path generation algorithm. The "System Model" block also calculates the heading and the lateral errors $y_{e,i}$ and $\psi_{e,i}$, respectively. The time gap Δt is incorporated in the design such that the desired longitudinal separation is obtained. The "Lateral Controller" block contains both the feedforward and feedback controllers such that the reference steering input $\delta_{ref,i}$ is obtained.

During simulation, string stability in the lateral sense is evaluated for the following scenarios:

1. The nominal case, where all vehicles are driven at nominal speed $v_{x,i} = 20\,\mathrm{m\,s^{-1}}$ and no uncertainty is present;

2. A worst-case scenario, where uncertainty in the cornering stiffnesses is considered;

3. The case where the vehicle is driving at a velocity other than the nominal speed, and no other uncertainties are present.

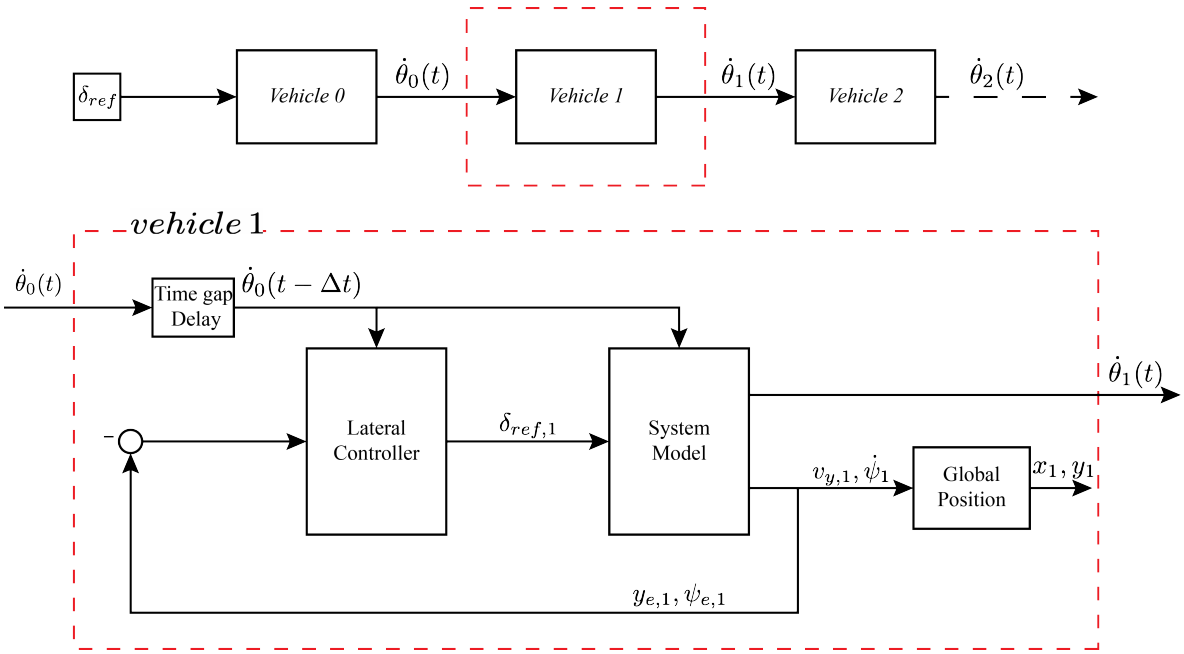

Figure 4-8: A schematic representation of the simulation model for a platoon consisting of three vehicles. The dotted line coming out of vehicle 2 indicates possible extension of this model.

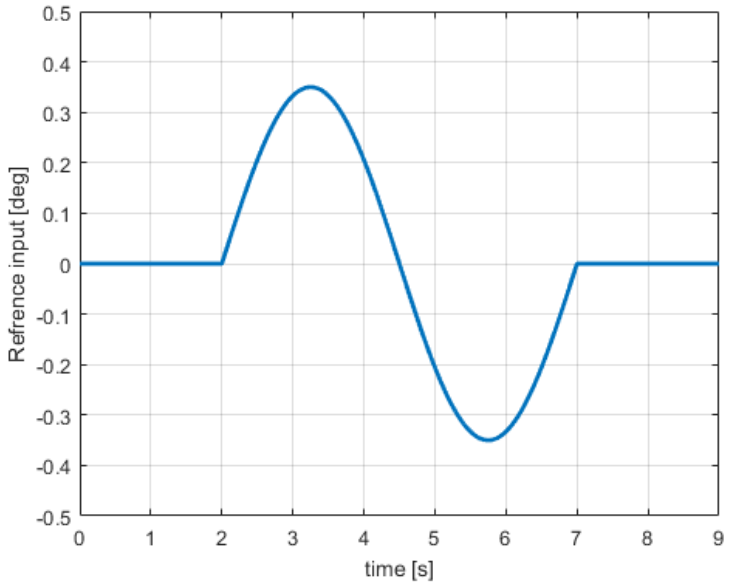

Figure 4-9: Reference steering input to the the leading vehicle.

For the time-domain simulations, a lane-change scenario is considered. Here all the vehicles drive in a platoon with an initial velocity of $20\,\mathrm{m\,s^{-1}}$ and a time-gap $\Delta t = 1\,\mathrm{s}$, i.e., a separation distance of 20 m. Such that, $\begin{pmatrix} x_{0,0} & y_{0,0} & \psi_{0,0} \end{pmatrix} = \begin{pmatrix} 0 & 0 & 0 \end{pmatrix}$, $\begin{pmatrix} x_{1,0} & y_{1,0} & \psi_{1,0} \end{pmatrix} = \begin{pmatrix} -20 & 0 & 0 \end{pmatrix}$, and $\begin{pmatrix} x_{2,0} & y_{2,0} & \psi_{2,0} \end{pmatrix} = \begin{pmatrix} -40 & 0 & 0 \end{pmatrix}$. Furthermore, the remaining initial conditions of the system states are all chosen to be equal to zero, such that, $x_{i,0} = \begin{pmatrix} v_{y,i,0}, & \dot{\psi}_{i,0}, & y_{e,i,0}, & \psi_{e,i,0}, & \delta_{i,0}, & \dot{\delta}_{i,0}, \end{pmatrix}^T = \mathbf{0}$. For the lane-change manoeuvre a reference steering input δ_{ref}, as depicted in Figure 4-9, is given to the leading vehicle. This results in the road profile of the lane-change manoeuvre having a sinusoidal rate of change of orientation $\dot{\theta}_0$ with a frequency of 0.2 Hz.

The nominal case

First the nominal case is considered, where no uncertainty is present and the vehicles are driving at $v_{x,i} = 20\,\mathrm{m\,s^{-1}}$. Figures 4-10a and 4-10b show the result of this lane-change manoeuvre for the state feedback-feedforward controller and the $\mathcal{H}_\infty$ controller, respectively. It can be observed that the system controlled by the state feedback-feedforward controller exerts string unstable behaviour in the lateral direction. This is concluded from the increasing overshoot of the path driven, and the amplification of the disturbance $\dot{\theta}_i(t)$. It should be noted that eventually the errors do converge to zero, which confirms that a stable system does not necessarily yield a string-stable interconnected system.

On the other hand, the $\mathcal{H}_\infty$ controller is able to perform the same lane-change manoeuvre whilst maintaining string stability. This can be concluded from the fact that the following vehicle follows the exact path driven by it's predecessor and that $\dot{\theta}_i(t)$ does not amplify in upstream direction, thereby confirming the results obtained in the frequency domain.

A worst-case scenario

In Section 4-2, it was noted that the designed controller is not robust against uncertainty, in the string-stability sense. However, it was stated that, regardless of this uncertainty, the controller is able to fulfil its path-following objective. In order to confirm that in simulation, a worst case scenario is considered. According to [38], a worst case is obtained when the cornering stiffness at the rear axle $C_{\alpha r}$ is decreased, since this could cause the poles to cross the imaginary axis. Considering a case where this parameter is varied by 10 %, yields the following perturbed rear cornering stiffness

$$C_{\alpha r} = 0.129\,\mathrm{MN\,rad^{-1}}. \tag{4-13}$$

The state feedback-feedforward controller was kept identical, as the parameter is assumed to have been determined incorrectly. The results of this simulation are presented in Figures 4-11a and 4-11b, for the same lane-change manoeuvre at a velocity $v_{x,i} = 20\,\mathrm{m\,s^{-1}}$, and the same initial conditions as before. From the response of $\dot{\theta}_i(t)$ at approximately 10 s it can be concluded that indeed the string stability condition has been violated, yet path-following was obtained for both controllers, which in the case of the $\mathcal{H}_\infty$-controller, again, confirms

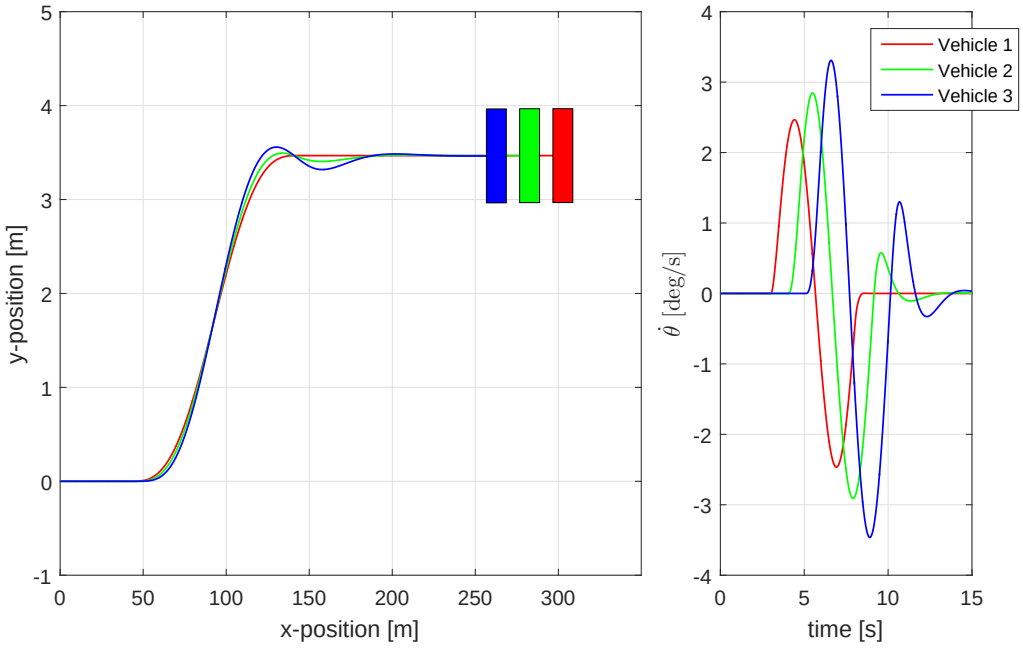

(a)

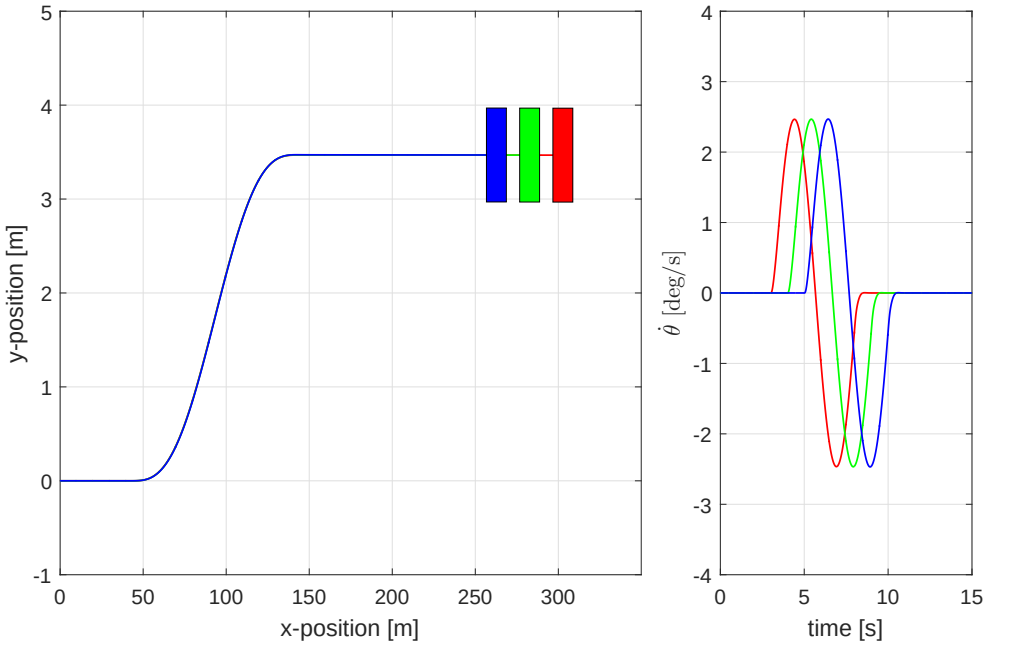

(b)

Figure 4-10: Simulation of a lane-change manoeuvre for the nominal case, where the vehicles drive at $v_{x,i} = 20\,\mathrm{m\,s^{-1}}$, (a) illustrates the results for the feedback-feedforward controller and (b) illustrates the results for the $\mathcal{H}_\infty$-controller. The colours red, green, and blue represent the first, second, and the third vehicle, respectively.

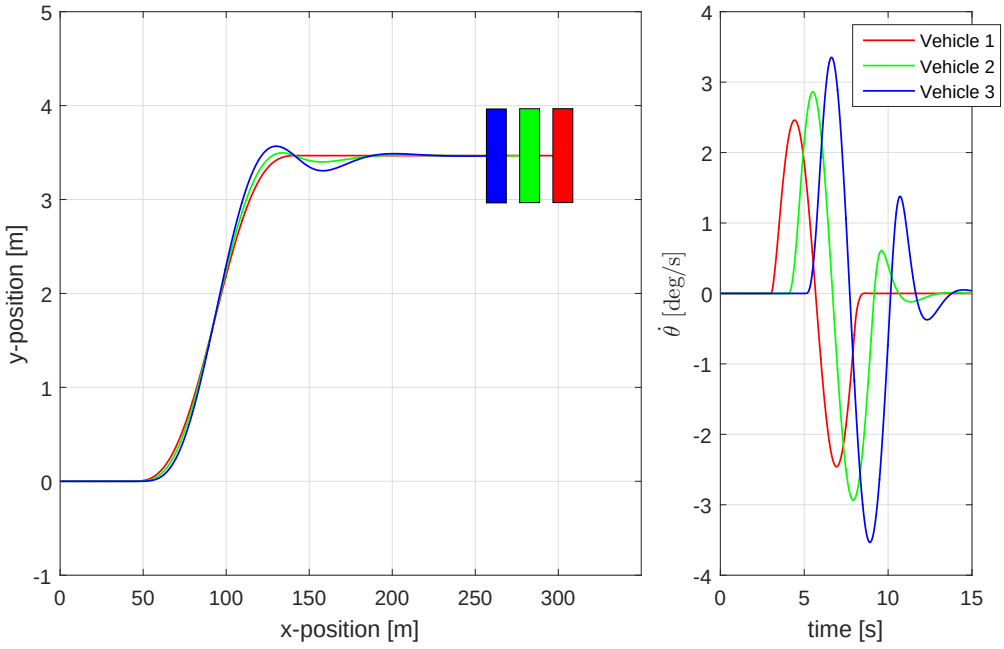

(a)

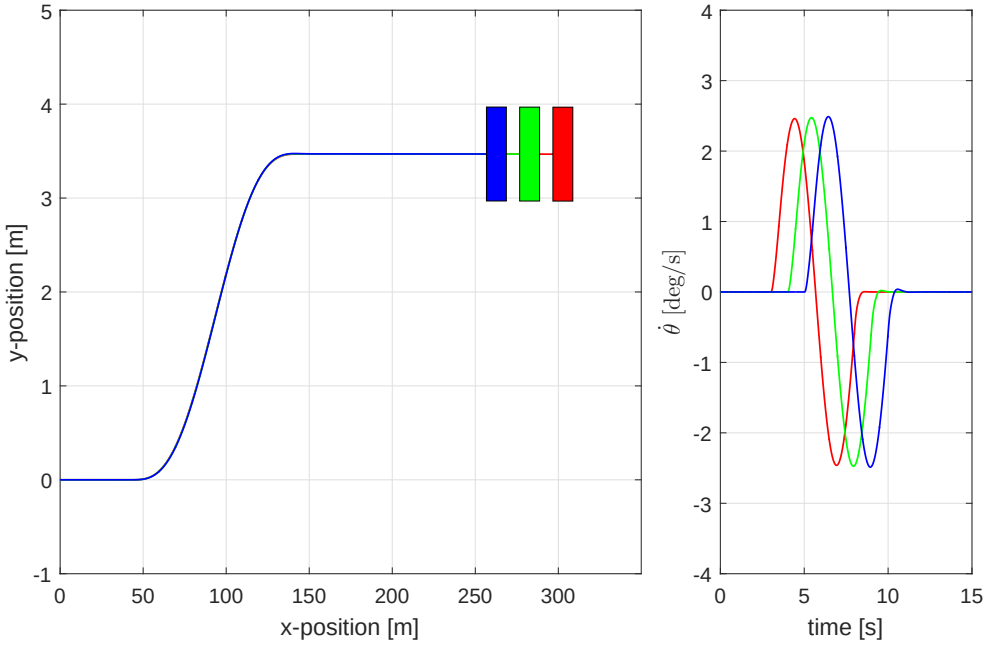

(b)

Figure 4-11: Simulation of a lane-change manoeuvre for a worst-case scenario, where the vehicles drive at $v_{x,i} = 20\,\mathrm{m\,s^{-1}}$, (a) illustrates the results for the feedback-feedforward controller and (b) illustrates the results for the $\mathcal{H}_\infty$-controller. The colours red, green, and blue represent the first, second, and the third vehicle, respectively.

the analysis performed in the frequency domain. However, it should be noted that the amplification of $\dot{\theta}_i(t)$ is contained, and the response still resembles string-stable like behaviour. Which shows that in a worst-case scenario, deploying the $\mathcal{H}_\infty$ controller would still be an improvement over the current controller.

Uncertainty in the velocity

Finally, a third case is considered where the vehicle parameters are nominal and the velocity is uncertain. Here an increase of 10 % from the nominal velocity was considered, such that $v_{x,i} = 22\,\mathrm{m\,s^{-1}}$. Since the longitudinal velocity is measurable, the gains for the state-feedback controller were recalculated accordingly, such that

$$\begin{aligned} K_{fb} &= \begin{pmatrix} k_{y_{e,i}} & k_{\psi_{e,i}} \end{pmatrix} = \begin{pmatrix} 0.0141 & 0.3523 \end{pmatrix} \\ K_{ff} &= 0.1994. \end{aligned} \tag{4-14}$$

The results of this simulation are presented in Figures 4-12a and 4-12b, for an identical lane-change manoeuvre with a separation distance of 22 m and the same initial conditions as before. From both the trajectory in the global coordinates as the response of $\dot{\theta}_i(t)$ it can be concluded that indeed the string-stability condition has been violated, yet path-following was obtained for both controllers, which again confirms the analysis performed in the frequency domain. Despite the state-feedback controller operating at its design speed, the response of the $\mathcal{H}_\infty$ controller is more subdued, and resembles a more string-stable-like response.

Further increasing the velocity causes, as expected, the performance of the $\mathcal{H}_\infty$-controller to degrade in the string stability sense. However, until velocities of $30\,\mathrm{m\,s^{-1}}$ the $\mathcal{H}_\infty$ controller is still able to maintain string-stable-like responses. At higher velocities the response of the feedback-feedforward controller remains similar whilst, whilst the $\mathcal{H}_\infty$ controller's response becomes more oscillatory, but with smaller overshoots.

Further decreasing the velocity on the other hand, causes both controllers to exhibit more string-stable-like responses. With the state feedback-feedforward controller having more accurate tracking and less overshoot. The $\mathcal{H}_\infty$ yields a string-stable response with $\dot{\theta}_i$ decreasing in the upstream platoon direction; however, the path tracking becomes less accurate. This is a result of controller being designed for higher velocities, which yields a controller inputs that are too small for low velocities.

4-6 Discussion

In this chapter the robustness properties of the controller designed in Chapter 3 were analysed. Here, robustness against parametric and dynamic uncertainty were of interest, which were analysed using complex perturbations. These perturbations were modelled using input-multiplicative uncertainty. From the analysis, it was concluded that the $\mathcal{H}_\infty$ optimal controller is not robust against this type of uncertainty. This was caused by the string-stability condition not being fulfilled, however the path-following condition was still met.

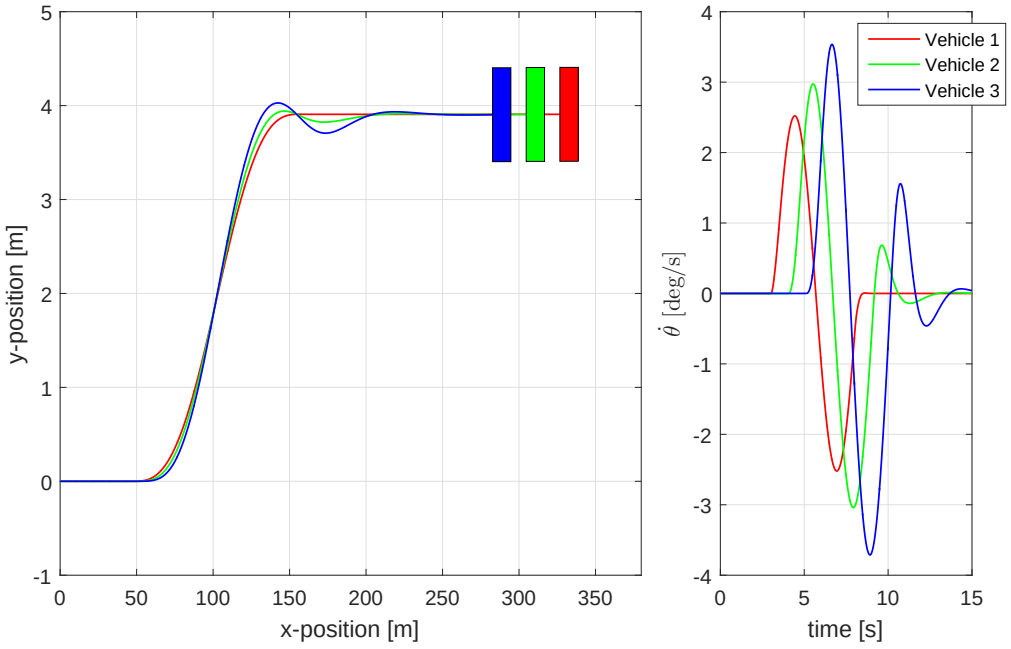

(a)

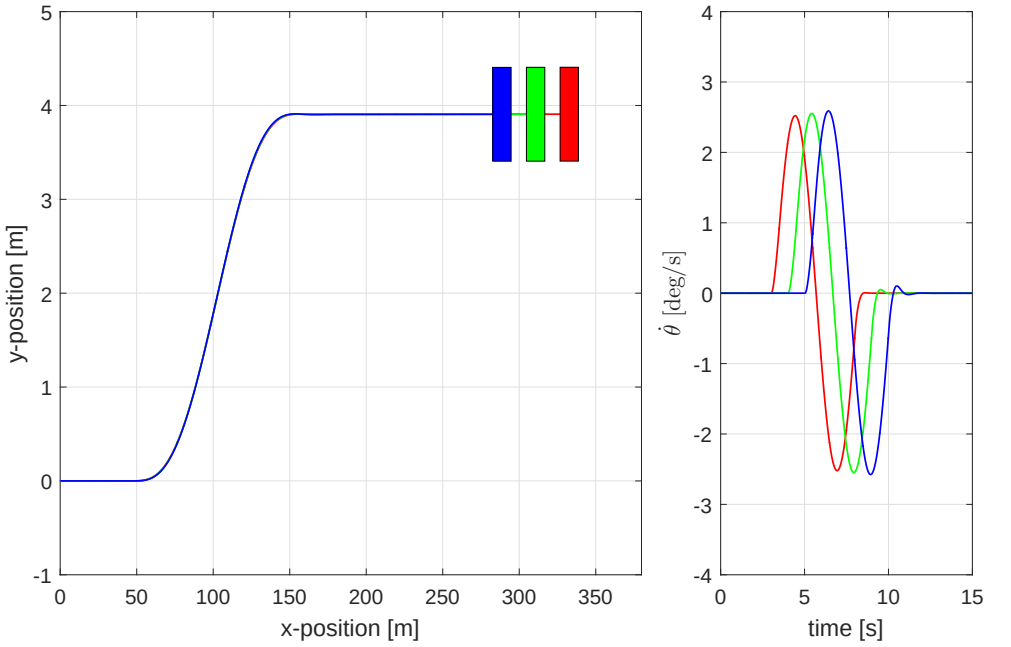

(b)

Figure 4-12: Simulation of a lane-change manoeuvre for a scenario, where the vehicles drive at $v_{x,i} = 22\,\mathrm{m\,s^{-1}}$, (a) illustrates the results for the feedback-feedforward controller and (b) illustrates the results for the $\mathcal{H}_\infty$-controller. The colours red, green, and blue represent the first, second, and the third vehicle, respectively.

In order to confirm these frequency-domain results, time-domain simulations were performed. Here the performance of the designed $\mathcal{H}_\infty$-controller was compared to a state-feedback controller, which is currently used at TNO. First the transient response of the controller was analysed, where it was observed that the $\mathcal{H}_\infty$-controller had a faster and overall more damped response to an initial condition deviation. It was also observed that the $\mathcal{H}_\infty$-controller exerted higher steering inputs, and a more aggressive response. This is caused by the relatively high derivative gains, which get excited by the initial condition perturbation. The difference in response and controller gains, was amounted to the different approaches to the control problem. Whereas the state feedback-feedforward controller was designed to deal with variations in velocity, the $\mathcal{H}_\infty$-controller was designed from an input-output point of view.

Finally, the string-stability properties of the controllers were examined in simulations by means of multiple lane-change scenarios. The first scenario considered the nominal case, where no uncertainties are present. Here it was indeed confirmed that the $\mathcal{H}_\infty$-controller yields a string-stable system, whilst the state-feedback controller was not able to do so. This implies a significant improvement in performance, compared to the current controller. For the second case, a worst-case scenario was considered where the rear cornering stiffness $C_{\alpha r}$ was varied by 10 %. It was observed that for the lane-change manoeuvre, both controllers yielded a string unstable response, thereby confirming the results obtained from the frequency-domain analysis. However, using the $\mathcal{H}_\infty$-controller resulted in a more string-stable-like response. Moreover, a case was considered where the lane-change manoeuvre was performed at a velocity $v_{x,i} = 22\,\mathrm{m\,s^{-1}}$. Similar to the second case both controllers yielded a string-unstable response. However, the $\mathcal{H}_\infty$-controller still yielded a better response in the string stability sense, despite the feedback-feedforward controller being designed to deal with these type of variations. For these case studies, it was confirmed that it would be more beneficial to deploy the $\mathcal{H}_\infty$-controller.

Chapter 5

Experimental validation

The aim of this chapter is experimentally validate the designed controller. First, Section 5-1 will discus the practical implementation of the vehicle following algorithm. Section 5-2 will introduce limitations encountered during practical implementation, which required adjusting the designed controller. In Section 5-3, the experimental implementation and the experimental results are discussed, and Section 5-4 concludes this chapter.

5-1 Implementation aspects

In this section, the practical implementation of the vehicle-following trajectory generation algorithm will be provided, see Figure 5-1. In case the equipped camera detects a vehicle ahead of the host vehicle, a measurement of the relative distance $(x_{r,i}\,, y_{r,i})\vec{\mathbf{e}}_i$, with respect to the rear of the preceding vehicle is provided. This can be interpreted as a single point on the path of the preceding vehicle, which is stored in a history buffer at the frequency rate of the camera, such that the resulting measurement series can be used for path-reconstruction via polynomial fitting. For every new measurement the history buffer is updated, such that the least recent measurement is discarded and the most recent one is added. Figure 5-1 shows these positions projected as fixed points in the global coordinate frame with $\vec{\mathbf{e}} = \begin{pmatrix} \vec{e}_x^{\,o} & \vec{e}_y^{\,o} \end{pmatrix}$.

During vehicle following, the host vehicle will change its position and orientation with respect to the global reference frame between samples; this effect is illustrated in Figure 5-2. Due to the change in coordinate frame caused by this motion, each time sample, the measurements stored in the history buffer are expressed with respect to the most recent coordinate frame of the host vehicle. For this compensation the following transformation is used:

$$\begin{pmatrix} x_r(k) \\ y_r(k) \\ 1 \end{pmatrix} = \underbrace{\begin{pmatrix} \cos\left(\Delta\psi_{k|k+1}\right) & -\sin\left(\Delta\psi_{k|k+1}\right) & \Delta x_{k|k+1} \\ \sin\left(\Delta\psi_{k|k+1}\right) & \cos\left(\Delta\psi_{k|k+1}\right) & \Delta y_{k|k+1} \\ 0 & 0 & 1 \end{pmatrix}}_{T} \begin{pmatrix} x_r(k+1) \\ y_r(k+1) \\ 1 \end{pmatrix}, \tag{5-1}$$

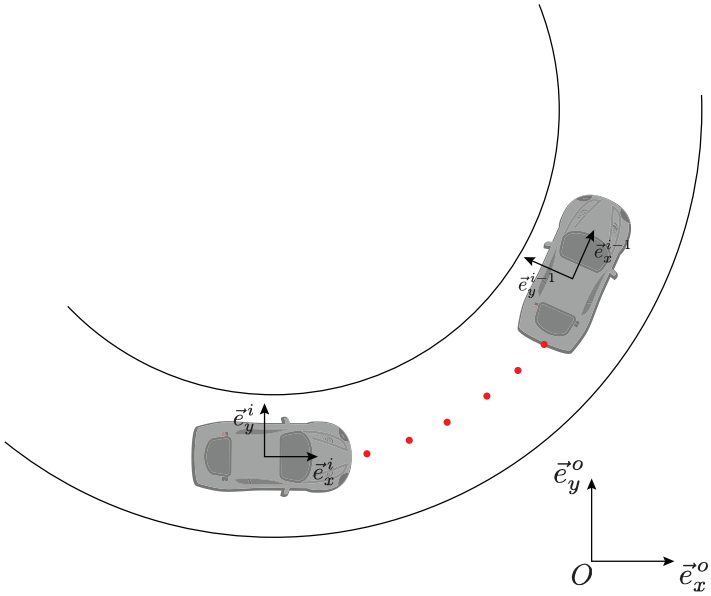

Figure 5-1: Schematic representation of the positions of the preceding vehicle in the global coordinate frame.

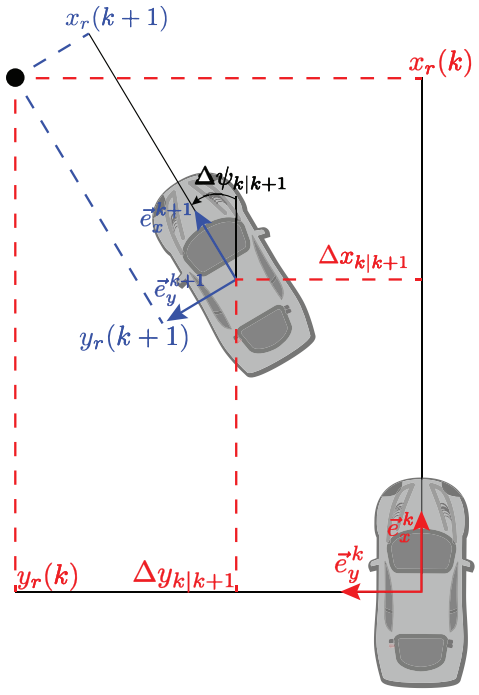

Figure 5-2: Schematic representation of the compensation for the vehicle's movement between samples k and $k+1$.

where $x_r(k)$ and $y_r(k)$ denote the relative longitudinal and lateral coordinates, and $\Delta x_{k|k+1}$, $\Delta y_{k|k+1}$, and $\Delta\psi_{k|k+1}$ are the translations in $x-$ and $y-$direction of the host coordinate frame $(\vec{e}_x^k, \vec{e}_y^k)$ and the rotation around $\vec{e}_z^k$ at sample k, respectively. The target positions as stored in the buffer, which are all expressed with respect to the host vehicle coordinate frame at sample k, need to be expressed with respect to the most recent host coordinate frame, i.e., at time k+1. This is implemented through the following coordinate transformation:

$$\begin{pmatrix} x_r(k+1) \\ y_r(k+1) \\ 1 \end{pmatrix} = T^{-1} \begin{pmatrix} x_r(k) \\ y_r(k) \\ 1 \end{pmatrix}. \tag{5-2}$$

This coordinate transformation applies to all buffer points and is repeated at every time instance, where the most recent motion information of the host are used to determine the transformation matrix T. This transformation is not sufficient to accurately reconstruct the path. Namely, there is a time delay between the time a new measurement starts and the time a measurement is added to the buffer, which is is primarily caused by the image recognition algorithms. Compensating for this delay is similar to compensating for the motion of the vehicle between samples. For a camera delay of ϕ, every new measurement is multiplied by a transformation matrix T_{dc}, which is the product of multiple transformation matrices T_k^{-1}, with $k \in 1, \ldots, n_i$,

$$T_{dc} = T_1^{-1} T_2^{-1} \ldots T_{n_i}^{-1}, \tag{5-3}$$

where each transformation matrix T_k^{-1} is equal to the inverse of the matrix introduced in Equation (5-1), and n_i denotes the amount of transformations required, and is equal to the delay time ϕ divided by the sampling time,

$$n_i = \phi / t_s. \tag{5-4}$$

If for example ϕ is a multiple of five larger than a time-step of the control system, a total of five transformations are required, i.e., $n_i = 5$. The transformation matrix T_{dc} is multiplied by the new relative measurement such that the compensated points can be stored in the buffer:

$$\begin{pmatrix} x_{r,cm}(k) \\ y_{r,cm}(k) \\ 1 \end{pmatrix} = T_{dc} \begin{pmatrix} x_r(k) \\ y_r(k) \\ 1 \end{pmatrix}, \tag{5-5}$$

here the subscript *cm* denotes the new compensated measurement stored in the buffer.

Using the least-squares method, a fifth-order polynomial is fitted through the j amount of buffered points. In order to do so, the points are put in the following linear set of equations,

$$\underbrace{\begin{pmatrix} x_{r,1}^5 & x_{r,1}^4 & x_{r,1}^3 & x_{r,1}^2 & x_{r,1} & 1 \\ x_{r,2}^5 & x_{r,2}^4 & x_{r,2}^3 & x_{r,2}^2 & x_{r,2} & 1 \\ \vdots & \vdots & \vdots & \vdots & \vdots & \vdots \\ x_{r,j}^5 & x_{r,j}^4 & x_{r,j}^3 & x_{r,j}^2 & x_{r,j} & 1 \end{pmatrix}}_{X} \underbrace{\begin{pmatrix} c_5 \\ c_4 \\ c_4 \\ c_3 \\ c_2 \\ c_1 \\ c_0 \end{pmatrix}}_{c_{pol}} = \underbrace{\begin{pmatrix} y_1 \\ y_2 \\ \vdots \\ y_j \end{pmatrix}}_{Y}. \tag{5-6}$$

The coefficients of the polynomial are found by solving

$$X^T X c_{pol} = X^T Y, \tag{5-7}$$

such that the following polynomial is obtained,

$$K(x) = c_5 x^5 + c_4 x^4 + c_3 x^3 + c_2 x^2 + c_1 x + c_0, \tag{5-8}$$

where, the longitudinal position x does not depend on time and K is the driven path of the preceding vehicle in the host frame of reference.

Calculating the errors

Now that a reference path is constructed, it is possible to obtain the lateral error $y_{e,i}$ and the heading error $\psi_{e,i}$. In this approach $y_{e,i}$, is defined as the shortest distance between the center of gravity **C** of the vehicle and the reference path, as depicted in Figure 2-2. The distance d from **C** to any point on $K(x)$ is defined as,

$$d = \sqrt{x^2 + y^2}. \tag{5-9}$$

The smallest distance $y_{e,i}$ is found by solving the minimisation problem where d is minimised as a function of x. The obtained x for which the d is minimised is denoted by x_{min}. This x_{min} can be approximated to be zero, effectively meaning that the shortest distance - which is the length of the vector from the path to C, in the direction perpendicular to the path - is approximated by the length of the vector from C to the path, in a direction perpendicular to the vehicle. In Appendix E, a numerical and a physical analysis are provided in which it is argued that the difference between the "true" error and the obtained error is negligible. This is desirable, as it reduces the computational effort required for finding the errors, as a result,

$$\begin{aligned} y_{e,i} &= K(x_{min}) \\ &= c_0. \end{aligned} \tag{5-10}$$

The heading error $\psi_{e,i}$ is the arctangent of the slope of the path (5-8) evaluated at x_{min}, which yields

$$\begin{aligned}\psi_{e,i} &= \arctan\left(\frac{\partial K(x_{min})}{\partial x}\right) \\ &= \arctan(c_1 + 2c_2 x_{min} + 3c_3 x_{min}^2 + 4c_4 x_{min}^3 + 5c_5 x_{min}^4),\end{aligned} \tag{5-11}$$

for $x_{min} = 0$ one obtains

$$\psi_{e,i} = \arctan\left(c_1\right). \tag{5-12}$$

Finally, the road curvature $\rho_{s,i}$ can also be extracted from the reconstructed path. This is useful as $\dot{\theta}_{s,i} \approx v_{x,i}\rho_{s,i}$ is used for feed-forward control. The curvature of a polynomial is defined as [39],

$$\begin{aligned}\rho_{s,i}(x) &= \frac{\frac{d^2K(x)}{x^2}}{\left(1 + \left(\frac{dK(x)}{dx}\right)^2\right)^{3/2}} \\ &= \frac{20c_5x^3 + 12c_4x^2 + 6c_3x + 2c_2}{\left(1 + \left(5c_5x^4 + 4c_4x^3 + 3c_3x^2 + 2c_2x + c_1\right)^2\right)^{3/2}},\end{aligned} \tag{5-13}$$

which at $x = x_{min} = 0$ yields,

$$\rho_{s,i} = \frac{2c_2}{(1 + c_1^2)^{3/2}}. \tag{5-14}$$

It should also be noted that in the computation of the heading error $\psi_{e,i}$ the body-slip angle β_i is not included. This is done since in practice it is not possible to measure this angle. Moreover, when operating in the linear tyre regime, β_i remains small. As a result, any estimates of this angle under these conditions will be heavily influenced by measurement noise. The inclusion of β_i will therefore not yield any significant gain in the accuracy of the estimate for $\psi_{e,i}$.

5-2 Adjustments for practical implementation

Upon implementation, it was discovered that the Park Assist System (PAS) has an input delay of 0.1 s. This delay will influence the string-stability properties of the closed-loop system, as the actuator will not be able apply the required input fast enough. Therefore, the $\mathcal{H}_\infty$ framework of Figure 5-3 was adopted, where $D_i(s)$ represents the delay in the frequency domain, such that,

$$D_i(s) = e^{-\tau_i s}, \tag{5-15}$$

with $\tau_i = 0.1$ representing the time delay. To express the delay as a transfer function, a second-order Padé approximation is taken [40]. Moreover, with $D_i(s)$ accounted for, one was

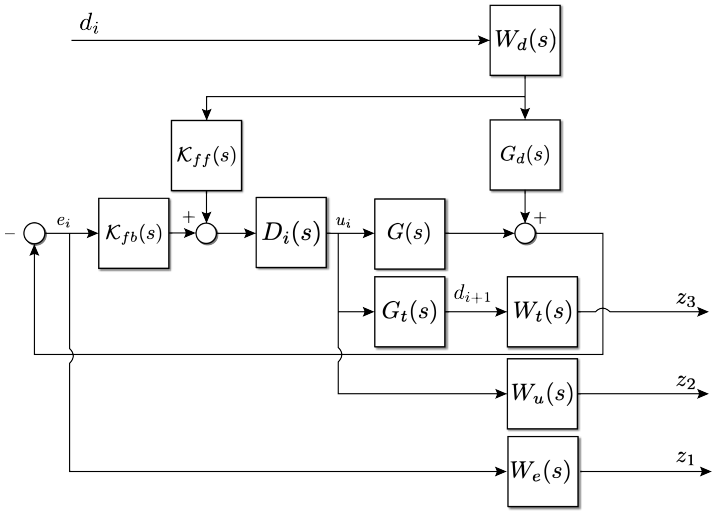

Figure 5-3: Block diagram of the system with input-delay.

not able to achieve strict string stability. In order to guarantee string stability, $W_d(s)$ in Figure 5-3 was introduced to capture the true disturbance acting on the plant. Since the frequency content of $\dot{\theta}_i$ is not expected to exceed 0.5 Hz [17], $W_d(s)$ is chosen to be a low-pass filter defined as

$$W_d(s) = \frac{1}{1 + \frac{s}{\omega_d}} \tag{5-16}$$

with $\omega_d = 2 \cdot 2 \cdot \pi$. Furthermore, in the control architecture deployed in the vehicles, the control signal u_i is saturated before it is sent to the actuator. Thus, for large control inputs, the signal sent to the steering wheel will not match the signal produced by the controller. To prevent high control inputs the input weighting filter was adjusted such that $W_u = 1$. The synthesised controller yields a closed-loop system with $\|N\|_{\mathcal{H}_\infty} = 1$, such that string stability is obtained. This controller was then reduced to a fourth-order transfer function, and the poles and zeros outside the frequency spectrum of interest were removed. Moreover, the controller was discretised with a sampling time $t_s = 0.01\,\text{s}$ such that the controller of Figure 5-4 was obtained, which is given by:

$$\begin{aligned}
\mathcal{K}_{ff}(z) &= \frac{0.1916z^2 - 0.2667z + 0.0805}{z^2 - 1.749z + 0.7757} \\
\mathcal{K}_{fb,y_e}(z) &= \frac{0.04867z^3 - 0.1274z^2 + 0.1109z - 0.0322}{z^4 - 3.338z^3 + 4.208z^2 - 2.384z + 0.5149} \\
\mathcal{K}_{fb,\psi_e}(z) &= \frac{0.0172z^3 - 0.04458z^2 + 0.03845z - 0.01105}{z^4 - 3.338z^3 + 4.208z^2 - 2.384z + 0.5149}.
\end{aligned} \tag{5-17}$$

Compared to the controller of (3-42), the controller of (5-17) has the same steady-state gain for $\mathcal{K}_{ff}$. Moreover, the steady-state gains for both $\mathcal{K}_{fb,y_e}$ and $\mathcal{K}_{fb,\psi_e}$ are larger in magnitude than those of (3-42). Furthermore, the derivative actions for all three controllers of (5-17) are smaller in magnitude, this is a result of the constraint imposed by choosing $W_u = 1$.

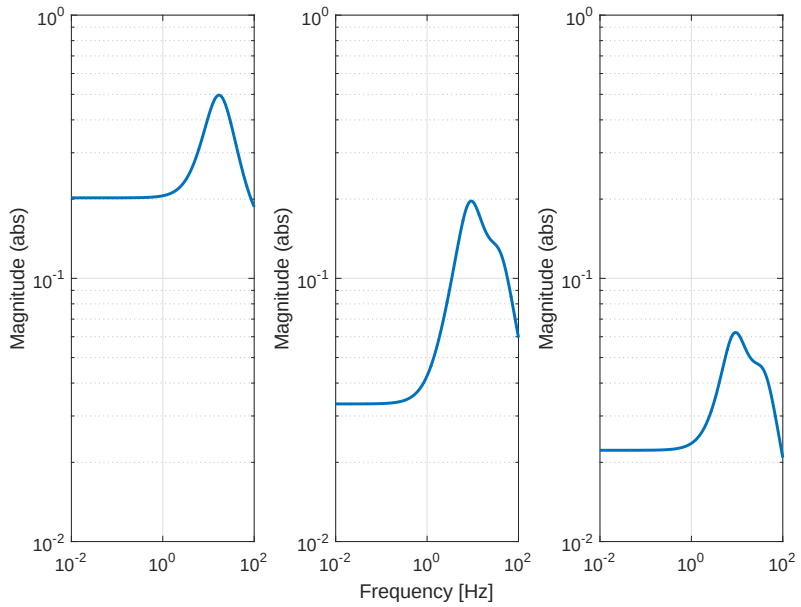

Figure 5-4: Frequency responses for the designed controller, from left to right $|\mathcal{K}_{ff}(z)|$, $|\mathcal{K}_{fb,y_e}(z)|$, $|\mathcal{K}_{fb,\psi_e}(z)|$.

5-3 Experiments

The controller is evaluated in practice on TNO Carlab. The Carlab is a Toyota Prius, which is equipped with instrumentation for cooperative driving, such as a real-time computing platform (Speedgoat) for rapid control prototyping, vehicle sensors (radar, camera, wireless communication, gyroscope, accelerometer, wheel speed encoders and GPS) for measuring, and a driver Human Machine Interface (HMI).

Figure 5-5, shows a close-up of the trunk of the test vehicle, where the hardware is located. The real-time platform is a computer equipped with a real-time operating system, on which algorithms developed in Matlab and Simulink can be run in real-time. The real-time platform is connected to the Vehicle Gateway through a Controller Area Network (CAN) bus, such that it is possible to communicate with the sensors and activate the actuators. Moreover, the real-time platform is connected via an Ethernet connection for communication with the HMI platform. The ITS-G5 Gateway module enables the wireless communication with other vehicles. Finally, the GPS sensor tracks the global position of the vehicle.

5-3-1 Experimental Results

Lane keeping

To validate the path-tracking performance of the designed controller, first a lane-keeping experiment was performed. This test was executed at Aldenhoven Testing Center in Germany (Figure 5-6). The lane-keeping algorithm deployed at TNO generates a reference path in the middle of the lane in the form of a polynomial similar to the vehicle following case. Therefore,

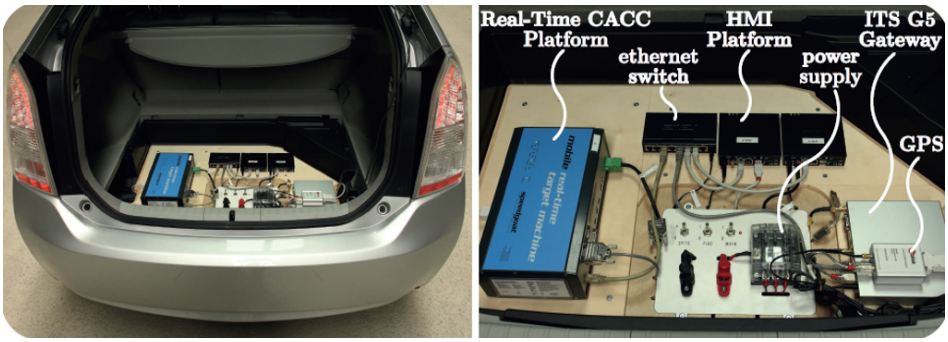

Figure 5-5: Overview (left) and close-up (right) of the vehicle instrumentation in the trunk [1].

Figure 5-6: Aldenoven Testing Center of RWTH Aachen University GmbH [2].

the path-following controller could be used for this application as well. In this experiment, the host vehicle was driven at a velocity of $65\,\mathrm{km\,h^{-1}}$, starting at an offset from the road's centreline. The velocity, at which the test was performed, was not the same as the design velocity; this should not cause a problem for lane-keeping, since in Chapter 4 it was concluded that path following is guaranteed in the face of uncertainty/variation in $v_{x,i}$.

Figure 5-7, presents the gathered experimental data. Here the position of the vehicle with respect to the centreline is given. The longitudinal coordinate x is approximated through integration of $\dot{x}_i = v_{x,i}\cos(\psi_i)$, which is the longitudinal kinematic equation of motion for a unicycle model [41], this method is often referred to as dead reckoning. The lateral position of the vehicle is obtained by subtracting the lateral error from the reference centerline defined at $y_{ref} = 0$, such that, $y_i = y_{ref} - y_{e,i} = -y_{e,i}$. Finally the measurements of the steering input, lateral error, reference curvature, and heading error are included as a function of time.

From the y-position and the lateral error $y_{e,i}$, it can be observed that the controlled vehicle converges slowly to the center of the lane, with an average steady-state error of approximately $0.05\,\mathrm{m}$. This is to be expected, since during the design of the controller it was stated that a maximum amplification, from the low-frequency disturbances of d_i to the error $y_{e,i}$, of three time was allowed. From the signal of the angular rate of orientation of the road, it can be observed that despite being on a straight path $\dot{\theta}_{s,i} \neq 0$. Which was caused by the camera not being able to detect the lanes reliably due to the weather conditions during testing. On a

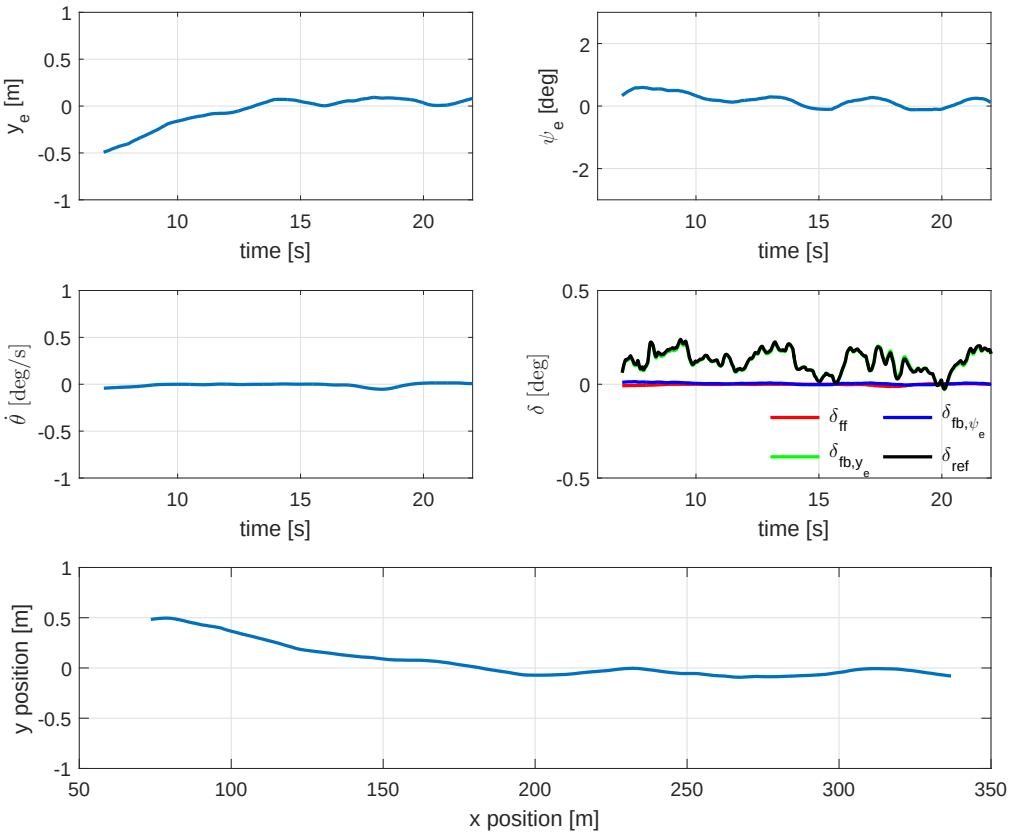

Figure 5-7: Experimental data of a lane-keeping test performed at $v_{x,i} = 65\,\mathrm{km\,h^{-1}}$ with an initial offset of approximately $0.5\,\mathrm{m}$.

longer path this error should eventually converge to zero. Moreover, it can be observed that the control input $\delta_{ref} \approx \delta_{fb,y_e}$, since $\dot{\theta}_{s,i} \approx 0$ and $\psi_{e,i}$ were relatively small, the control signals δ_{ff} and δ_{fb,ψ_e} were relatively small. If a faster response is desired, a controller with a higher bandwidth can be designed. However, as has been stated during controller design, this comes at the cost of string stability.

A similar scenario was simulated using the simulation model presented in Section 4-5, such that the test scenario can be approximated. Similarly, the longitudinal velocity $v_{x,i} = 65\,\mathrm{km\,h^{-1}}$ and the offset is approximately $0.5\,\mathrm{m}$. The response of the system is given in Figure 5-8, where the lateral error $y_{e,i}$, the heading error $\psi_{e,i}$, and the global position are plotted. In this simulation the conditions are assumed to be ideal, such that no noise was present in the system. The response in the simulation is very similar to that of the experiment, i.e., slow convergence with approximately the same settling time and near zero heading error. The results of the experiment are more oscillatory, this is due to the presence of measurement noise, which gets amplified by the derivative action.

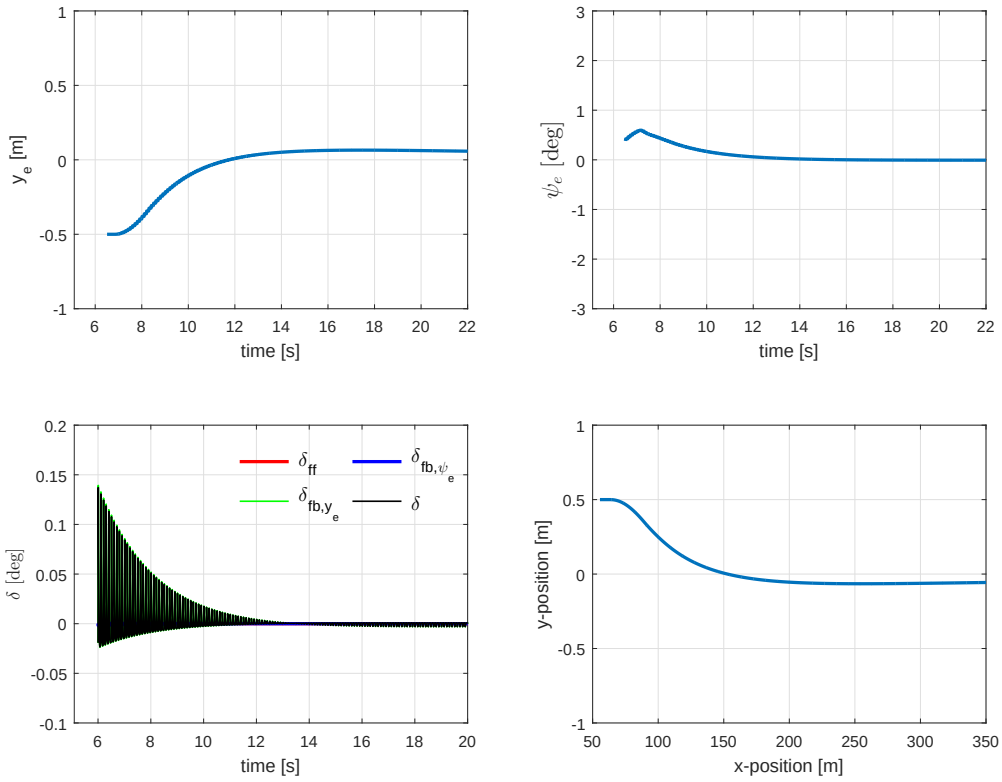

Figure 5-8: Simulation data of the same lane-keeping test performed at $v_{x,i} = 65\,\mathrm{km\,h^{-1}}$ with an initial offset of approximately $0.5\,\mathrm{m}$.

String stability

Now that the path-following objective has been verified by using lane-keeping, it is desired to test the string-stability properties of the controller. This can be done by means of following a predefined lane-change or a sinusoidal path driven by the preceding vehicle; as this means that $\dot{\theta}_{s,i}$ will not be constant, thus a conclusion can be drawn about string stability.

Unfortunately during the experimental validation vehicle following could not be tested. This has been identified to not be a shortcoming of the designed controller, but rather due to inaccurate path reconstruction. Namely the same phenomenon occurred using the controller developed at TNO, which has been confirmed to have fulfilled the vehicle-following objective at previous times; it was thus concluded that the path-generation algorithm was not functioning properly.

To still be able to draw a conclusion about string stability a lane-change manoeuvre was performed using a predefined reference path. In here, the reference path is calculated based on the velocity of the vehicle at which the lane-change manoeuvre is initiated, such that $\dot{\theta}_s$ has a period of 7.5 s. This experiment was conducted at TNO's Vehicle Hardware In the Loop (VeHIL) facility, which has an approximately 80 m long test road with lane markings, see Figure 5-9 (lane markings not visible). This stretch of road is too small for any manoeuvres at $v_x = 70\,\mathrm{km\,h^{-1}}$, therefore, the operating velocity had to be adjusted to $v_x = 40\,\mathrm{km\,h^{-1}}$. For this experiment to yield conclusive results, a controller had to be tuned for this specific velocity. At lower velocities the vehicle dynamics have more damped characteristics, as a result, less additional damping is required to obtain string stability. Therefore, the weighting filter $w_{e,22}$ was adjusted, it was found that $w_{e,22} = 10$ yields a string-stable closed-loop system with $\|N\|_{\mathcal{H}_\infty} = 1$. Reducing the generated controller to a fourth-order transfer function, and discretising it with a sampling time of $t_s = 0.01\,\mathrm{s}$ yields the controller depicted in Figure 5-10, which is given by:

$$\begin{aligned}
\mathcal{K}_{ff}(z) &= \frac{0.11869(z+1.253)(z-0.9237)(z^2-1.798z+0.8185)}{(z^2-1.853z+0.8616)(z^2-1.323z+0.4936)} \\
\mathcal{K}_{fb,y_e}(z) &= \frac{-0.0007924(z-30.73)(z-0.9957)(z^2-1.74z+0.7761)}{(z^2-1.93z+0.932)(z^2-1.418z+0.5382)} \\
\mathcal{K}_{fb,\psi_e}(z) &= \frac{0.0009283(z+11.9)(z-0.9746)(z^2-1.759z+0.7893)}{(z^2-1.93z+0.932)(z^2-1.418z+0.5382)}.
\end{aligned} \tag{5-18}$$

In comparison to the controllers designed for $v_x = 70\,\mathrm{km\,h^{-1}}$, the steady-state gain of the feedforward controller is larger, since at lower velocities larger steering angles are permitted, as they will not result in the system becoming unstable. Moreover, the derivative action is smaller, which ties in to the expectation that less additional damping is required at lower velocities.

Two lane-change manoeuvres were performed to experimentally validate the string-stability properties of the controller. The results of the first lane-change manoeuvre, performed at $v_x = 30\,\mathrm{m\,s^{-1}}$, is depicted in Figure 5-11. In here, the reference path is a polynomial K whose coefficients c_i, with $i \in \{1, 2, 3, 4, 5\}$, are determined such that the a lane-change manoeuvre is generated with $\dot{\theta}_s$ having a period of 7.5 s and a velocity-appropriate magnitude. It can be observed that the vehicle tracks the reference path smoothly without any overshoot. To

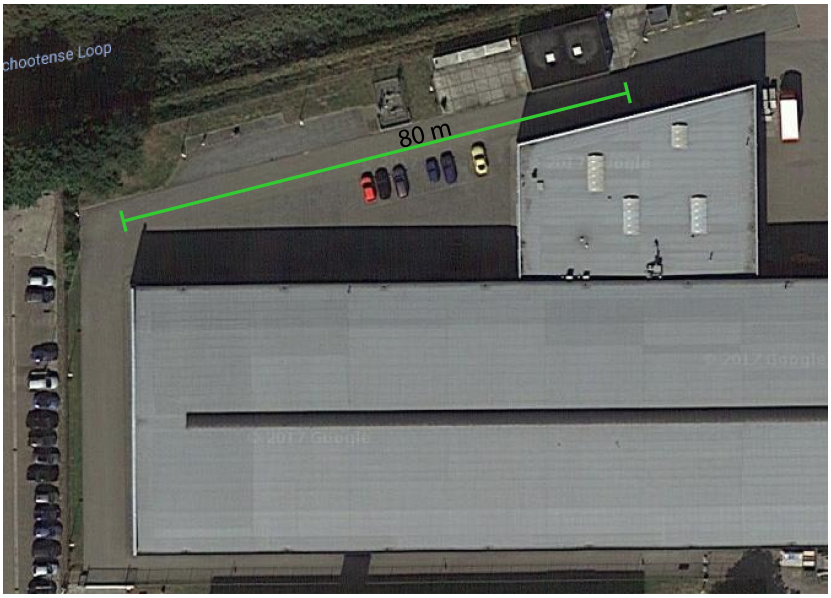

Figure 5-9: Test road at TNO's VeHIL facility.

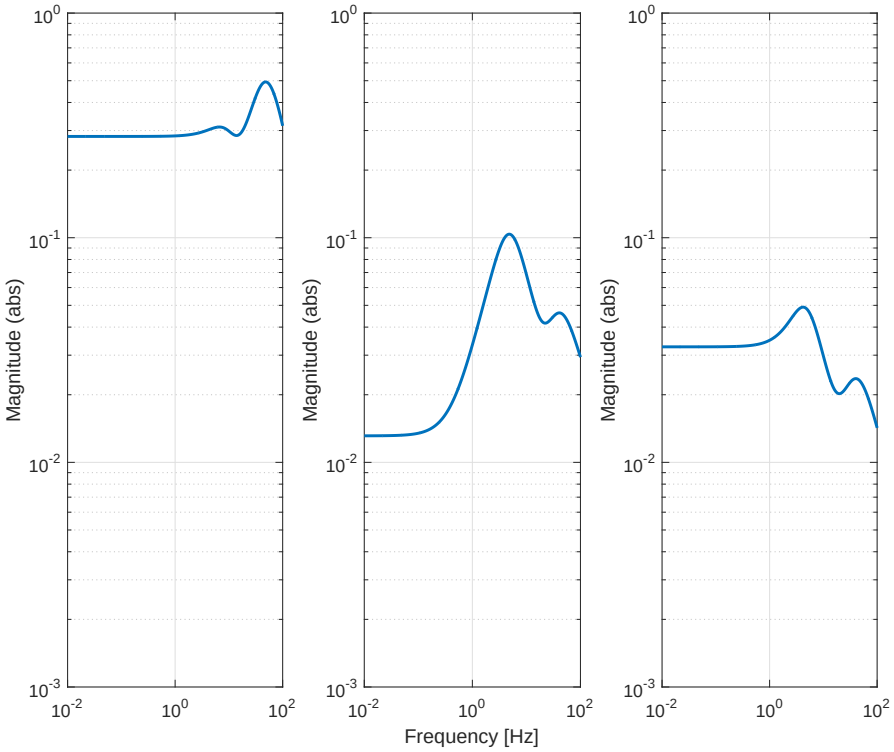

Figure 5-10: Frequency responses for the designed controller, from left to right $|\mathcal{K}_{ff}(z)|$, $|\mathcal{K}_{fb,y_e}(z)|$, $|\mathcal{K}_{fb,\psi_e}(z)|$.

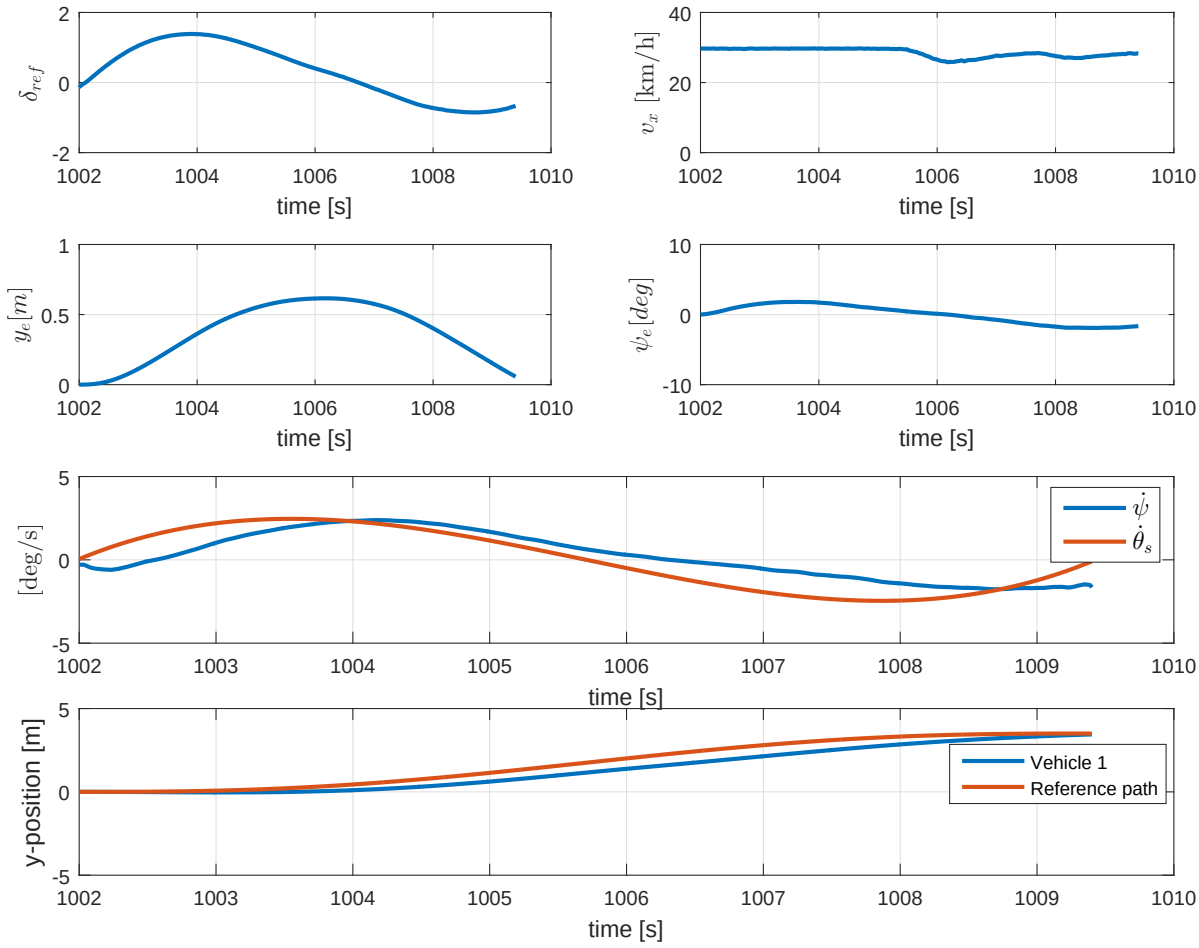

Figure 5-11: Experimental data of a lane-change manoeuvre performed at $v_x = 30\,\mathrm{km\,h^{-1}}$.

analyse the string stability properties of the system, $\dot{\theta}_s$ was compared to $\dot{\psi}$ as it is not possible to obtain $\dot{\beta} + \dot{\psi}$. From these signals it can be observed that the magnitude of $\dot{\psi}$ is smaller than or equal to the magnitude $\dot{\theta}_s$ at all times, meaning that string stability is obtained. Moreover, from y_e and ψ_e nearing zero, it can be concluded that the path-following objective is fulfilled.

The second experiment was conducted at design velocity, i.e., $v_x = 40\,\mathrm{km\,h^{-1}}$. The results of this experiment are as depicted in Figure 5-12. Here it can be observed that the lane-change manoeuvre is not completed, this is caused by the road not being long enough, forcing the driver to brake and manually take over before reaching the end of the manoeuvre. However, from the results obtained from driving at $v_x = 30\,\mathrm{km\,h^{-1}}$ it was confirmed that path following was obtained, therefore, it is expected that for a long enough road the manoeuvre will be completed. From these results, it is possible to draw a conclusion about the string-stability properties of the controller. In the plot of $\dot{\theta}_s$ and $\dot{\psi}$, it can be observed that for the part where the controller is actively steering, the response of $\dot{\psi}$ is damped and smaller than the $\dot{\theta}_s$,

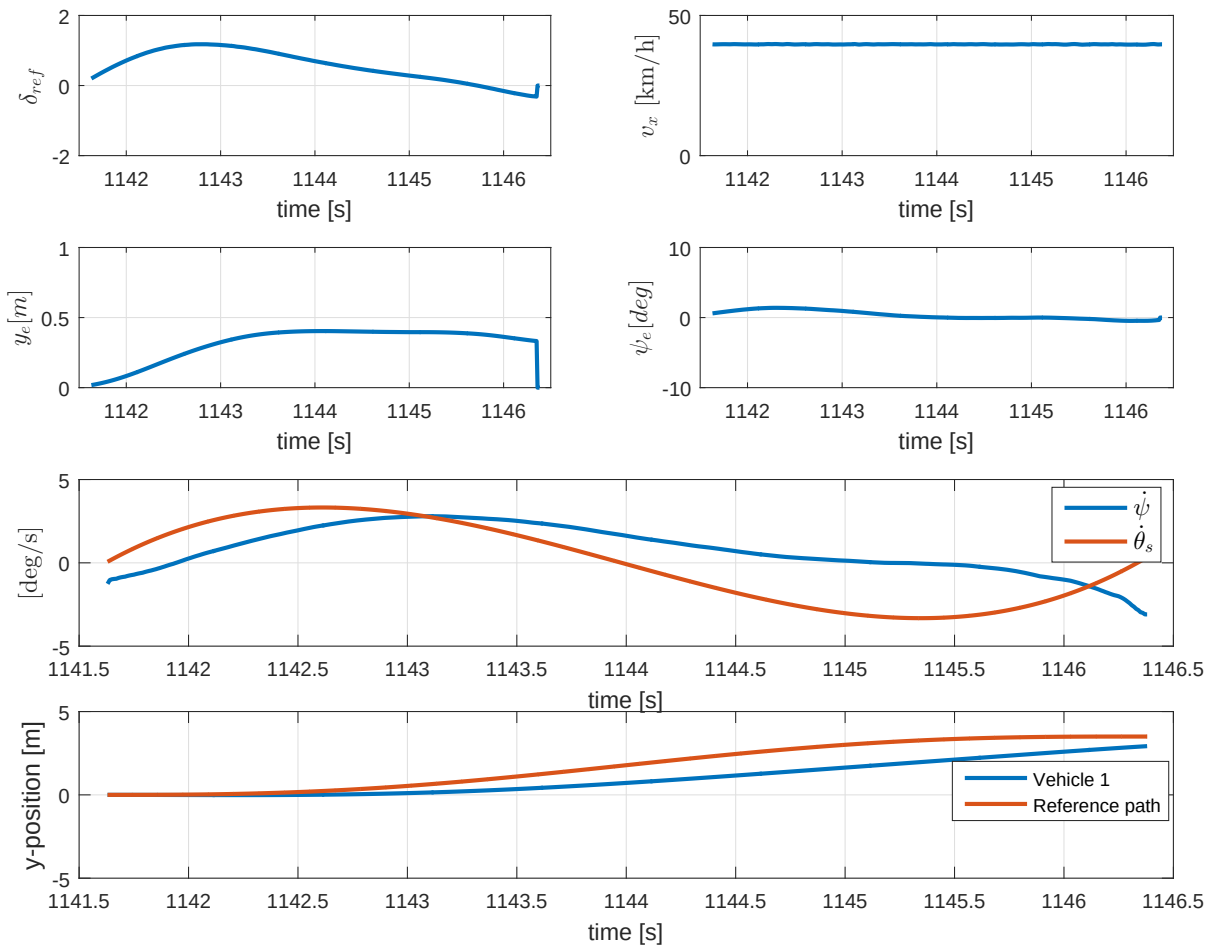

Figure 5-12: Experimental data of a lane-change manoeuvre performed at $v_{x,i} = 40\,\mathrm{km\,h^{-1}}$.

from which it can be concluded that string-stable behaviour is obtained. To further confirm this result it is recommended to conduct this experiment at a larger stretch of road, that way the behaviour of the vehicle at the last part of the lane-change manoeuvre is also taken into account.

5-4 Discussion

In this chapter, the practical implementation of the controller on an experimental set-up has been discussed. Here, the path-following objective has been verified by means of lane keeping. For this experiment, the vehicle started at an offset of 0.5 m from the lane's centreline. The vehicle was able to converge towards the lane's centreline and maintain this position, with an average offset of 0.05 m. From the obtained results, it could be concluded that the path-following objective as defined in Chapter 3 has been fulfilled. These results have been validated

in simulation, where for a similar scenario, comparable results were obtained.

Unfortunately, it was not possible to test the string-stability properties for the designed controller using vehicle following, as the path generation algorithm was not functioning properly at the time of the experiments. Instead, a reference trajectory was provided to the vehicle, such that a lane-change manoeuvre was conducted. Due to the constraints imposed by the location of testing, the experiments were conducted at low velocities, i.e., $v_x = 30\,\mathrm{km\,h^{-1}}$ and $v_x = 40\,\mathrm{km\,h^{-1}}$. To produce meaningful results regarding string stability, a controller was tuned for a design velocity of $v_x = 40\,\mathrm{km\,h^{-1}}$. The experiments at $v_x = 30\,\mathrm{km\,h^{-1}}$ showed accurate and smooth path tracking, with the errors y_e and ψ_e converging to zero. Moreover, the response of $\dot{\psi}$ showed string-stable behaviour. However, since this experiment was not conducted at design velocity, the results for string stability are not conclusive.

In order to do that, the string-stability properties were validated at design velocity $v_x = 40\,\mathrm{km\,h^{-1}}$. The road used for testing was not long enough to complete the entire lane-change manoeuvre, as a result, only part of this manoeuvre was performed. In the part where the controller was active, smooth path following was obtained, combined with the results obtained at $v_x = 30\,\mathrm{km\,h^{-1}}$ it is expected that the path would have been accurately tracked had the manoeuvre been completed. Moreover, string-stable behaviour was obtained, with $\dot{\psi}$ being smaller than $\dot{\theta}_s$ at all times.

Overall, the experimental results illustrated the possibility of obtaining a string-stable path-following controller using $\mathcal{H}_\infty$ optimisation control. To further solidify these results it is recommended to perform more tests, such that the experiments can be performed for different manoeuvres and at higher velocities.

Chapter 6

Conclusions and recommendations

6-1 Conclusions

Recent advancements in the field of Intelligent Transportation Systems (ITS) have led to an acceleration in the development of smart driving solutions. One of these solutions is vehicle platooning, which has the potential to increase road capacity and reduce fuel consumption. In a platoon, vehicles drive cooperatively in an automated manner with small inter-vehicular distances whilst maintaining a constant velocity. Here, automation is required such that safety of the passengers is not compromised. An important property of such an interconnected system is string stability, which characterises the propagation of the effect of disturbances over the interconnected system. A string-stable system prevents the amplification of system states in the presence of noise, such as the acceleration, velocity and the inter-vehicular distance. Hence the reason why this property is sought after for cooperative driving. Most advancements in research regarding this topic have been done in the context of longitudinal string stability, due to the nature of the application. However, to enable driving at smaller inter-vehicle distances and higher velocities, one cannot rely on the human driver to react quickly enough to perform certain steering manoeuvres such as a lane-change or steady-state cornering. Therefore, lateral automation has to be implemented as well in order to enable platooning in practice.

The main contribution of this MSc thesis was to formulate and provide a lateral control strategy that achieves string stability of homogeneous platoons. Here, an $\mathcal{H}_\infty$ optimal control strategy was proposed as a solution to the defined problem, which proved to be useful for obtaining a linear controller that guarantees string stability *a-priori*. Moreover, it was possible to obtain both path following and string stability simultaneously, which is compared to other linear control methods a significant benefit. However, obtaining a controller with the desired properties requires significant tuning of the weighting functions assigned to the outputs of the control problem. The amount of weighting functions required, increased the degrees of freedom to this control problem, which added to the complexity of the problem. Finally, the experimental results demonstrated the ability to obtain a controller that fulfils both the path-following and the string-stability objectives.

In Chapter 1, it was argued that for lateral control at smaller inter-vehicular distances, it would be more advantageous to use a path-following approach, as opposed to the more common vehicle-following method, since this avoids the corner-cutting phenomenon, thereby preventing potential hazardous situations. Moreover, a generic definition for string stability was introduced, based on the concept of $\mathcal{L}_p$ string stability. In a review of the limited amount of publications available for this topic, an investigation was made on how to assess the string-stability condition in the lateral sense. From this assessment, it was concluded that the ratio between the curvature of the path driven by the following vehicle and the preceding vehicle is an appropriate measure for string stability.

Based on the aforementioned information, Chapter 2 opted to develop an error model for a controlled path-following vehicle. Here it was shown that a linearised bicycle model with a linear tyre model is sufficient to describe the lateral dynamics. Moreover, it was argued that, in order to follow a path, one needs to distinguish two types of errors, those being a lateral deviation and a heading error. Finally, using the error model, a system model was developed to relate the states of the preceding vehicle with the reference path. This interconnection was realised by relating the angular velocity of the road orientation, to the states of the preceding vehicle. It was found however that there is a time delay Δt between the system states of the preceding and the following vehicle, as a result of the constant separation distance.

In Chapter 3, this system model was used to create a linear homogeneous platoon model, such that the string stability conditions could be defined. Here it was shown that it is possible to exclude the aforementioned delay Δt during string-stability analysis, without consequence. The prerequisite for this condition to hold is that the time gap Δt should remain constant, which in the case of platooning is reasonable to assume. The time delay will only change during critical scenarios, such as harsh braking for emergency scenarios. This results in a platoon model where all the vehicles are virtually driving the same path at the same time. This platoon model was adopted into the $\mathcal{H}_\infty$ control framework, as it provides the means for multiple input controller design. Moreover, its properties allowed for the explicit inclusion of the $\mathcal{L}_2$ string-stability requirements a-priori, whilst enforcing the path-following condition. By selecting the appropriate input and output signals and their respective weighting filters, strict $\mathcal{L}_2$ string stability was obtained for the control system.

The use of the $\mathcal{H}_\infty$ control framework allows for performing sensitivity analysis against uncertainties. In Chapter 4, the designed controller was analysed against both parametric and dynamic uncertainties. It was concluded that the designed controller is not robust against uncertainties since string stability could not be guaranteed, however, path-following was still maintained. The results obtained in the frequency domain were validated using time-domain simulations, where the $\mathcal{H}_\infty$-controller was compared to the controller currently implemented at TNO. The transient response of both controllers to an initial condition perturbation was first investigated, such that the difference in behaviour could be identified. In a lane-change scenario, the string-stability properties of both controllers were investigated. Here it was indeed confirmed that the $\mathcal{H}_\infty$-controller yields a string-stable system, implying a significant improvement over the existing controller. At parameter values other than the nominal values, it appeared that, despite the $\mathcal{H}_\infty$-controller not being robust to this type of uncertainty, an overall better response than the state-feedback controller regarding string stability was obtained. This showed that even in an uncertain platooning scenario, it would be more beneficial to use the $\mathcal{H}_\infty$-controller.

Finally, the designed controller was experimentally validated, using path-following. The controller was adjusted to account for the actuator delay, and the control architecture used for the experimental set-up. First, the controller was used in a lane-keeping scenario, since lane-keeping is done by means of a similar path-following algorithm. From the experimental results it was concluded that the path-following objective of the controller was met. This conclusion was confirmed by having the data obtained from simulations match the loggings. Unfortunately, due to an unsolved issue in the path-generation algorithm for vehicle following, it was not possible to perform any vehicle-following experiments. Instead the string-stability properties were tested by making the vehicle follow a predefined lane-change manoeuvre. The results showed that the controller yields lateral string-stable behaviour.

6-2 Recommendations

In this work, a method to obtain a controller suitable for platooning applications was presented. Due to problems with the path-generation algorithm and time constraints, string stability was tested using a reference lane-change manoeuvre. Although string stability was concluded, the location of testing limited the possible testing scenarios and maximum velocities. To obtain better results it is therefore recommended to perform more tests. Moreover, it is also desired to test the performance using vehicle following, as it is still required for lateral automation within platoons.

In the experimental implementation of the controller, the actuator delay was included in the control framework such that it could be accounted for. To gain more insight into the influence of the actuator delay on string stability, a more in-depth analysis on the influence of the actuator delay on the string stability of the system is desired.

The vehicle model used in this work considers the problem of lateral and longitudinal dynamics to be decoupled for driving at low accelerations and velocities. This allows to treat the longitudinal and lateral control problem separately, and, as a result, the string-stability problem can also be treated separately. However, this limits the possible scenarios for platooning; in other words, including the longitudinal dynamics would result in a more generic platooning scenario, such as, for obstacle avoidance. The ability of the $\mathcal{H}_\infty$-control framework to handle multivariable systems could enable the design of a controller that takes both dynamics into account. Therefore, this could be the natural evolution in controller design in automation for platooning.

Moreover, the designed controller was linear, designed for a fixed velocity. Hence, string stability can only be guaranteed for the design velocity of choice, as was concluded from the uncertainty analysis. The use of robust control methods is not recommended as string stability for all velocities can then only be achieved at the cost of the path-following performance. Instead it is suggested to use a Linear Parameter Varying (LPV) controller instead. For instance, one could use a grid-based approach or a Linear Fractional Transformation (LFT) method to approximate the model non-linearity in the velocity, which then can be used to generate a parameter varying controller, using a framework similar to the one presented in this thesis. This controller should potentially be able to guarantee string stability for a set of parameters with bounded parameter rates. It is also possible to use constrained Model Predictive Control, such that actuator saturation is taken into account.

Finally, the results of this thesis only apply to homogeneous platoons, assuming identical dynamic behaviour for all platoon members. However, in practice, this will almost never be the case. One way to approach this problem is to treat heterogeneity as uncertainty, or design a controller that yields identical dynamic behaviour regardless of system parameters. It is highly recommended to investigate this topic, since it essential for the practical realisation of platooning.

Appendix A

Remark on the $\mathcal{H}_\infty$orm

In analysing string stability the $\mathcal{H}_\infty$ norm is a recurring notion. There exist different interpretations in literature, this section will serve as a clarification of the interpretation used. The infinity norm used in this section is a system norm. System norms predominantly focus on transfer functions. The H_∞ or $\mathcal{H}_\infty$ norm of a transfer function $G(s)$ can be defined as follows,

$$\begin{aligned} \|G(s)\|_{\mathcal{H}_\infty} &:= \sup_{Re(s)>0} \bar{\sigma}(G(s)) \\ &= \sup_{Re(s)>0} \max_i \sqrt{\lambda_i(G(s)^H G(s))} \\ &= \sup_{Re(s)>0} \|G(s)\|_{i_2}. \end{aligned} \tag{A-1}$$

Here, $\bar{\sigma}(G(s))$ denotes the largest singular value of matrix $G(s)$ and $\|G(s)\|_{i_2}$ the induced matrix 2-norm [26]. The induced matrix 2-norm for a matrix A is defined as follows,

$$\begin{aligned} \|A\|_{i_2} &:= \max_{u\neq 0} \frac{\|Au\|_2}{\|u\|_2} \\ &= \max_{u\neq 0} \frac{\sqrt{u^H A^H A u}}{\sqrt{u^H u}} \\ &= \max_i \sqrt{\lambda_i(A^H A)} \\ &= \bar{\sigma}(A). \end{aligned} \tag{A-2}$$

Here, $\|u\|_2$ denotes the vector norm of u, $\lambda_i(A^H A)$ denotes the i-th eigenvalue of matrix $A^H A$. Given that $G(s)$ is stable and causal, $\bar{\sigma}(G(s))$ can be computed along the imaginary axis such that $\sup_{Re(s)>0} \bar{\sigma}(G(s)) = \sup_{\omega\in\mathcal{R}} \bar{\sigma}(G(j\omega))$.

Appendix B

The Single-Track Bicycle Model

This section presents the derivation of the equations of motion for the single track bicycle model; such that the lateral dynamics can be described. An illustration of the bicycle model is given in Figure B-1, where the physical parameters are included. Here F_i with $i \in \{xr, xf, yr, yf\}$, represents the external forces acting on the vehicle, which are generated by the slip between tyre and road. The front and rear tyre slip angles are denoted by α_f and α_r, respectively, β denotes the the vehicle's body slip angle, and δ denotes the steering angle. Furthermore, L_r and L_f denote the distance from the vehicle's center of gravity to the rear and front axle, respectively. Finally, $\vec{V}_r$ and $\vec{V}_f$ represent the velocity vectors of the rear and front tyre, respectively.

For the bicycle model as presented in Figure B-1 two sets of reference frames can be defined using a rectangular coordinate system. Those are defined as the space fixed reference frame $P^O = \{\mathbf{O}, \underline{\vec{e}}^o\}$ and the body-fixed frame $P^C = \{\mathbf{C}, \underline{\vec{e}}^c\}$. Here $\underline{\vec{e}}^i$, $i \in [o, c]$, represents the coordinate system as described by a set of orthogonal unit vectors,

$$\underline{\vec{e}}^i = \begin{pmatrix} \vec{e}_x^i & \vec{e}_y^i \end{pmatrix}^T. \tag{B-1}$$

The origin C of the body-fixed frame of reference is defined at the vehicle's center of gravity, and the unit vector $\vec{e}_x^c$ is oriented along the vehicle's longitudinal axis at angle ψ with respect to $\vec{e}_x^o$. Therefore, the body-fixed frame of reference can be transformed to the space fixed frame of reference using the rotation matrix $R(\psi)$ around the z-axis, yielding,

$$\begin{aligned} \underline{\vec{e}}^c &= R(\psi)^T \underline{\vec{e}}^o \\ &= \begin{pmatrix} \cos\psi & \sin\psi \\ -\sin\psi & \cos\psi \end{pmatrix} \underline{\vec{e}}^o. \end{aligned} \tag{B-2}$$

Furthermore, the position of C is defined as,

$$\vec{r}_c = \begin{pmatrix} x & y \end{pmatrix} \underline{\vec{e}}^o, \tag{B-3}$$

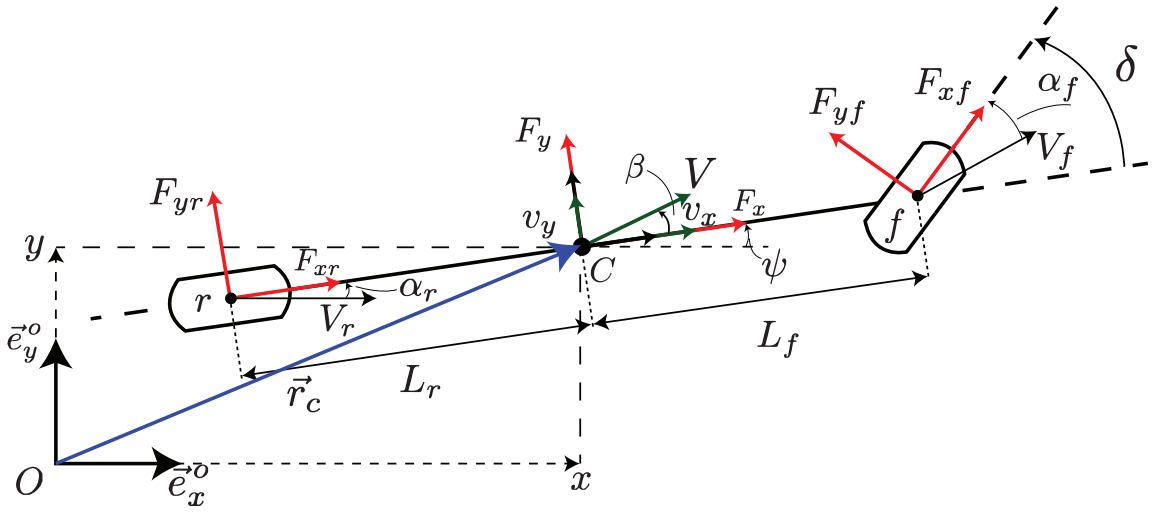

Figure B-1: Dynamic Bicycle model

the velocity as,

$$\begin{aligned}\dot{\vec{r}}_c &= \begin{pmatrix}\dot{x} & \dot{y}\end{pmatrix}\underline{\vec{e}}^o \\ &= \begin{pmatrix}v_x & v_y\end{pmatrix}\underline{\vec{e}}^c.\end{aligned} \tag{B-4}$$

The acceleration is obtained by taking the derivative of the velocity with respect of time and applying the chain rule, giving

$$\ddot{\vec{r}}_c = \begin{pmatrix}v_x & v_y\end{pmatrix}\dot{\underline{\vec{e}}}^c + \begin{pmatrix}\dot{v}_x & \dot{v}_y\end{pmatrix}\underline{\vec{e}}^c. \tag{B-5}$$

Using the relations in Equation (B-2) and the chain rule $\dot{\underline{\vec{e}}}^c$ can be expressed as:

$$\begin{aligned}\dot{\underline{\vec{e}}}^c &= \dot{R}(\psi)^T\underline{\vec{e}}^o + R(\psi)^T\underline{\vec{e}}^o \\ &= \dot{\psi}\begin{pmatrix}0 & 1\\ -1 & 0\end{pmatrix}\begin{pmatrix}\cos\psi & \sin\psi\\ -\sin\psi & \cos\psi\end{pmatrix}\underline{\vec{e}}^o \\ &= \begin{pmatrix}0 & \dot{\psi}\\ -\dot{\psi} & 0\end{pmatrix}\underline{\vec{e}}^c.\end{aligned} \tag{B-6}$$

Here $\dot{\psi}$, represents the angular velocity of the vehicle often referred to as the yaw rate. Substitution of Equation (B-6) in Equation (B-5), the following expression for the acceleration is obtained:

$$\ddot{\vec{r}}_c = \begin{pmatrix}\dot{v}_x - \dot{\psi}v_y & \dot{v}_y + \dot{\psi}v_x\end{pmatrix}\underline{\vec{e}}^c. \tag{B-7}$$

Since the expressions for the acceleration have now been obtained the equations of motion can now be obtained. Using Newton's second law,

$$m\ddot{\vec{r}}_c = \sum \vec{F}_c, \tag{B-8}$$

with m being the mass of the vehicle. Equation (B-8) can be expressed in terms of its longitudinal and lateral components, yielding

$$\begin{aligned} m(\dot{v}_x - \dot{\psi} v_y) &= \sum F_x \\ m(\dot{v}_y + \dot{\psi} v_x) &= \sum F_y. \end{aligned} \tag{B-9}$$

If small angles are assumed for δ, the small angle approximation can be used, such that $\sin\delta \approx \delta$ and $\cos\delta \approx 1$. The sum of all longitudinal forces can then be written as $\sum F_x = F_{xr} + F_{xf}$, analogously the sum of all lateral forces $\sum F_y = F_{yr} + F_{yf}$. The forces exert a moment on the vehicle around its center of gravity C. The vehicle has a moment of inertia I_z around the z-axis, which is pointing out of the paper, i.e., $\vec{e}_z^{\,c} = \vec{e}_x^{\,c} \times \vec{e}_y^{\,c}$. Therefore, the sum of the yaw moments,

$$I_z \ddot{\psi} = \sum M_z \tag{B-10}$$

which is equal to $L_f F_{yf} - L_r F_{yr}$. The equations harnessing the vehicle's motion can then be written as,

$$\begin{aligned} m(\dot{v}_x - \dot{\psi} v_y) &= F_{xr} + F_{xf} \\ m(\dot{v}_y + \dot{\psi} v_x) &= F_{yr} + F_{yf} \\ I_z \ddot{\psi} &= L_f F_{yf} - L_r F_{yr} \end{aligned} \tag{B-11}$$

The lateral forces in Equation (B-11) are generated by the tyres, and are a function of the slip angle α_i with $i \in \{r, f\}$.

Appendix C

Analysis of the TNO-controller

In this chapter a comparison between the magnitudes of the controller gains of the TNO-controller and the $\mathcal{H}_\infty$ controller is given. From Figure C-1 it can be observed that the steady-state feedforward gain of the $\mathcal{H}_\infty$ controller is approximately equal to the feedforward gain of the TNO controller. Moreover, a the steady-state gain of the control action on y_e of the $\mathcal{H}_\infty$ controller is approximately a factor three smaller than the gain of the TNO controller. Finally, the steady-state gain of the $\mathcal{H}_\infty$ controller on ψ_e is a factor ten smaller than the TNO-controller.

String stability analysis

For the model in (4-7), one can define

$$\begin{aligned} G_a(s) &= C_a(sI - A_a)^{-1}B_{a,1} \\ G_{a,d}(s) &= C_a(sI - A_a)^{-1}B_{a,2}, \end{aligned} \tag{C-1}$$

with

$$C_a = \begin{pmatrix} 0 & 0 & 1 & 0 & 0 & 0 \\ 0 & 0 & 0 & 1 & 0 & 0 \end{pmatrix}, \tag{C-2}$$

and $B_{a,1} = \begin{pmatrix} 0 & 0 & 0 & 0 & 0 & \omega_n^2 \end{pmatrix}^T$, $B_{a,2} = \begin{pmatrix} 0 & 0 & 0 & 1 & 0 & 0 \end{pmatrix}^T$, and A_a is as defined in (4-7). Moreover, it is possible to define

$$G_{a,t}(s) = C_{a,t}\left(sI - A_a\right)^{-1} B_{1,a}, \tag{C-3}$$

with the output matrix $C_{a,t}$ defined as

$$C_{a,t} = \left(\tfrac{1}{v_{x,i}^2}\tfrac{C_{\alpha r}+C_{\alpha f}}{m}, \quad \tfrac{1}{v_{x,i}^2}\tfrac{C_{\alpha r}L_r - C_{\alpha f}L_f}{m}, \quad 0, \quad 0, \quad -\tfrac{1}{v_{x,i}}\tfrac{C_{\alpha f}}{m}, \quad 0 \right), \tag{C-4}$$

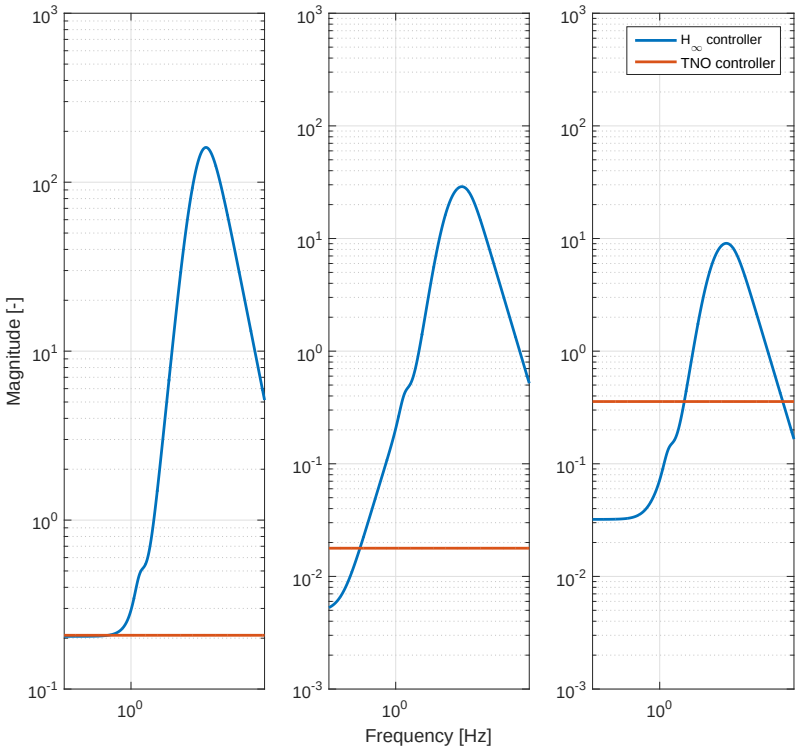

Figure C-1: Comparison between the $\mathcal{H}_\infty$ controller and the TNO controller, from left to right $|\mathcal{K}_{ff}|$, $|\mathcal{K}_{fb,y_e}|$, $|\mathcal{K}_{fb,\psi_e}|$.

where A_a and $B_{a,1}$ are identically defined as for (4-7). With these transfer functions defined and the TNO-controller $\mathcal{K}$, one can compute the string stability complementary sensitivity function Γ_a as defined in (3-24)

$$\Gamma_a = G_{a,t}\left(\left(1+\mathcal{K}_{fb}G_a\right)^{-1}\mathcal{K}_{ff} - \mathcal{K}_{fb}\left(I+G_a\mathcal{K}_{fb}\right)^{-1}G_{a,d}\right). \tag{C-5}$$

For the nominal parameters this yields a string stability complementary sensitivity function Γ_a with $\|\Gamma_a\|_{\mathcal{H}_\infty} = 1.221$, i.e., the system is not string stable.

Appendix D

Closed-loop poles

In this appendix the closed-loop poles of the closed-loop systems G_{cl}, related to the dynamic and static controllers are presented, with $v_{x,i} = 20\,\mathrm{m\,s^{-1}}$. The closed-loop system is given by,

$$G_{cl}(s) = \frac{G(s)\mathcal{K}_{fb}}{(I + G(s)\mathcal{K}_{fb}(s))} \tag{D-1}$$

which yields for the $\mathcal{H}_\infty$-controller:

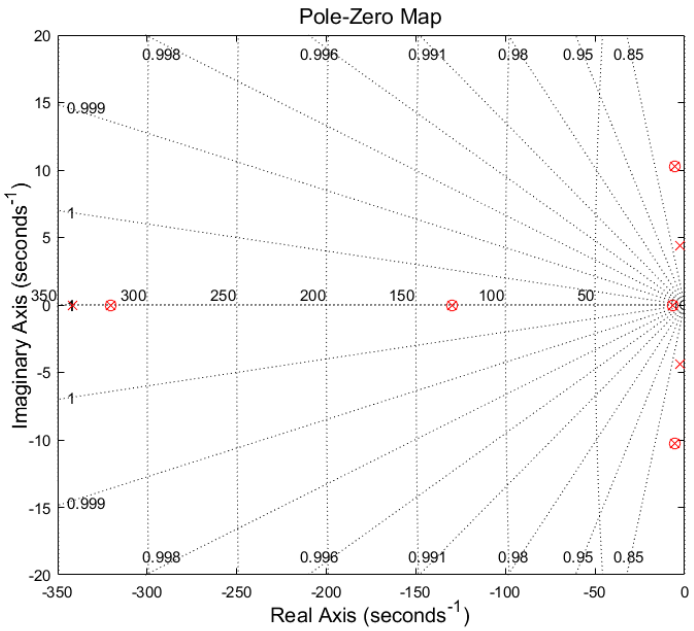

Figure D-1: Pole ($\times$) zero (o) map of the closed-loop system with the $\mathcal{H}_\infty$-controller at $v_{x,i} = 20\,\mathrm{m\,s^{-1}}$.

And for the static controller,

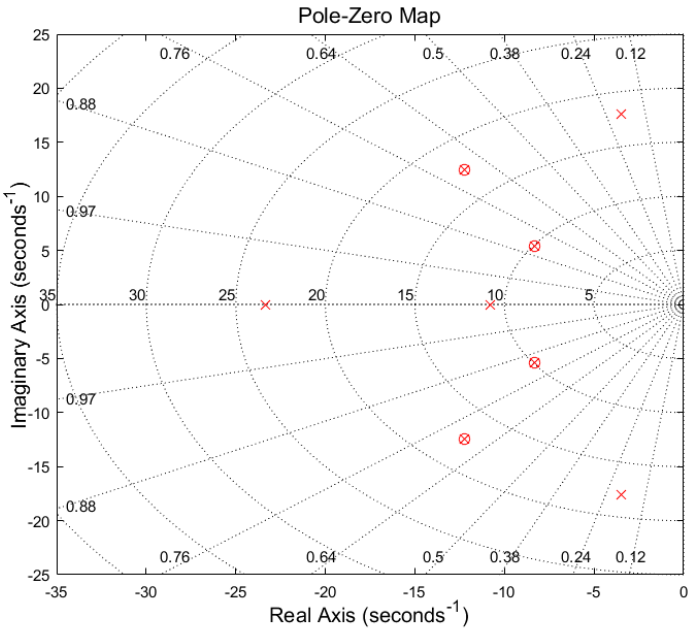

Figure D-2: Pole ($\times$) zero (o) map of the closed-loop system with the static controller at $v_{x,i} = 20\,\mathrm{m\,s^{-1}}$.

It can be observed from Figure D-1 that the $\mathcal{H}_\infty$-controller has faster and more damped poles and zero along the real axis, compared to the static controller. Which explains the more aggressive reaction to the initial condition response, moreover, the more damped poles are what makes this system string-stable.

Appendix E

Significance of error deviation

In this appendix the dynamics for the error perpendicular to the vehicle's longitudinal axis will be derived, it will be shown that given the right assumptions the right assumptions the error dynamics are not that different from the error dynamics defined perpendicular to the road. Moreover, these results will be verified by means of a numerical analysis.

Physical analysis

Let us define the heading error ψ_e as,

$$\psi_e = \beta + \psi - \theta_s \tag{E-1}$$

its time derivative $\dot{\psi}_e$ can be written as,

$$\begin{aligned} \dot{\psi}_e &= \dot{\beta} + \dot{\psi} - \dot{\theta}_s \\ &= \frac{\dot{v}_y}{v_x} - \frac{v_y}{v_x^2}\dot{v}_x + \dot{\psi} - \dot{\theta}_s \\ &\approx \frac{\dot{v}_y}{v_x} + \dot{\psi} - \dot{\theta}_s \end{aligned} \tag{E-2}$$

where use was made of the following approximation $\beta = \arctan\left(\frac{v_y}{v_x}\right) \approx \frac{v_y}{v_x}$ and it was assumed that v_x is constant such that $\dot{v}_x = 0$. Before continuing with the lateral error the following relation is defined:

$$\underline{\vec{e}}^c = R(\psi)^T \underline{\vec{e}}^o \tag{E-3}$$

with $R(\psi)^T$ the rotation matrix defined as,

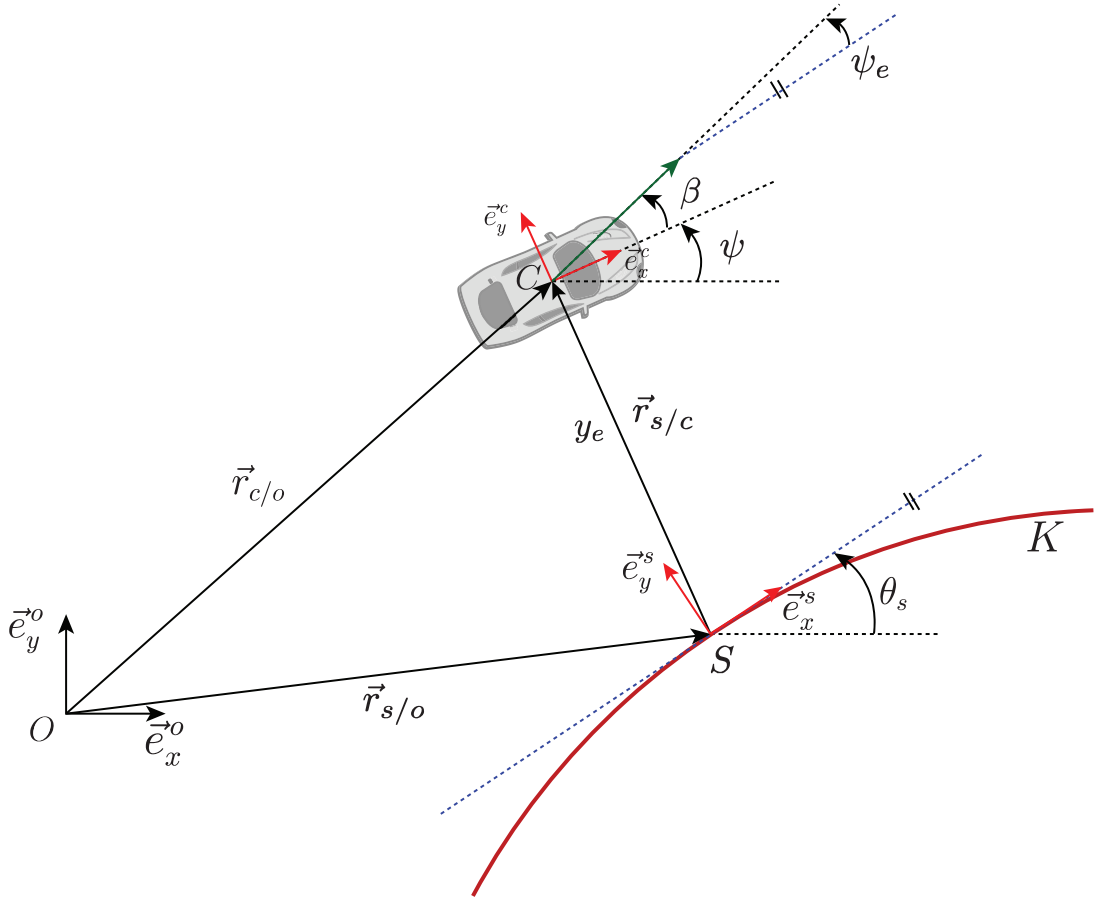

Figure E-1: Representation of the error dynamics perpendicular to the vehicle's longitudinal axis with respect to a reference path.

$$R(\psi)^T = \begin{pmatrix} \cos\psi & \sin\psi \\ -\sin\psi & \cos\psi \end{pmatrix} \tag{E-4}$$

the time derivative of $\underline{\vec{e}}^c$ is then equal to,

$$\begin{aligned} \dot{\underline{\vec{e}}}^c &= \dot{R}(\psi)^T \underline{\vec{e}}^o + R(\psi)^T \dot{\underline{\vec{e}}}^o \\ &= \dot{\psi} \begin{pmatrix} 0 & 1 \\ -1 & 0 \end{pmatrix} R(\psi)^T \underline{\vec{e}}^o \\ &= \begin{pmatrix} 0 & \dot{\psi} \\ -\dot{\psi} & 0 \end{pmatrix} \underline{\vec{e}}^c \end{aligned} \tag{E-5}$$

The lateral error y_e is defined as the distance from the the vehicle's CoG to the road, perpendicular to the vehicle's longitudinal axis. From Figure E-1 it follows that,

$$\dot{\vec{r}}_{s/o} = \dot{\vec{r}}_{c/o} - \dot{\vec{r}}_{s/c} \tag{E-6}$$

moreover, from the bicycle model in Appendix B we know that,

$$\dot{\vec{r}}_{c/o} = \begin{pmatrix} v_x & v_y \end{pmatrix} \underline{\vec{e}}^c. \tag{E-7}$$

Furthermore, from Figure E-1 it can be seen that

$$\vec{r}_{s/c} = y_e \vec{e}_y^c \tag{E-8}$$

from which it follows that,

$$\dot{\vec{r}}_{s/c} = \dot{y}_e \vec{e}_y^c + y_e \dot{\vec{e}}_y^c \tag{E-9}$$

using Equation (E-5) this can be written as,

$$\dot{\vec{r}}_{s/c} = \dot{y}_e \vec{e}_y^c - y_e \dot{\psi} \vec{e}_x^c \tag{E-10}$$

As a result Equation (E-6) yields,

$$\dot{\vec{r}}_{s/o} = \begin{pmatrix} v_x + y_e \dot{\psi} & v_y - \dot{y}_e \end{pmatrix} \underline{\vec{e}}^c \tag{E-11}$$

Per definition the origin **S** of frame P^S moves only in the tangential direction, yielding

$$\begin{aligned} \dot{\vec{r}}_{s,o} &= \begin{pmatrix} \dot{s} & 0 \end{pmatrix} \underline{\vec{e}}^s \\ &= \begin{pmatrix} \dot{s} & 0 \end{pmatrix} R\left(\psi - \theta_s\right) \underline{\vec{e}}^c \\ &= \begin{pmatrix} \dot{s}\cos\left(\psi - \theta_s\right) & -\dot{s}\sin\left(\psi - \theta_s\right) \end{pmatrix} \end{aligned} \tag{E-12}$$

From Equations (E-11) and (E-12) we get,

$$\begin{aligned} \dot{y}_e &= v_y + \dot{s}\sin\psi - \theta_s \\ &= v_y + \left(v_x + y_e\dot{\psi}\right)\tan\left(\psi - \theta_s\right) \\ &\approx v_y + \left(v_x + y_e\dot{\psi}\right)\left(\psi - \theta_s\right) \end{aligned} \tag{E-13}$$

using the convention that $\psi - \theta_s = \psi_e - \beta$ and $\beta \approx \frac{v_y}{v_x}$ and assuming that $v_x \gg y_e\dot{\psi}$ one obtains,

$$\begin{aligned} \dot{y}_{e,c} &= v_y + v_x\left(\psi_e - \frac{v_y}{v_x}\right) \\ &= v_x\psi_e \end{aligned} \tag{E-14}$$

which is the exact same equation as for the error defined as perpendicular to the road given in Equation (2-26). So to summarise the two errors are equal if $v_x \gg y_e\dot{\psi}$.

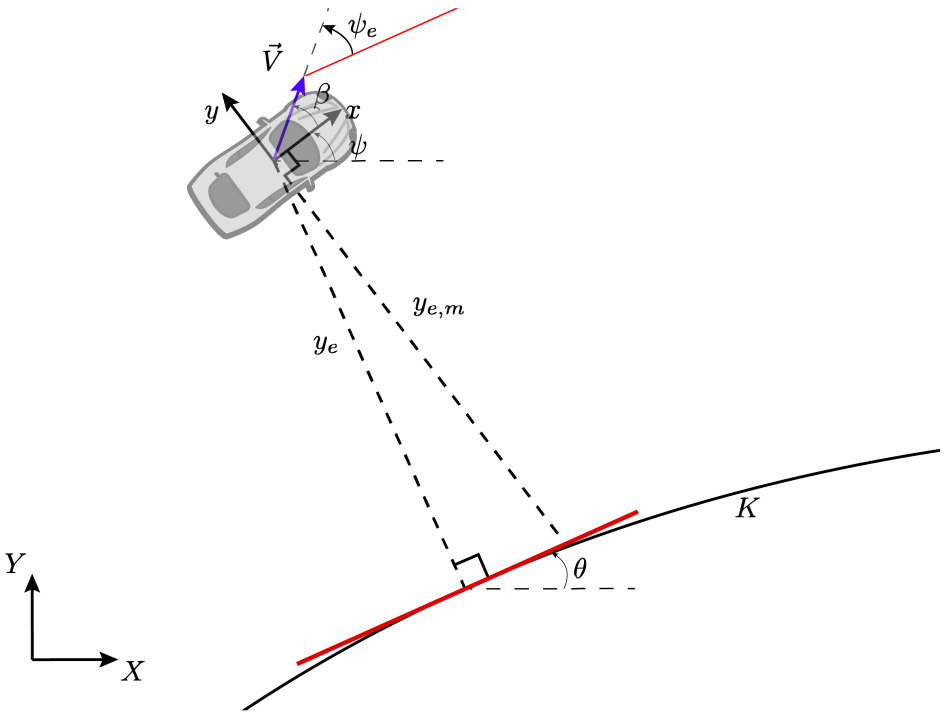

Figure E-2: The true error y_e versus the measured error $y_{e,m}$

Numerical analysis

In this section a numerical analysis of the significance of the difference in error definition will be provided. Here the true error will be defined as a function of the measured error. Figure E-2 serves to illustrate the problem at hand, where the measured error (perpendicular to the longitudinal axis) is denoted by $y_{e,m}$ and the true error is given by y_e. The true error can be written as a function of the measured error such that one obtains,

$$y_e = y_{e,m} + \underbrace{(y_e - y_{e,m})}_{d_e} \tag{E-15}$$

where d_e is the difference between the true error and the measured error from the reconstructed polynomial.

The reconstructed polynomial is given as a function of the vehicle's local x-coordinate $y = K(x)$. In order to find the error that is perpendicular to the road, one has to obtain the line $L(x)$ perpendicular to $K(x)$ which goes through the point $(0, 0)$, i.e., the origin defined at the vehicle's centre of gravity. The line perpendicular to the polynomial is obtained using the following relation,

$$\begin{aligned} \frac{dK}{dx} * L'(x) &= -1 \\ L' &= -1/\left(\frac{dK}{dx}\right) \end{aligned} \tag{E-16}$$

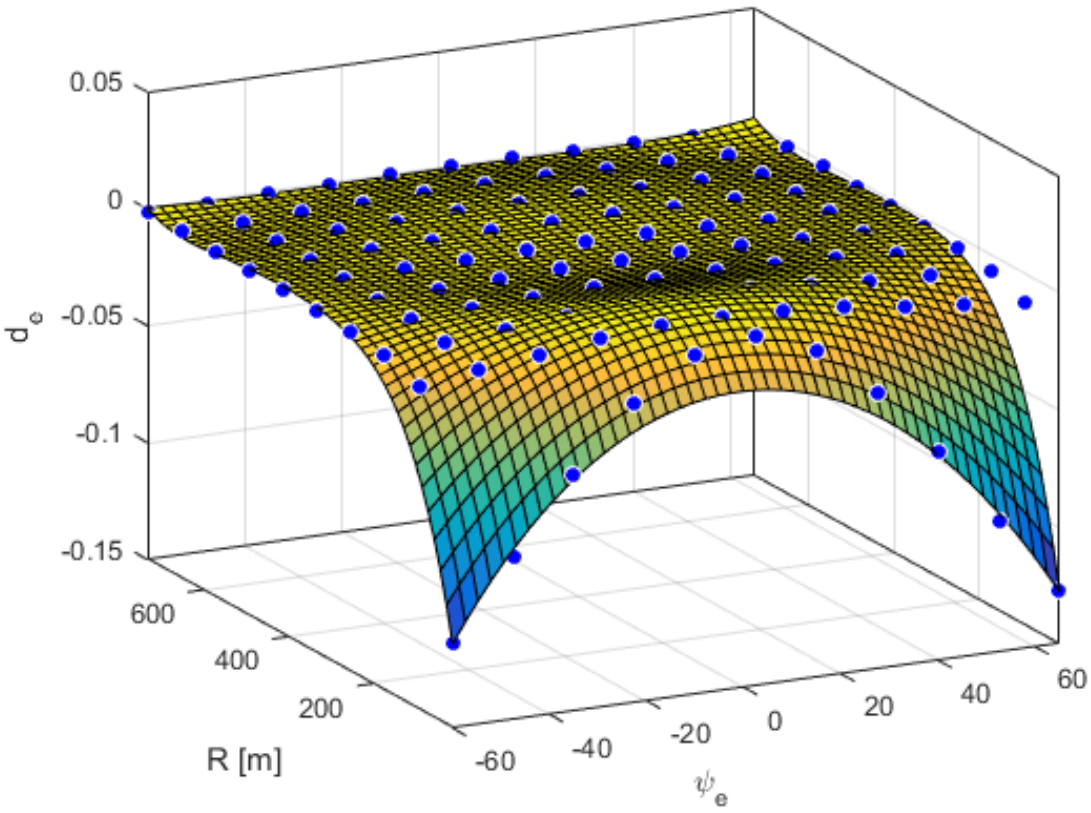

Figure E-3: Surface of the error as a function of ψ_e and R, the blue dots represent the data points

The line $L(x)$ is then equal to $L(x) = L' \cdot x + c$ since the line goes through $(0, 0)$, therefore $L(x) = L'(x) \cdot x$. Now that this line is determined, one can solve for the x-coordinate where $L(x)$ intersects $K(x)$, yielding x_{int}. Plugging x_{int} into $K(x)$ then gives the error perpendicular to the road, i.e., $y_e = K(x_{int})$. For a fifth order polynomial this problem does not have a simple analytical solution. Therefore a numerical demonstration of the effect of this difference in definition as a function of the heading error ψ_e and the road's radius R is given. This is given in the plot of Figure E-3, where a surface was fitted into the obtained values for d_e using a fifth order polynomial $d_e = P(\psi_e, R)$

Form Figure E-3 it can be observed that the surface for most combinations of ψ_e and R has a d_e of approximately 0. So even if both ψ_e and R have a noisy input the difference would still be negligible, except for when R is small, for example at a roundabout. Here d_e would be affected significantly by ψ_e. The difference would be in the centimetre region, and so the use of this compensation would be advised. However in most cases it would not make sense to apply this transformation since d_e would be approximately zero in most operation conditions, even in the presence of signal noise on R and ψ_e.

Bibliography

[1] J. Ploeg, "Analysis and design of controllers for cooperative and automated driving," Ph.D. dissertation, Technische Universiteit Eindhoven, 2014.

[2] "Siersdorf-Aldenhoven - FEV Group." [Online]. Available: http://www.fev.com/en/who-we-are/locations/subsidiaries/siersdorf-aldenhoven.html

[3] "Future of Highways," http://www.arup.com/future_of_highways, accessed: 2017-04-12.

[4] K. M. Hymel, K. A. Small, and K. V. Dender, "Induced demand and rebound effects in road transport," *Transportation Research Part B: Methodological*, vol. 44, no. 10, pp. 1220–1241, 2010.

[5] U.S. Department of Transportaion, "Traffic Safety Facts," National Highway Traffic Safety Administration, Washington, DC, Tech. Rep. February, 2015.

[6] SAE International, "Automated Driving," SAE International, Tech. Rep.

[7] V. Turri, B. Besselink, J. Martensson, and K. H. Johansson, "Fuel-efficient heavy-duty vehicle platooning by look-ahead control," *Proceedings of the IEEE Conference on Decision and Control*, vol. 2015-February, no. February, pp. 654–660, 2014.

[8] B. A. Bakermans, "Truck platooning: Enablers, Barriers, Potential and Impacts," 2016.

[9] S. Sheikholeslam and C. A. Desoer, "Control of Interconnected Nonlinear Dynamical Systems: The Platoon Problem," *IEEE Transactions on Automatic Control*, vol. 37, no. 6, pp. 806–810, 1992.

[10] D. Naffin, G. Sukhatme, and M. Akar, "Lateral and longitudinal stability for decentralized formation control," *Proceedings of the International Symposium on Distributed Autonomous Robotic Systems*, pp. 1–10, 2004.

[11] G. L. G. Lu and M. Tomizuka, "A practical solution to the string stability problem in autonomous vehicle following," *Proceedings of the 2004 American Control Conference*, vol. 1, pp. 780–785, 2004.

[12] R. Kianfar, M. Ali, P. Falcone, and J. Fredriksson, "Combined longitudinal and lateral control design for string stable vehicle platooning within a designated lane," *2014 17th IEEE International Conference on Intelligent Transportation Systems, ITSC 2014*, pp. 1003–1008, 2014.

[13] S. Solyom, A. Idelchi, and B. B. Salamah, "Lateral Control of Vehicle Platoons," *2013 IEEE International Conference on Systems, Man, and Cybernetics*, pp. 4561–4565, 2013.

[14] H. Summala, "Brake Reaction Times and Driver Behavior Analysis," *Transportation Human Factors*, vol. 2, no. 3, pp. 217–226, 2000.

[15] G. D. Lee, S. W. Kim, Y. U. Yim, J. H. Jung, S. Y. Oh, and B. S. Kim, "Longitudinal and lateral control system development for a platoon of vehicles," *Proceedings 199 IEEE/IEEJ/JSAI International Conference on Intelligent Transportation Systems (Cat. No.99TH8383)*, pp. 605–610, 1999.

[16] L. E. Peppard, "String Stability of Relative-Motion PID Vehicle Control Systems," *IEEE Transactions on Automatic Control*, vol. 19, no. 5, pp. 579–581, 1974.

[17] W. Jansen, "Masters Thesis: Lateral Path-Following Control for Automated Vehicle Platoons," p. 92, Technische Universiteit Delft, 2016.

[18] I. Papadimitriou, G. Lu, and M. Tomizuka, "Autonomous lateral following consideration for vehicle platoons," *IEEE/ASME International Conference on Advanced Intelligent Mechatronics, AIM*, vol. 1, pp. 401–406, 2003.

[19] J. H. H. M. . Alleleijn, "Lateral string stability of vehicle platoons," 2014.

[20] R. Rajamani, *Vehicle Dynamics and Control*, ser. Mechanical Engineering Series. Springer US, 2011.

[21] S. Gehrig and F. Stein, "A trajectory-based approach for the lateral control of car following systems," *SMC'98 Conference Proceedings. 1998 IEEE International Conference on Systems, Man, and Cybernetics (Cat. No.98CH36218)*, vol. 4, pp. 3596–3601, 1998.

[22] G. O. Burnham, J. Seo, and G. A. Bekey, "Identification of Human Driver Models in Car Following," *IEEE Transactions on Automatic Control*, vol. 19, no. 6, pp. 911–915, 1974.

[23] S. Shladover, "Longitudinal Control of Automated Guideway Transit Vehicles Within Platoons," *Journal of Dynamic Systems*, pp. 302–310, 1978.

[24] P. A. Ioannou and C. C. Chien, "Autonomous Intelligent Cruise Control," *IEEE Transactions on Vehicular Technology*, vol. 42, no. 4, pp. 657–672, 1993.

[25] D. Swaroop and J. K. Hedrick, "String stability of interconnected systems," *IEEE Transactions on Automatic Control*, vol. 41, no. 3, pp. 349–357, 1996.

[26] J. Ploeg, "A Not-So-Short Overview of Vector , Matrix , Signal , and System Norms," 2016.

[27] J. Ploeg, N. Van De Wouw, and H. Nijmeijer, "$\mathcal{L}_p$ String Stability of Cascaded Systems: Application to Vehicle Platooning."

[28] S. C. Warnick and A. A. Rodriguez, "Longitudinal control of a platoon of vehicles with multiple saturating nonlinearities," *Proceedings of 1994 American Control Conference - ACC '94*, vol. 1, 1994.

[29] R. D. Castro, A. Schaub, C. Satzger, and J. Brembeck, "A Vehicle Following Controller for Highly-Actuated Vehicles," *International Symposium on Advanced Vehicle Control 2016*, 2016.

[30] D. Schramm, M. Hiller, and R. Bardini, "Vehicle Dyanmics." Springer-Verlag Berlin Heidelberg 2014, 2014, ch. Chapter 10, pp. 223–245.

[31] R. Rajamani and C. Zhu, "Semi-autonomous adaptive cruise control systems," *IEEE Transactions on Vehicular Technology*, vol. 51, no. 5, pp. 1186–1192, 2002.

[32] J. Craens and N. Das, "Taking over the steering of a toyota prius using the electric steering motor," Fontys, Tech. Rep., 2014.

[33] S. Skogestad and I. Postlethwaite, "Multivariable feedback control analysis and design." *International Journal of Robust and Nonlinear Control*, vol. 8, no. 14, pp. 144–145, 1998.

[34] M. Huang, W. Gao, and Z. P. Jiang, "A data-based lane-keeping steering control for autonomous vehicles: A human-in-the-loop approach," in *2016 35th Chinese Control Conference (CCC)*, July 2016, pp. 8974–8979.

[35] P. Ruijs, R. van der Horst, and P. Broeren, "Ontwerpen van horizontale bogen," RWS DVS, Tech. Rep., 2012.

[36] I. Besselink, "Lecture notes in vehicle dynamics," August 2008.

[37] A. Schmeitz, J. Zegers, J. Ploeg, and M. Alirezaei, "Towards a generic lateral control concept for cooperative automated driving theoretical and experimental evaluation," in *2017 5th IEEE International Conference on Models and Technologies for Intelligent Transportation Systems (MT-ITS)*. IEEE, jun 2017, pp. 134–139. [Online]. Available: http://ieeexplore.ieee.org/document/8005653/

[38] M. Alirezaei, S. T. H. Jansen, A. J. C. Schmeitz, and A. K. Madhusudhanan, "Collision Avoidance System using State Dependent Riccati Equation Technique : An Experimental Robustness Evaluation," *International Symposium on Advanced Vehicle Control 2016*, 2016.

[39] E. W. Weisstein, "Radius of Curvature." [Online]. Available: http://mathworld.wolfram.com/RadiusofCurvature.html

[40] H. Xing, J. Ploeg, and H. Nijmeijer, "Pade approximation of delays in cooperative acc based on string stability requirements," *IEEE Transactions on Intelligent Vehicles*, vol. 1, no. 3, pp. 277–286, Sept 2016.

[41] R. Carona, A. P. Aguiar, and J. Gaspar, "Control Of Unicycle Type Robots Tracking, Path Following and Point Stabilization." [Online]. Available: http://users.isr.ist.utl.pt/{~}jag/publications/08-JETC-RCarona-vcontrol.pdf